

Vladimer Birkadze

Optimization and engineering geological evaluation of headrace tunnel system of Akavreta HPP in Georgia

Master's thesis in Hydropower Development

Supervisor: Krishna Kanta Panthi

Co-supervisor: Bikash Chaudhary

June 2022

Vladimer Birkadze

Optimization and engineering geological evaluation of headrace tunnel system of Akavreta HPP in Georgia

Master's thesis in Hydropower Development
Supervisor: Krishna Kanta Panthi
Co-supervisor: Bikash Chaudhary
June 2022

Norwegian University of Science and Technology
Faculty of Engineering
Department of Geoscience and Petroleum



Your ref.: MS/I23T67/IGP/LBKPP

Date: 07.02.2022

**TGB4945 ENGINEERING GEOLOGY - MSc thesis
for
HPD student Vladimer Birkadze**

Optimization and engineering geological evaluation of headrace tunnel system of Akavreta HPP in Georgia

Background

Design and optimization of a hydropower project is heavily influenced on the site location and correct placement of both surface and sub surface (underground) structures. Failure in locating underground structures at the right place brings additional cost overruns and substantial delays in construction. This is especially the case while planning and design of the underground structure passing through the volcanic rock formations where there is a great variation in the rock mass conditions. The planned Akavreta Hydropower Project in Georgia consists of two headrace tunnels that utilize water from two different rivers. The discharge from these two rivers is collected through free flow tunnels to a forebay from where water is discharged through a common penstock pipe aligned along the topographic surface leading to the powerhouse located to open ground.

MSc thesis task

This MSc thesis is to focus on the planning and design aspects of Akavreta hydropower project, with a focus on the following issues:

- Review planning & design principles of hydropower structures. Review the tunnel stability challenges and stability assessment methods practiced in rock engineering which are relevant to be used for the stability assessment of headrace system of Akavrete HPP.
- Briefly describe Akavreta Hydropower Project. Review the extent of engineering geological investigations carried out at this project.
- Carry out critical assessment of existing lay-out design and placement of headrace tunnels and other elements of the project. Highlight major deficiency of the existing design.
- Suggest an alternative lay-out design and improved placement of the headrace system.

- Carry out extensive assessment on the type of stability challenges that different underground elements may experience during excavation. Evaluate each of the challenges using prevailing rock engineering theory discussed in the theory review chapter.
- Carry out stability assessment of the selected segments of headrace system using numerical modelling.
- Discuss the analysis results and conclude the work.

Relevant computer software packages

Candidate shall use *roc-science package* and other relevant computer software.

Background information for the study

- Relevant information such as reports, maps, information, and data collected by the candidate.
- Scientific papers, reports and books related to hydropower, rock and tunnel engineering.
- Literatures on rock mass properties, in-situ stress, rock mass quality and rock support.

Co-supervisor

PhD fellow Mr. Bikash Chaudhary will be the co-supervisor of this MSc thesis work.

The project work has started on 10th January 2022 and to be completed by 11th June 2022.

The Norwegian University of Science and Technology (NTNU)
Department of Geoscience and Petroleum

February 07, 2022



Dr. Krishna K. Panthi
Professor of geological engineering, main supervisor

Note: This MSc task must be inserted in the MSc thesis after cover page

Preface

This master thesis titled “Optimization and engineering geological evaluation of headrace tunnel system of Akavreta HPP in Georgia” is submitted to the Department of Geoscience and Petroleum at the Norwegian University of Science and Technology (NTNU) as the final requirement for fulfillment of Master of Science in Hydropower Development Program (2020-2022).

The thesis mainly focuses on the documentation and evaluation of plastic deformation analysis of tailrace tunnel of Akavreta HPP, Georgia. The applied methods for plastic deformation analysis involve empirical, semi-analytical and numerical methods. Current and alternative designs were evaluated and recommendations were given. The thesis work started during the winter semester of 2022 and is submitted at the end of the spring semester of 2022 and is supervised by Prof. Dr. Krishna Kanta Panthi.

Vladimer Birkadze
NTNU, Norway
June 2022

Acknowledgement

I would like to express my gratitude to my main supervisor Prof. Dr. Krishna Kanta Panthi. During thesis work he guided me and gave me recommendations, which was very valuable during my thesis writing journey. Furthermore, I would like to extend my gratitude to my co-supervisor, Mr. Bikash Chaudhary who helped me in RS2 software and gave me insightful tips.

I am grateful to Mr. Irakli Janashvili, Director of Georgian Hydro Power LLC (GHP) for his help and legal support for data collection (maps, 3D contour lines, hydrological and geological investigation technical reports) of Akavreta HPP. I would also like to thank the employees at the GHP, Georgia for their support and cooperation on creating alternative alignment for Akavreta HPP headrace tunnel.

Abstract

Current thesis is about designing and evaluating Akavreta HPP headrace tunnel system in Georgia. Akavreta HPP is 20 MW hydropower project located in Adjara region. There are three dams, which collect water from three different rivers and transfer discharge through five free flow channels and two headrace tunnels to forebay, where it is directed to the powerhouse with surface penstock. The project was purposed by Georgian Hydro Power LLC (GHP). First, the tunnel stability challenges, and stability assessment methods, which are relevant to be used for the stability assessment of headrace tunnel system of the project were reviewed. Initial design was evaluated and major deficiencies were highlighted. After deciding that the current alignment is not safe and reliable, because of very small overburden in major weakness zones, alternative one was introduced. In alternative alignment the headrace tunnel N1 size increases from 2150 m to 2750 m, but it eliminates the 820 m of free flow channel with 820 m of the road, it also highly increases the overburden at major weakness zones. Empirical, semi-analytical and numerical analysis were carried out. With empirical and semi-analytical calculations, it was found that in weak rock type, which is tuff-breccias, there would be small squeezing. For support system design, the Q system was used, which is one of the most widely used rock mass classification system. Further, elastic and plastic analysis were carried out for numerical modeling to find headrace tunnel deformation and to find optimal tunnel support system. After getting results, the conclusion and recommendations were given.

TABLE OF CONTENTS

Preface.....	i
Acknowledgement.....	ii
Abstract	iii
1. Introduction	1
1.1. Background.....	1
1.2. Objective of the study.....	2
1.3. Methodology of the study.....	3
2. Planning and design	4
2.1. Hydropower and tunneling	4
2.2. Tunnel alignment and location	5
2.2.1. Tunnel alignment.....	5
2.2.2. Tunnel location.....	6
2.3. Optimization of tunnel shape and size.....	8
2.4. Groundwater and leakage in tunnels	9
3. Rock mass quality and stability assessment.....	10
3.1. Rock mass properties.....	11
3.1.1. Discontinuities.....	11
3.1.2. Weathering	12
3.1.3. Rock mass classification systems.....	13
3.1.4. Rock mass quality	21
3.2. Rock stresses.....	24
3.3. Stability assessment methods	28
3.3.1. Failure criteria	28
3.3.2. Rock burst	30
3.3.3. Squeezing	31
4. Case description	36
4.1. Akavreta HPP	36
4.1.1. River Akavreta catchment area	37
4.1.2. Hydraulic structures	38
4.1.3. Precipitation	38
4.1.4. Hydrology.....	39
4.1.5. Climate	42

4.2.	General geology of Georgia	43
4.2.1.	Regional geology.....	45
4.2.2.	Project geology.....	47
4.3.	Rock mass quality along the headrace tunnels	53
4.3.1.	Modulus of deformation.....	53
4.3.2.	Rock mass strength.....	54
4.3.3.	Rock mass classification	56
5.	Critical assessment of existing design.....	56
5.1.	Brief description of current design	56
5.2.	Evaluation of current design.....	57
6.	Alternative possibility	61
6.1.	Evaluation on the possible alternative	61
6.2.	Stability assessment and rock support design.....	66
6.2.1.	Squeezing and rock burst/spalling analysis.....	66
6.2.2.	Support design.....	68
7.	Numerical assessment	69
7.1.	Input parameters	69
7.2.	Principle stress direction	71
7.3.	Elastic analysis	74
7.4.	Plastic analysis	77
7.5.	Support system	82
8.	Conclusion and recommendations	85
8.1.	Conclusion.....	85
8.2.	Recommendations	86
	References	88
	APPENDICES.....	90

1. Introduction

1.1. Background

Georgia is located east of Black Sea, bordering Russia to the north, Turkey, Armenia to the South and Azerbaijan to the South-east. Georgia covers a territory of 69,700 square kilometers and its population is around 3.72 million people (Georgia Energy Policy Review 2020).



Figure 1. 1 - Map of Georgia ("Georgia" 2008)

Currently main goal in energy sector of Georgia is to become energy independent country and to be less energy import oriented. Georgia is very rich with natural and renewable energy resources. The problem is that a major part of it is not utilized. For example, there are 26,000 rivers in Georgia, which makes the country one of the top in water resources per capital in world rankings, but only 20-22% of the total hydro potential is utilized ("Factsheet: Renewable Energy in Georgia 2021" 2021). Hydropower potential is estimated to be around 50 TWh/year ("Factsheet: Renewable Energy in Georgia 2021" 2021).

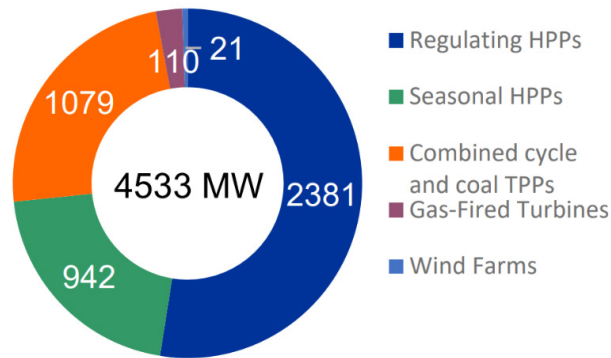


Figure 1. 2 - Pie chart of total installed capacity in Georgia (Ten-Year Network Development Plan of Georgia 2021-2031, 2021)

Currently, total installed capacity of Georgian power system is 4533 MW (Figure 1. 2), from which the installed capacity of regulated hydropower plant is 2381 MW, the run-of-river hydropower plant is 942 MW, 21 MW for wind farm, 110 MW for gas-fired turbines and 1079 MW for combined cycle and coal thermal power plant (Ten-Year Network Development Plan of Georgia 2021-2031, 2021). About 74% of total power production comes from Hydropower plants. Thus, the hydropower provides a major part of Georgia's electricity generation.

1.2. Objective of the study

Key points of objective of the study:

- Give brief description of planning and design principles of hydropower structures. Review the tunnel stability challenges and stability assessment methods practiced in rock engineering, which are relevant to be used for the stability assessment of headrace tunnel system of Akavrete HPP.
- An overview of Akavreta HPP Hydropower Project. Analyze the extent of engineering geological investigations undertaken for this project.
- Analyze the existing layout design and the placement of headrace tunnels and other components of the project. Identify major shortcomings in the project.
- If necessary, propose a different layout and location for the headrace system.
- Assess in detail what kind of stability challenges different underground elements may face during excavation. Utilize the rock engineering theory described in the theory review chapter to evaluate each of the challenges.
- Utilize numerical models to determine the stability of selected segments of the headrace tunnel system.
- Conclude the work by discussing the analysis results and give recommendations.

1.3. Methodology of the study

- Various literature, reports, maps and articles will be used as a reference to this thesis.
- Evaluate the current design of the headrace tunnel, which was purposed by Georgian Hydro Power LLC.
- If the headrace tunnel meets all the safety requirements and is feasible, it will remain as it is, if not, there will be new design proposal with detailed evaluation and calculations.
- For headrace tunnel evaluation the empirical and semi-analytical methods will be used. As for numerical part the RS2 software package will be used.
- At the final stage the conclusion and recommendations will be given.

2. Planning and design

In this chapter the design approach of the tunneling system and its characteristics will be discussed. The Figure 2. 1 demonstrates the main principles for engineering geological design.

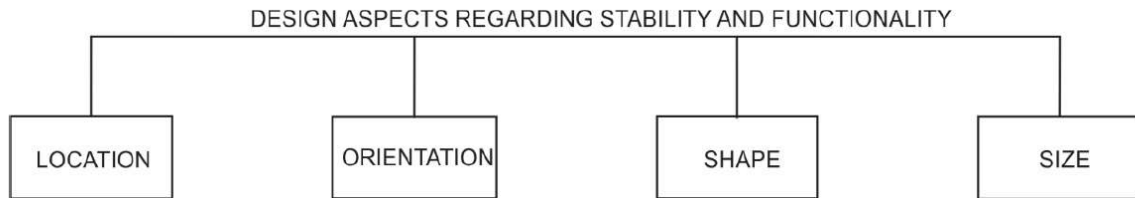


Figure 2. 1 - Elements controlling stability and long-term functionality of an underground opening (Panthi & Broch, 2022)

2.1. Hydropower and tunneling

Tunneling in Hydropower projects have been used for many years and in modern days plays big role in many hydropower systems. Norwegian hydropower has more than 100 years of experience in constructing more than 4000 km long unlined pressure shafts and tunnels with maximum static water head of 1047 m (Panthi & Basnet, 2016).

Headrace tunnels can be pressurized, which means full cross section covered with water, or non-pressurized, meaning there is some portion of the tunnel section, which is not covered by water. In this thesis the non-pressurized headrace tunnel will be analyzed.

There is a substantial difference between tunnel for traffic and for water conveying. In the case when the tunnel is used for water transport, first, while excavating it is dry, but while operation of hydropower plant it gets wet. While power plant operates, the changes in head may induce stress differences along the tunnel periphery.

Tunnels can also be lined and unlined. Lined tunnels are with support and unlined are without support. The unlined tunnel system is used in case when the rock mass is strong enough to withstand induced stresses on its own.

Some advantages of the tunnels in hydropower system:

- Its more secure
- Health and safety of society
- On many occasions cost effective
- Provides possibility to reduce the distance and increase long term stability
- It has freedom of design and possibility for future expansion

- It can be used while having limited space on the surface

2.2. Tunnel alignment and location

2.2.1. Tunnel alignment

To avoid or to reduce the instability problems in the tunnel, it is essential to have a favorable location and alignment of the tunnel axis. There are many different reasons for having optimal tunnel alignment and location, several of them are:

- To have the shortest length possible
- To avoid weakness zones
- To have a favorable orientation with respect to the major joint sets
- To have favorable orientation with respect to in-situ rock stresses if they are very high
- To have optimal tunnel overburden

In the best-case scenario, all upper given goals will be achieved, but unfortunately in practice it is nearly impossible. There is always compromise to make, the best practice is to evaluate what will be the best choice between upper given options in terms of tunnel construction time, stability, and cost. When making decision, there are many modern tools to help. For example, the areal images and LIDAR scanning can be used to map the major weakness zones and discontinuities. For conventional method, various graphical tools can be used, for example the so-called Join Rosette (Figure 2. 2). It is the map, which illustrates the joint sets, their number and orientation (strike-dip).

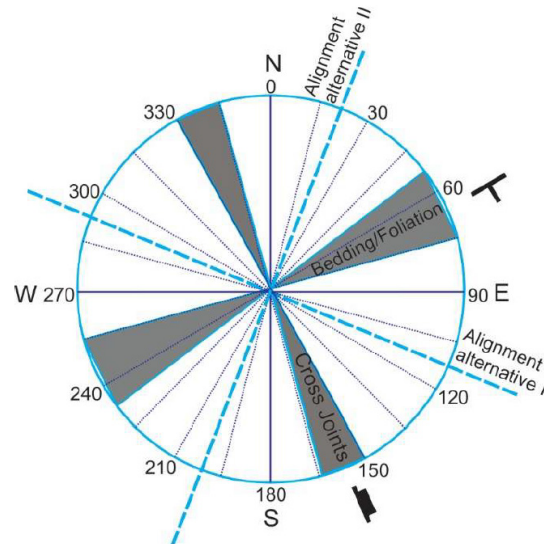


Figure 2. 2 - Discontinuity interpretation in a joint rosette with possible tunnel axis alignment alternatives (Panthi & Broch, 2022).

For the best tunnel alignment, in case of one joint set, tunnel axis should be as much as possible perpendicular to the joint set, because it gives us the most reasonable solution, with less possible chances of having instabilities in the tunnel caused by discontinuity. In case of several joint sets, the tunnel alignment should be planned, so it bisects the angle between given joint sets, it means tunnel will be in equal angular distance between joints. For example, two most reasonable tunnel axis alignments are shown in Figure 2. 2, the first “alignment alternative I” and second option “alignment alternative II”. In the worst-case scenario, the tunnel alignment will be parallel to the joints. In this case, continues joints will be running parallel to the tunnel, which will create instabilities.

2.2.2. Tunnel location

The location of the tunnel depends on the rock mass quality. For example, when making location decisions, the young sedimentary rocks should be avoided, because they may induce instabilities in the tunnel. Depending on, if there is a shallow or deep-seated tunnel, there are different techniques to determine its location. In general, the portals are in shallow areas. In this case, it must be seated deep enough to leave the unweathered rock mass above the roof at some specific distance. In Norway as a rule of thumb, the cavern should be at least 5 m (up to 20 m) bellow depth of weathering area (Figure 2. 3).

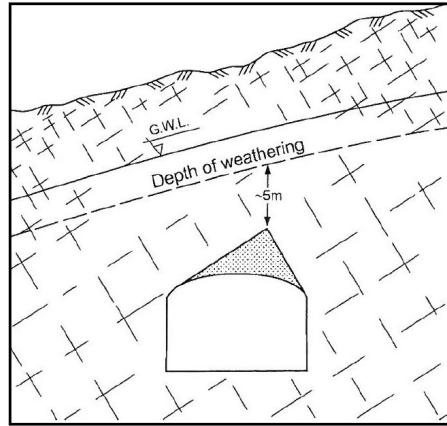


Figure 2. 3 - Minimum distance of the tunnel from depth of weathering area (Selmer-Olsen & Broch, 1978)

The overburden depth is necessary to maintain self-supporting capabilities of the roof. Unfortunately, not always it is possible to maintain the safe distance, in this case the tunnel alignment should be changed or installation of more support and lining will be required to maintain the safe environment and the cost of the tunnel will increase. This happens because of the low distance to the surface, as a result there is a low vertical stress in the rock mass and interlocking effect (arching effect) between rock blocks is reduced, it can induce the rock fall phenomena in tunnel area. The tunnel and slope adjacent to it may have serious problems due to inadequate confining forces caused by an insufficient depth of burial of the tunnel (Hoek, 2007). In case of deep-seated situation, the location should be planned to avoid high vertical stress level, because if it exceeds the rock mass strength than the instability problems may occur.

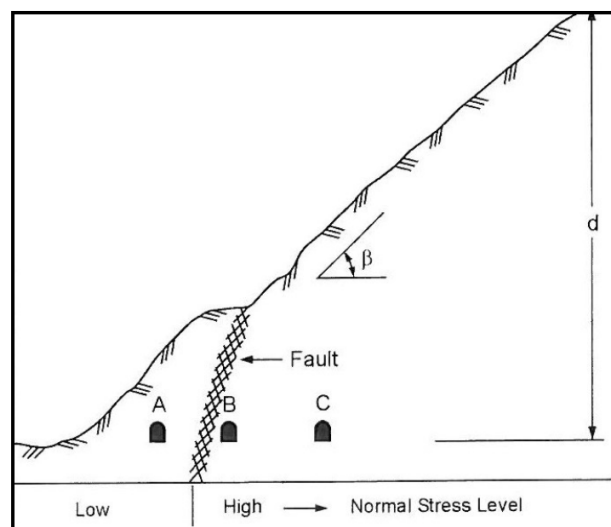


Figure 2. 4 – Different cavern locations in the steep Valley with fault zone (Selmer-Olsen & Broch, 1978)

The fault zones may have big impact on the cavern location decision making, because it can influence different instabilities. For example, from the Figure 2. 4 at the option “A”, because of the fault zone, the horizontal stresses will not be transformed, and the depth is shallow. As a result, it will make the area where the “A” is located, distressed. If the tunnel will be built at this location, there might be instabilities associated with rock fall. For case “B” the scenario will be more or less the same as for “A”, because it is also close to the fault zone. Between these three options the “C” will be the best, because the overburden will be sufficient and it is not close to the fault zone.

2.3. Optimization of tunnel shape and size

As a basic principle of design, one should not only look for an optimum orientation for underground openings, but also strive to distribute compressive stresses evenly along the entire excavation (Selmer-Olsen & Broch, 1978). It is good practice to avoid sharp corners in the tunnel profile, because rock mass at these points will be distressed, resulting in instabilities, such as overbreak.

In theory, it is possible to design the tunnel profile knowing the orientation of the major principal stresses, but it is easier said than done. As shown in Figure 2. 5 depending on the orientation of major principal stresses, the impact will be different at different locations of the tunnel opening.

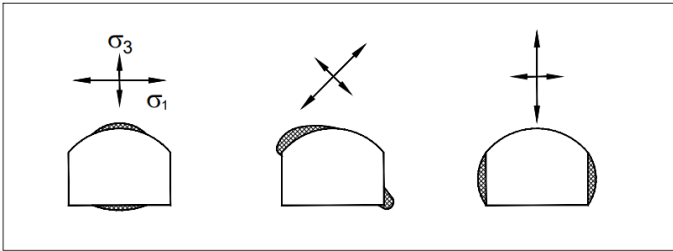


Figure 2. 5 - Effect on different locations of the opening, depending on the major principal stress orientation (modified from (Selmer-Olsen & Broch, 1978))

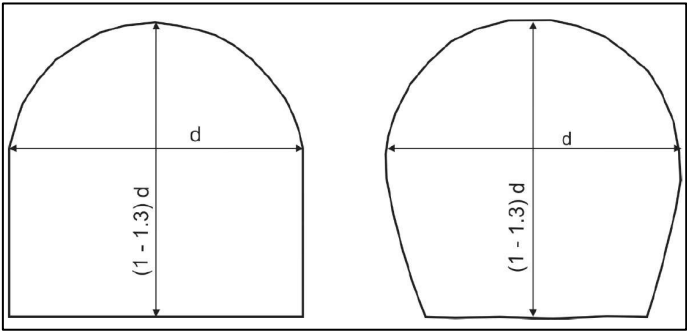


Figure 2. 6 - Recommended inverted D-shape (left) horseshoes shape (right) tunnel (Panthi, 2015)

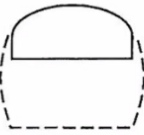
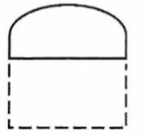
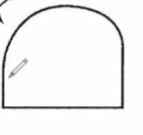
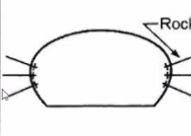
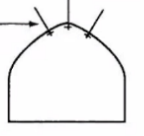
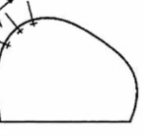
STRESS LEVEL Design principle	DIRECTION OF MAJOR PRINCIPLE STRESS		
	VERTICAL	HORIZONTAL	INCLINED
MODERATE Even distribution of stresses to avoid local stability problems	 High walls should be curved to avoid buckling	 High walls can be straight	 Assymetric profile when large anisotropy in stresses
HIGH Concentration of stresses to reduce unstable area and costs of support	 High walls should be avoided	 The roofarch should be pointed	 Assymetric profile with curved walls

Figure 2. 7 - The shape of the tunnel profile at different stress conditions (Nilsen and Thidemann 1993 in (Panthi, 2020))

Depending on the different stress conditions in the rock mass and the orientation of major principal stresses, the shape of the tunnel profile can be defined. For example, according to Figure 2. 7, if there is a high vertical major principal stress, the shape of the tunnel profile will be elongated, and dynamic release of the stress could be controlled with anchored rock bolts as additional support. For the case of drill and blast tunneling method the best practice is to use the inverted D or horseshoe shaped tunnels (Figure 2. 6).

2.4. Groundwater and leakage in tunnels

Groundwater plays important part in tunnel design. If while construction the unexpected water flood occurs, it can have big impact on stability and safety of the tunnel. Groundwater prediction is very difficult and tedious task. Main source of the water in rock mass is from groundwater, which leaks through pores or open joints. If the gradient of energy head does not equal to zero, then the water movement will take place.

Slope stability problems are caused mainly by groundwater pressure, and therefore to implement reliable slope design, it is crucial to understand the role of the groundwater (Hoek & Bray, 1981). For the hydropower projects water leakage is major problem because water loss equals energy production loss. Beside reason for instabilities in the tunnel, the water leakage interferes with drill and blast tunnel excavation process.

There are various sources of water in rock mass. It can be stored in some minerals (e.g. Gypsum, salt and anhydrite) as a chemical bonding and the water can flow inside porose zones of the

rock mass. Different rock types have different porosity, for example magmatic and metamorphic rocks rarely have more than 2% of porosity, while soft limestone can vary between 20 and 50%. Despite low porosity in certain rock mass, the water can flow through open joints. In some cases, when certain minerals (e.g. smectites) get wet the chemical reaction occurs, they tend to swell and expand in size, which become the reason of instabilities (rock fall) in the tunnel.

3. Rock mass quality and stability assessment

Rock mass is a complex block of materials. Rock mass quality and mechanical processes affecting the rock mass are the two main characteristics of the rock mass (Panthi, 2006). Tectonic forces and environmental processes have created complex geometric and mechanical assemblages within rock masses. In another words, rock mass is the combination of stresses, discontinuities, joint sets, groundwater and intact rock. To determine various properties of the rock mass similar to deformation, strength and failure properties, in-situ measurements are carried out or the intact rock sample is analyzed in the lab. Intact rock is gathered through drilling. It is a part of rock mass, homogeneous and not affected by fractures. To predict the behavior of the rock mass during excavation the information about the full stress-strain behavior of the rock mass and its strength characteristics is needed, as well as how time influences their properties. Tunnel stability depends on the rock mass, its quality and strength. The relationship is shown in Figure 3. 1 .

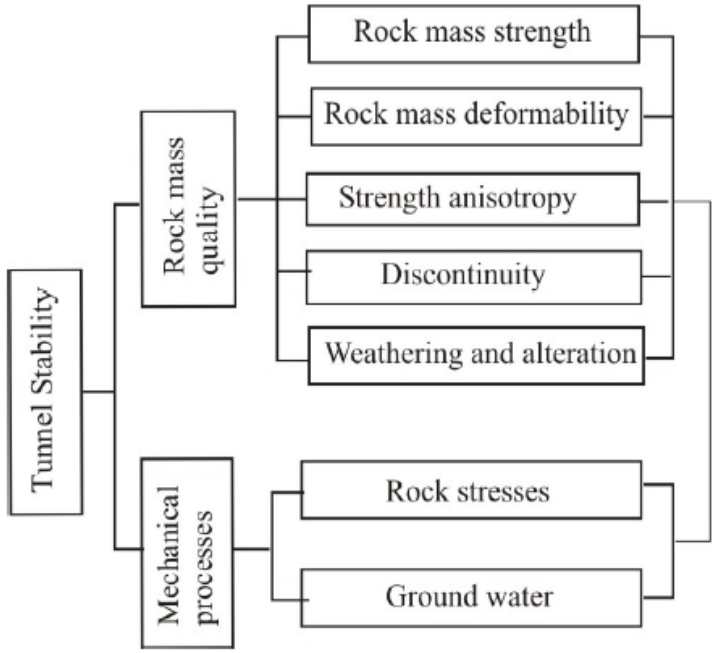


Figure 3. 1 - Factors influencing tunnel stability (Panthi, 2006)

3.1. Rock mass properties

Almost any type of analysis used for designing slopes, foundations, and underground excavations requires reliable estimates of rock mass strength and deformation characteristics. In the following chapters several crucial rock mass properties will be discussed. Generally, as shown in Table 3. 1, there are two types of methods to determine rock mass properties: direct and indirect method.

Table 3. 1 - Methods to determine rock mass properties (Based on (Brown, 1993)).

Direct method	Indirect method
<ul style="list-style-type: none"> • Laboratory tests • In situ tests 	<ul style="list-style-type: none"> • Empirical or theoretical correlations • Combination of intact rock and discontinuity Properties using analytical or numerical methods • Back-analysis using field observations of prototype observations

3.1.1. Discontinuities

The word ‘discontinuity’ is used to describe the natural faults (weakness zones), joints (also set of joints), fissures, fractures, and bedding planes. The deformability, strength and permeability of a rock mass can be determined by discontinuities in an engineering context. An excavation or surface can be significantly affected by continuous discontinuity and particularly with large one. That is why it is crucial to understand the geometrical, mechanical, and hydrological properties of discontinuities and how it affects the rock mass.

The most common way to study the discontinuities in rock mass is by bore hole analysis. The geometric properties of the discontinuities can be defined as (Figure 3. 2):

- Orientation (dip/strike angles) - Due to the assumption that the discontinuity is planar, the dip direction and dip angle are the only factors determining its orientation.
- Aperture – It describes two rock surfaces of the discontinuity perpendicular to each other.
- Discontinuity sets – It is the cluster of discontinuities and their number.
- Roughness – It describes the roughness of the discontinuity surface.
- Block size – It shows the presence of the rock blocks and its size.
- Spacing and frequency – Spacing describes the distance between two discontinuities and the frequency the number per unit distance.
- Size and shape – It simply describe the shape and size of discontinuity.

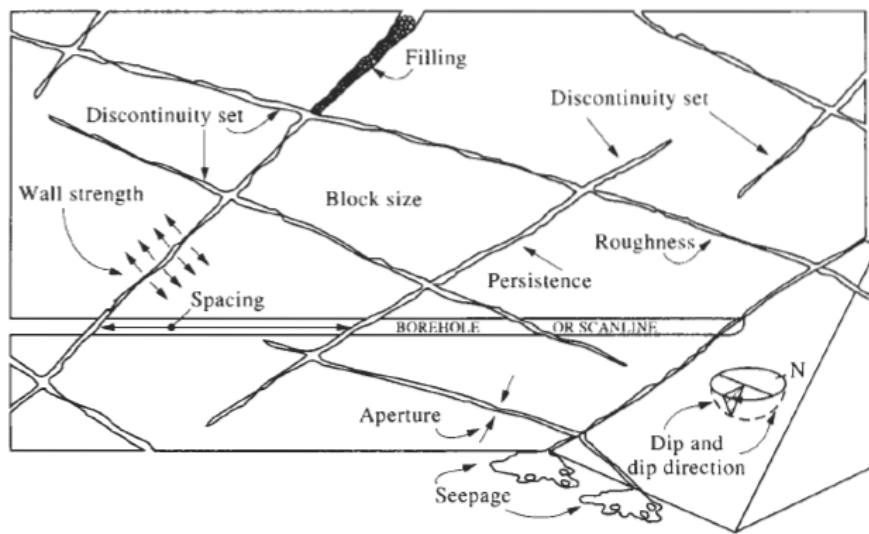


Figure 3. 2 - Geometric properties of discontinuities (Hudson & Harrison, 1997).

3.1.2. Weathering

Typically, rock is composed of natural mineral grains that are permanently bonded together. The weathering process weakens the bonding force and dismantles bigger mass to smaller pieces. Generally, there are two types of weathering mechanisms:

- **Mechanical weathering** – It occurs when the external forces, such as temperature and freezing water in fissures, physically dismantle the material. The erosion due to rain and wind play important part in mechanical weathering processes. The roots of the plants can also influence the physical disintegration of the rock.
- **Chemical weathering** – It is also called decomposition, it describes the process when the hard rock is transformed into soft by chemical reactions, such as: oxidation, leaching, desilication, carbonation and hydration.

Weathering profile changes along the depth. The closer the material is to the surface, more weathered it is (Figure 3. 3).

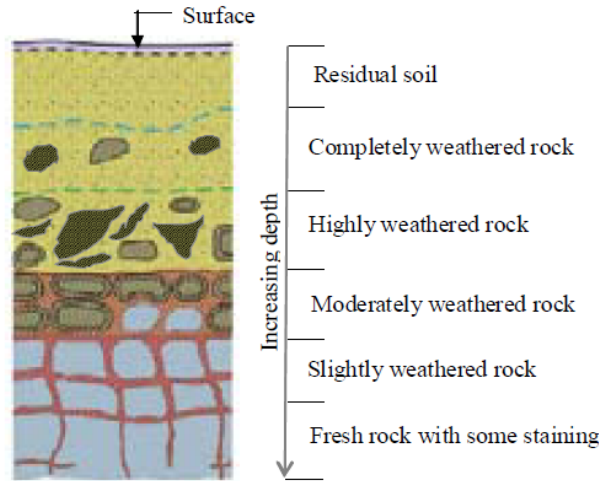


Figure 3.3 - Weathering profile changes due to depth (Panthi, 2006)

The weathering process diminishes rock mass qualities such as strength, deformation, slaking durability, and frictional resistance (Panthi, 2006). It also increases permeability of the rock mass. The weathering influence on different rocks and their properties is demonstrated in Figure 3.4

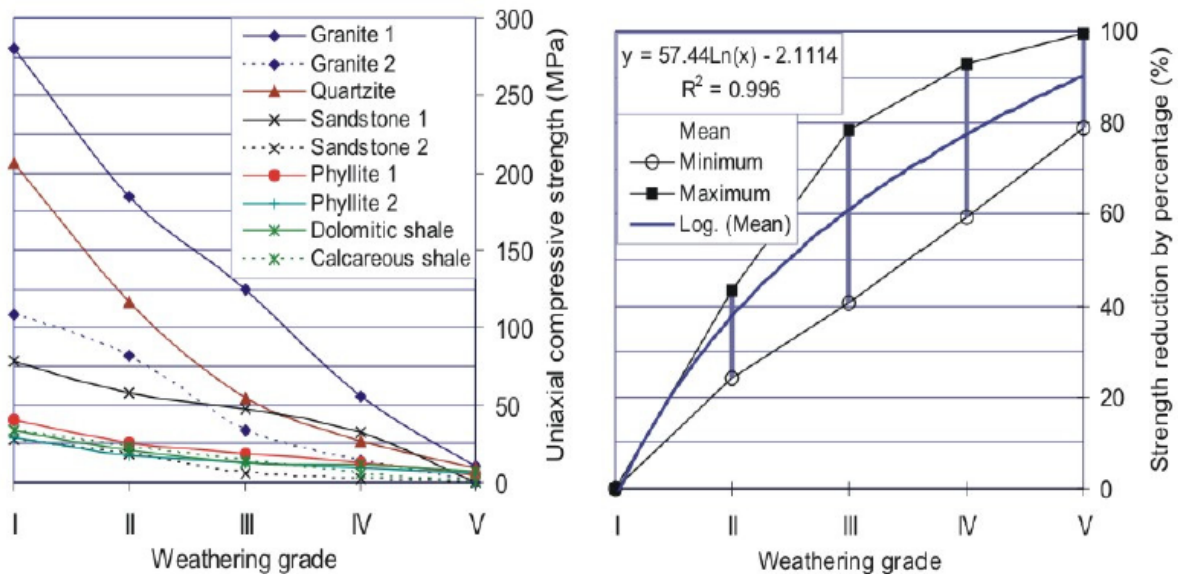


Figure 3.4 - Compressive strength of rock (left) and strength reduction in percentage (right) as function of weathering grade (based on data in Beavis et al, 1982; Beavis, 1985 and Gupta and Rao, 2000) (Panthi, 2006)

3.1.3. Rock mass classification systems

A rock mass classification systems are collection of empirical tools to describe quantitatively the geological characteristics of rock masses and to compute rock support requirements during the preconstruction phase of a project. The system is essential for estimating the rock behavior

and creating countermeasures to ensure safe and economical tunnel construction. Rock mass classification is also crucial during construction phase because it is used for monitoring, recording, and comparing the predicted and actual conditions of rock mass.

There are many different rock mass classification systems based on their form, type and main application. In Table 3. 2 the most widely used are shown.

Table 3. 2 - Rock mass classification systems (modified from (Aksoy, 2008))

N	Classification system	Form and type	Main applications	Reference
1	Terzaghi rock load classification system	Descriptive and behavioristic form Functional type	Design of steel support in tunnels	Terzaghi, 1946
2	Geological strength index (GSI)	Numerical form Functional type	Design of support in underground excavation	Hoek, 1994
3	Rock mass rating (RMR)	Numerical form Functional type	Design of tunnels, mines, and foundations	Bieniawski, 1973
4	Q-System	Numerical form Functional type	Design of support in Underground excavation	Barton et al., 1974

It is important to point out that while selecting rock support, rock mass classification system should be used with a grain of salt. The engineers shouldn't be fully dependent on it, because as shown in Figure 3. 5 the results aren't always accurate and, in many cases, it is very different from real world situation.

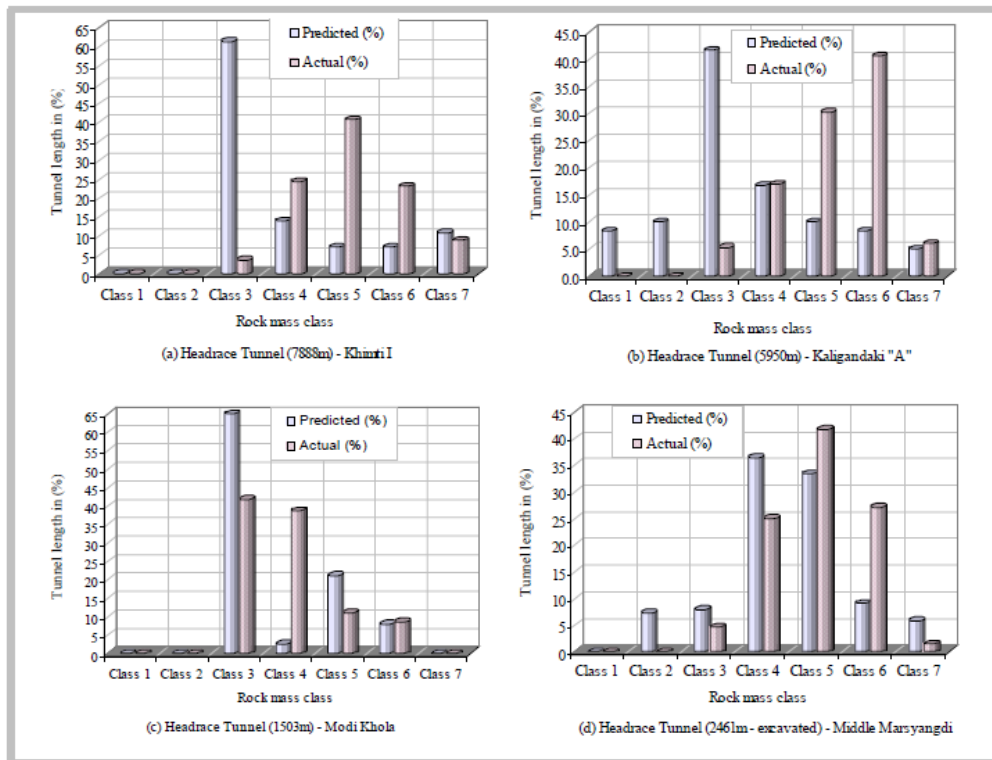


Figure 3. 5 - Predicted and actual rock mass conditions of the four tunnel cases located in different geological conditions in Nepal (Panthi & Nilsen, 2005).

For example, from Figure 3. 5 in Khimtri I case, 60% of the tunnel length predicted was to be Class 3 (Fair to good), but after excavation, it was much smaller in percentage. Inaccurate planning can significantly increase the tunnel cost and the time of construction, because for example if the rock mass is Class 2 and the prediction is Class 5, the excessive amount of support will be installed, which is not necessary. As shown in Figure 3. 6, the information about rock quality and the level of uncertainty is derived from project stages and it is time-dependent knowledge.

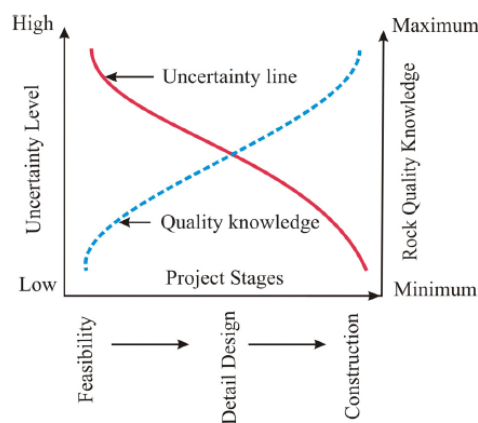


Figure 3. 6 - Schematic illustration of uncertainty level and rock quality knowledge at different (Panthi, 2006)

In modern days two the most widely used rock mass classification systems are Q-System and Rock mass rating (RMR) classification system. In the best practice, upper mentioned two systems are used in combination with each other.

3.1.3.1. Q-System

It was first proposed by Barton (1974). It is an empirical analysis of 200 tunnel construction projects in Scandinavia led to the development of this study. It’s the most popular classification system used in modern days. Q-system is mainly used in hard rock conditions, and it is less valid for soft grounds. The main usage of Q-system is to predict rock mass characteristics and to design the tunnel support system.

$$Q = \frac{RQD}{J_n} * \frac{J_r}{J_a} * \frac{J_w}{SRF} \qquad 3-1$$

Where:

RQD – Rock quality designation

J_n – Joint set number

J_r – Joint roughness number

J_a – Joint alteration number

J_w – Joint water reduction factor

SRF – Stress reduction factor

Table 3.4 – Ranges of Q-system parameters and its description (modified from (Kolymbas, 2008)).

Quality	Range
Q	0.001 (exceptionally poor) - 1,000 (exceptionally good quality rock)
RQD	0 - 100 %. Values lower than 10 % should not be used
J_n	0.5 (massive rock with no or few joints) - 20 (crushed, earth like rock)
J_r	0.5 (slickenside planar joints) - 4 (discontinuous joints)
J_a	0.75 (unaltered joint walls) - 20 (thick zones of swelling clay)
J_w	1.0 (dry excavation) - 0.05 (exceptionally high inflow)
SRF	1.0 (medium rock pressure) - 20 (heavy rock pressure)

To predict the stability of the tunnel and to calculate the required support, so called “Equivalent Dimension” D_e was introduced by Barton (1974):

$$D_e = \frac{\text{Excavation span (m)}}{\text{Excavation support ratio (ESR)}} \quad 3-2$$

ESR represents the support value for different purpose of excavation and its safety factor. In Table 3. 3 some values are shown, the left side of the table represents the old values of ESR (recommended in year 1993) and to the right the most recent values are given (updated in 2014).

Table 3. 3 - Updated values of ESR values (Barton, 2015)

Type of Excavation		ESR	ESR recommended
A	Temporary mine openings, etc.	ca. 2-5	ca. 2-5 (unchanged)
B	Permanent mine openings, water tunnels for hydropower (exclude high pressure penstocks), pilot tunnels, drifts and headings for large openings, surge chambers	1.6-2.0	1.6-2.0 (unchanged)
C	Storage caverns, water treatment plants, minor road and railway tunnels, access tunnels	1.2-1.3	0.9-1.1 Storage caverns 1.2-1.3 (unchanged)
D	Power stations, major road and railway runnels, civil defence chambers, portals, intersections	0.9-1.1	Major road and rail tunnels 0.5-0.8
E	Underground nuclear power stations, railway stations, sports and public facilities, factories, major gas pipeline tunnels	0.5-0.8	0.5-0.8 (unchanged)

Q-System has involved during past years and the latest version is published by Grimstad (2007) as shown in Figure 3. 7. With the help of Q-system graph, engineers can easily predict the support system needed based on various rock classes.

In 2006 Palmstrom and Broch have investigated Q-System and came into conclusion that it is the most effective in the certain range, which is shown by grey box in Figure 3. 8.

As shown in Table 3. 4 squeezing phenomena can also be estimated using Q-system.

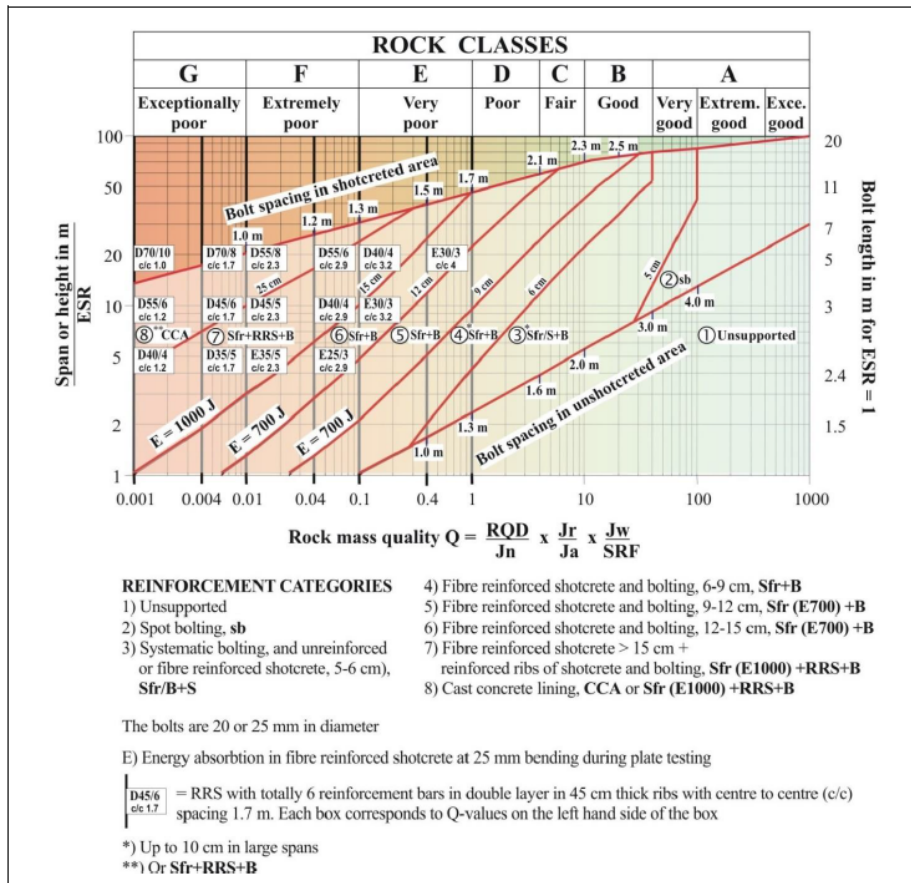


Figure 3. 7 - Latest version of Q-System published by Grimstad (2007) (Barton, 2015)

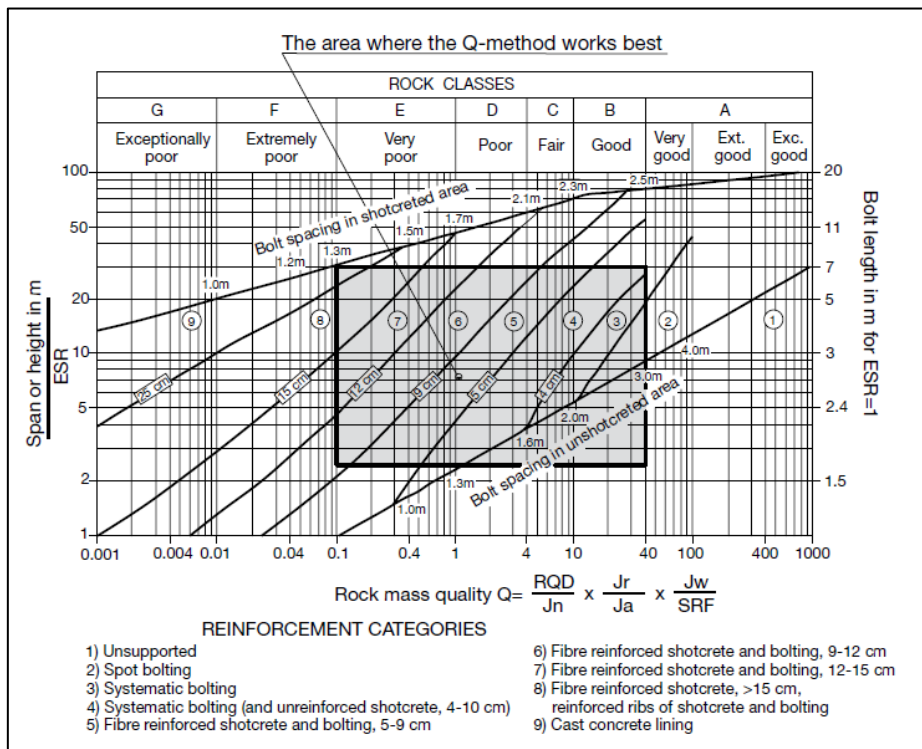


Figure 3. 8 - The most effective area in Q-system according to Palmstrom and Broch (Chapman et al., 2018)

Table 3. 4 - Estimating squeezing using Q-system (Barton, 2002)

Squeezing rock: plastic flow of incompetent rock under the influence of high rock pressure	$\sigma_{\theta max}/\sigma_{cm}$	SRF
Mild squeezing rock pressure	1-5	5-10
Heavy squeezing rock pressure	>5	10-20

Where:

$\sigma_{\theta max}$ – Maximum tangential stress

σ_{cm} – Rock mass strength

SRF – Stress reduction factor

3.1.3.2. Rock Mass Rating (RMR)

The Rock Mass Rating (RMR) classification system (also known as Geomechanics Classification) was introduced by Bieniawski in 1989. To describe rock mass using RMR classification method, following six parameters are used:

- Uniaxial compressive strength of the rock
- Rock quality designation (RQD)
- Spacing of discontinuities
- Condition of discontinuities
- Ground water conditions and
- Orientation of discontinuities

To quantify the upper given parameters, the field and lab investigations are required. The RMR final number is sum of each parameter rating values (Appendix A). Similar to Q-System, RMR is used for temporary and permanent support design. RMR is also capable of giving the relation between stand-up time and roof span after excavation (Figure 3. 9).

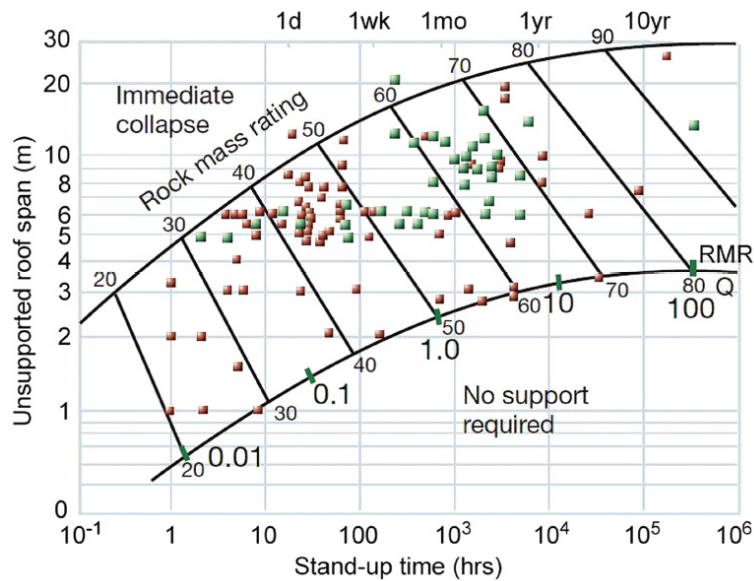


Figure 3. 9 - Graph for estimating the stand-up time of tunnels (Celada & Bieniawski, 2020)

3.1.3.3. Geological Strength Index (GSI)

GSI is arguably the classification system. It was introduced by Hoek and Brown (1997) to be used in failure criteria calculations, which will be discussed in following chapter. Determination of GSI value is based on visual inspection of geological conditions. The table is given in appendix B. It is possible, for people with different experience to estimate different GSI values from the chart due to the lack of measurable parameters for describing the rock mass structures and the discontinuity surface conditions. For structural description, GSI uses five main qualitative classifications:

- Intact/Massive
- Blocky
- Very blocky
- Blocky/Disturbed
- Disintegrated

Discontinuities are classified with five different surface conditions:

- Very good
- Good
- Fair
- Poor
- Very poor

GSI value can also be empirically estimated given RMR value using following equation (Hoek & Brown, 1997):

$$GSI = RMR - 5 \qquad 3-3$$

3.1.4. Rock mass quality

Rock mass quality is related to rock mass strength, deformability properties, strength anisotropy, presence of discontinuities and weathering effect over the geological history (Panthi & Broch, 2022). To define failure modes and to assess the stability of an underground cavern or tunnel, strength and deformability properties of the intact rock and rock mass are crucial. Weathering and anisotropy effect has big impact on overall strength of the rock mass. Meaning, it is important to know the weathering and schistosity condition of the in-situ rock mass where the intact rock specimen is taken. In Figure 3. 4 the weathering effect on rock strength is shown, while in Figure 3. 10 the effect of Schistosity or anisotropy at different degrees on rock strength is demonstrated.

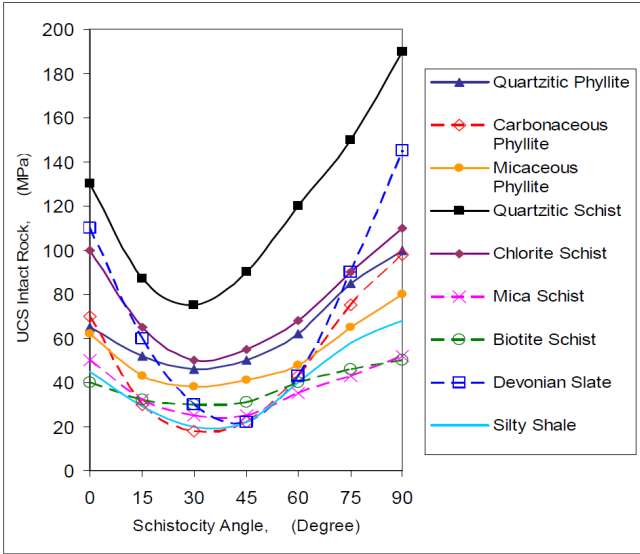


Figure 3. 10 - Variation of intact rock strength at varying schistosity angle (Panthi, 2006)

It is possible to estimate the rock strength and deformability properties with field investigation (Appendix D), but the most common way is to use intact rock specimen taken from in-situ and analyze it in the lab using uniaxial compressive strength test (UTS).

Intact rock is the part of rock mass. It is characterized to be homogeneous and with few or no discontinuities. According to Hoek and Brown (1980) the homogeneity of the material directly depends on its size (size effect), the smaller it is the more homogeneous it becomes (Figure 3. 11).

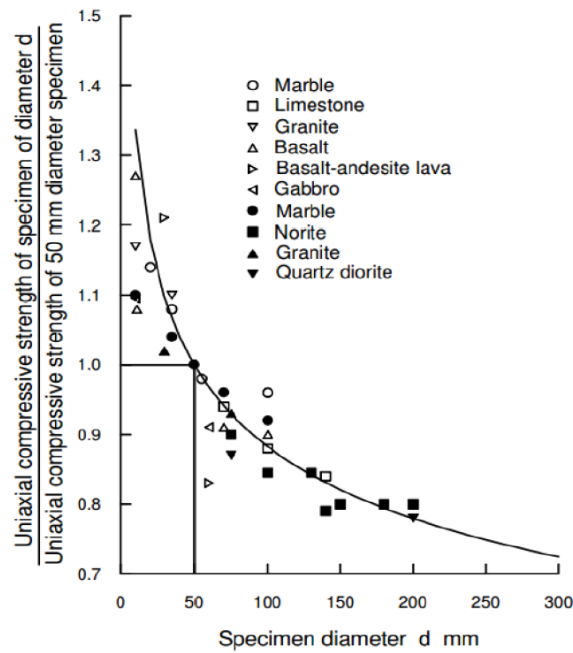


Figure 3. 11 - Influence of specimen size on the strength of intact rock. After Hoek and Brown (1980a) (Hoek, 2007)

That is why the intact rock is much stronger, with higher young's modulus than in situ rock mass and it becomes very challenging task to translate the lab test results from intact rock to rock mass. There are numerical and empirical ways to achieve it. Numerically Rocscience RS2 software could be used, while empirical equations are given in Table 3. 5 from various researchers.

Table 3. 5 - Empirical equations for rock mass strength calculation from different researchers

Author	Rock mass strength
Bieniawski (1989)	$\sigma_{cm} = \sigma_c * e^{\left(\frac{RMR-100}{18.75}\right)}$
Barton (2002)	$\sigma_{cm} = 5\gamma \left(\frac{\sigma_{ci}}{100} * Q\right)^{\frac{1}{3}}$
Hoek et al (2002)	$\sigma_{cm} = \sigma_{ci} \left[\exp\left(\frac{GSI - 100}{9}\right) \right]^a$
Panthi (2006)	$\sigma_{cm} = \frac{\sigma_{ci}^{1.5}}{60}$
Panthi (2018)	$\sigma_{cm} = \frac{\sigma_{ci}^{1.6}}{60}$

Where:

σ_{cm} – Unconfined compressive strength of rock mass

σ_{ci} – Laboratory test result of UTS

RMR - rock mass rating

a – Material constant related to Hoek and Brown failure criteria

Q – Rock mass quality rating

γ - Rock density in t/m³

In Table 3. 5 Panthi (2006) equation is used in case of foliated and schistose rock mass, while Panthi (2018) is used for brittle and homogeneous rock mass.

The deformability property of the rock mass explains its mechanical behavior. Laboratory test results are affected strongly by the size effect due to this parameter's sensitivity to ground discontinuities. There are different ways to perform in-situ deformability tests on rock mass. The most used are plate loading test (PLT), radial jacking test (RJT) and plate jacking test (PJT). All mentioned test methods are very time consuming and expensive. That is why various researchers have provided empirical equations (Table 3. 6) for calculation of modulus of deformation (E_m).

Table 3. 6 - Empirical equations for modulus of deformation from different researchers

Author	Modulus of deformation
Bieniawski (1989)	$E_m = 2 * RMR - 100$
Serafim and Pereira (1983)	$E_m = 10 \frac{(RMR - 10)}{40}$
Palmstrom (1995)	$E_m = 5.6 * RMI^{0.375}$
Hoek and Brown (1997)	$E_m = \sqrt{\frac{\sigma_{ci}}{100}} * 10^{\frac{GSI-10}{40}}$
Barton (2002)	$E_m = 10 * Q_c^{\frac{1}{3}} = 10 * \left(\frac{Q * \sigma_{ci}}{100}\right)^{1/3}$
Hoek and Diederichs (2006)	$E_m = E_{ci} * \left[0.02 + \frac{1 - \frac{D}{2}}{1 + e^{\left(\frac{60+15*D-GSI}{11}\right)}} \right]$
Panthi (2006)	$E_m = E_{ci} * \left(\frac{\sigma_{cm}}{\sigma_{ci}}\right)$

Where:

E_m - Modulus of deformation

E_{ci} - Modulus of deformation of the intact rock, obtained in the laboratory

RMR - Bieniawaski (1989) rock mass rating

RMi – Palmstrom’s rock mass index

Q_c - Normalized rock mass quality rating

Q – Rock mass quality rating

When there is no laboratory data available for modulus of deformation of intact rock, it is possible to use modulus ratio (MR) proposed by Deere (1968) (Cai et al., 2007) to approximate the modulus of deformation of intact rock (E_{ci}).

$$E_{ci} = MR * \sigma_{ci} \quad 3-4$$

3.2. Rock stresses

It is important to determine rock stresses in rock mass. In addition to providing the input parameters for preliminary analysis and modelling of a tunnel, this will assist in determining which tunneling method would be appropriate, whether ground improvement methods would be necessary and allow for an appropriate selection of tunnelling technique. In-situ vertical and horizontal stresses (Panthi, 2012) could be estimated using following equations:

$$\sigma_v = \gamma H \quad 3-5$$

$$\sigma_h = k_0 \sigma_v + \sigma_{tec} \quad 3-6$$

Where:

σ_h – Horizontal stress [MPa]

σ_v – Vertical stress [MPa]

γ – Unit weight of overburden rock mass

H – The distance between surface and the opening in rock mass [m]

k_0 – Coefficient of earth lateral pressure

σ_{tec} – Horizontal tectonic stress [MPa]

As shown in Figure 3. 12 vertical stress is caused mainly due to gravity and changes over depth, higher the depth, higher the value. Horizontal stress calculation is more complicated. As shown in Figure 3. 13, like vertical stress, it also depends on the depth, gravity and location around globe. Several effects influence the horizontal stress: tectonic, topographical, erosion and lithostatic pressure. Coefficient of earth lateral pressure (k_0) can be calculated using Possion's ratio:

$$k_0 = \frac{\mu}{1 - \mu} \tag{3-7}$$

Where:

μ - Possion's ratio ($0 \leq \mu \leq 0.5$)

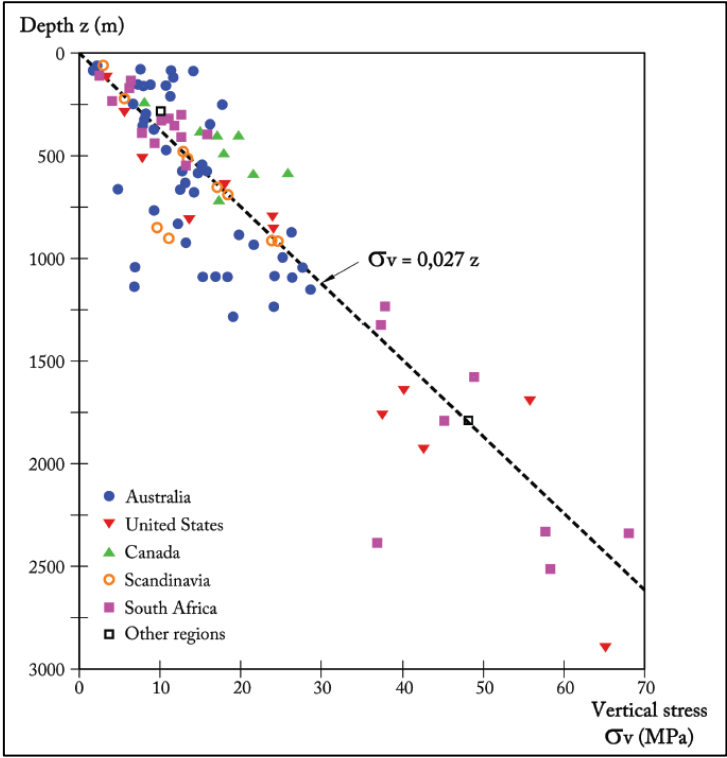


Figure 3. 12 - Vertical in situ stress variation with depth (Hoek and Brown, 1980.) (Celada & Bieniawski, 2020)

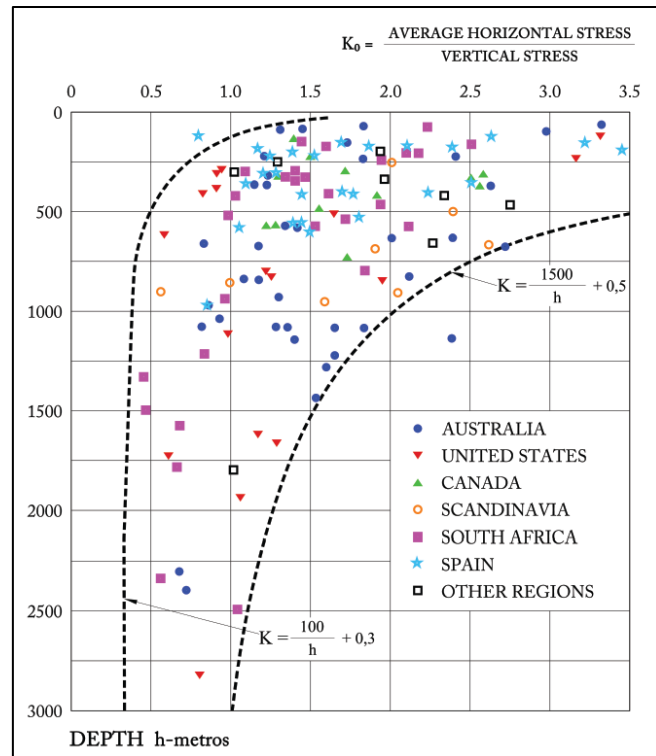


Figure 3. 13 - Changes of K_0 with depth (Hoek and Brown, 1980) (Celada & Bieniawski, 2020).

After tunnel excavation, the virgin (original in-situ) stresses will be disturbed. The natural in-situ stress will be forced to follow the contour of the tunnel, as a result tangential stresses will be developed around the opening area. In case of elastic rock material and isostatic stress condition ($\sigma_v = \sigma_h = \sigma$), the stress will be redistributed around the opening of a circular tunnel as shown in Figure 3. 14.

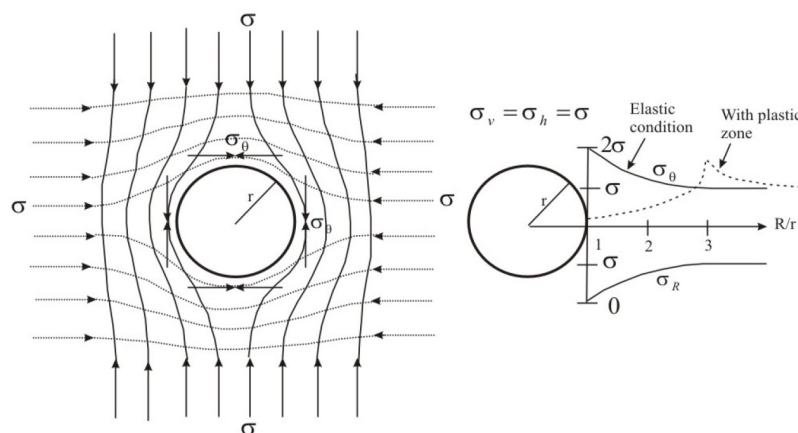


Figure 3. 14 - Stress trajectories in rock mass surrounding a circular opening (left) and tangential and radial stress distribution in elastic and non-elastic conditions (right) (based on Hoek and Brown, 1980; Nilsen and Thidemann, 1993 and Bray, 1967) (Panthi, 2006)

According to Figure 3. 14 (right), maximum tangential stress will be near the wall of the opening and equal to 2σ , radial stress (σ_R) will be zero and tangential stress will be normalized at about $3R$ distance from the center of opening. The equations for tangential stress (σ_θ) and radial stress (σ_R) calculations are given below:

$$\sigma_\theta = \sigma * \left(1 + \frac{r^2}{R^2}\right) \quad 3-8$$

$$\sigma_R = \sigma * \left(1 - \frac{r^2}{R^2}\right) \quad 3-9$$

Where:

σ_θ – Tangential stress

σ_R – Radial stress

r – Radius of the circle

R – Distance from the center of the circle

In most cases where there is anisotropic condition in the rock mass, meaning tangential stress vary around the periphery of an opening. In this case maximum tangential stress and minimum tangential stress can be calculated using Kirsch's equations:

$$\sigma_{\theta \text{ (max)}} = 3\sigma_1 - \sigma_3 \quad 3-10$$

$$\sigma_{\theta \text{ (min)}} = 3\sigma_3 - \sigma_1 \quad 3-11$$

Where:

$\sigma_{\theta \text{ (max)}}$ – Maximum tangential stress

$\sigma_{\theta \text{ (min)}}$ – Minimum tangential stress

σ_1 – Major principal stress

σ_3 – Minor principal stress

In case if minor principal stress (σ_3) is too low, the minimum tangential stress may end up being negative, which will cause tensile cracks in the tunnel. It is major problem for hydropower water convey tunnels, because the water will leak through the cracks causing reduction of discharge and overall power generation.

The validity of Kirsch solution is limited for a homogeneous, isotropic, and elastic rock mass with widely spaced and tight joints (Panthi, 2006). In case of weak rocks, as seen in Figure 3. 14 (right, dotted line), there is a plastic zone, caused by reduction of rock mass strength due to tangential stress.

3.3. Stability assessment methods

A tunnel's or cavern's stability is directly influenced by three engineering geological factors: rock mechanical properties, in situ stress conditions and groundwater inflow through fractures and fault zones (Panthi, 2012). For the tunnel with high overburden there is a possibility of instability caused by induced rock stresses. In relatively unjointed and massive rock mass, if the rock mass strength is less than the induced stresses, rock spalling or rock bursting may become the primary cause of instability. Whereas, if the rock mass is weak, deformed and schistose, the squeezing maybe the result of instability.

3.3.1. Failure criteria

Engineers use failure criteria to predict when and where the failure occurs. For many years different rock mass failure criterions were developed. In modern days, two most used ones are Mohr-coulomb and Generalized Hoek-Brown.

3.3.1.1. Mohr-coulomb failure criterion

Mohr-coulomb failure criterion structure contains a linear envelope touching all the Mohr's circle points, which represent the combinations of principal stresses (Figure 3. 15). It is mainly used in rock mass with elastic, isotropic and unjointed characteristics.

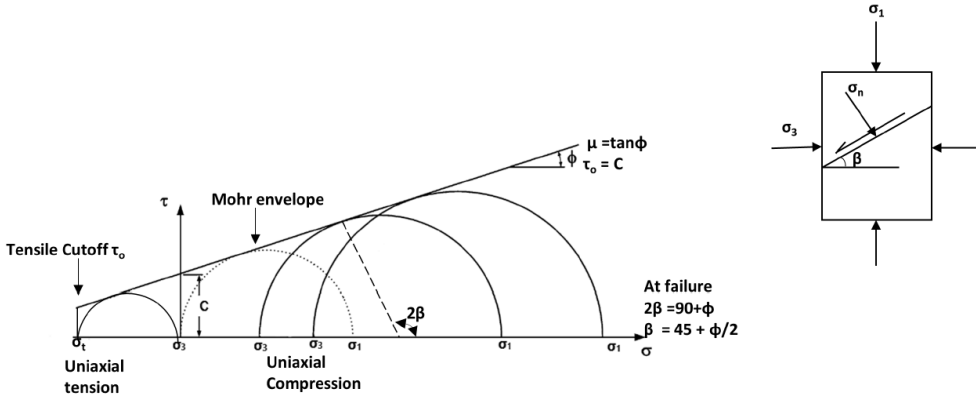


Figure 3. 15 - Mohr-Coulomb Failure Criteria (Hudson & Harrison, 2000)

Mohr-Coulomb failure criteria for the rock mass strength is defined by cohesive strength c' and the angle of friction φ (Hoek & Brown, 1997). The failure criteria is calculated with following equation:

$$\tau_p = c + \sigma_n \tan \varphi \quad 3-12$$

Where:

τ_p – Shear stress

c – Cohesion

σ_n – Normal stress

Shear stress is maximum in a plane inclined at 45° degrees to the horizontal and can be defined by equation 3-13.

$$\tau_{max} = \frac{\sigma_1 - \sigma_3}{1} \quad 3-13$$

3.3.1.2. Generalized Hoek-Brown failure criterion

The Hoek-Brown (HB) failure criterion is an empirical relation that characterizes the stress conditions that lead to failure in intact rocks and rock masses (Zuo & Shen, 2020). It is the most widely used failure criterion up to date.

To estimate the strength of rock mass, the generalized Hoek-Brown criterion is expressed as follows:

$$\sigma_1 = \sigma_3 + \sigma_{ci} * \left(m_b * \frac{\sigma_3}{\sigma_{ci}} + s \right)^a \quad 3-14$$

Where:

σ_1 – Major principal stress

σ_3 – Minor principal stress

σ_{ci} - Uniaxial compressive strength of intact rock

m_b, s, a – Rock property parameters, derived from the following equations:

$$m_b = m_i * \exp\left(\frac{GSI - 100}{28 - 14 * D}\right) \quad 3-15$$

$$s = \exp\left(\frac{GSI - 100}{9 - 3 * D}\right) \quad 3-16$$

$$a = \frac{1}{2} + \frac{1}{6} * \left(e^{-\frac{GSI}{15}} - e^{-\frac{20}{3}}\right) \quad 3-17$$

Where:

GSI – Geological Strength Index

D – Disturbance factor (found in Appendix C)

m_i - curve fitting parameter (Found in Appendix F)

Depending on rock mass homogeneity and jointing system, the Hoek-Brown or Mohr-Coulomb criteria is used. For example, in case if instability is controlled by single joint, the Mohr-Coulomb should be used, because failure will be related to normal stress and shear strength of the joint. In case of rock mass with many joints, then the Hoek-Brown is used. It is illustrated in Figure 3. 16

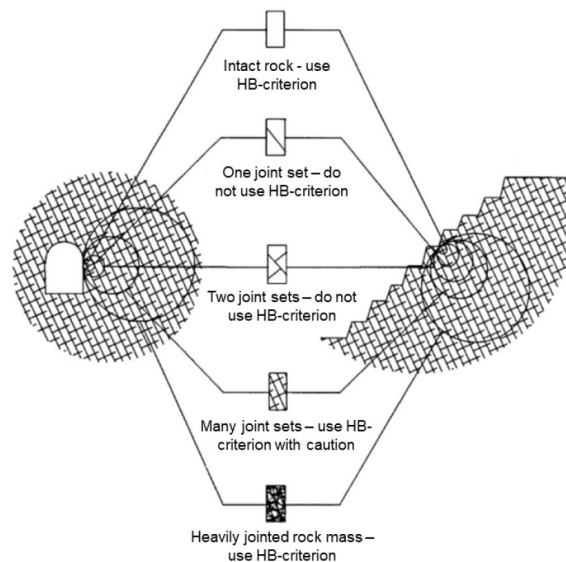


Figure 3. 16 - Mohr-Coulomb and Hoek-Brow criterion usage (Hoek, 2007)

3.3.2. Rock burst

Construction of tunnels is best done in environments with extremely hard and massive rock masses. However, problems can arise at deeper depths because the rock mass may be under a

great deal of pressure. Generally, rock bursts and spalling occur at depths of more than 1000 meters in rock masses with high strength (greater than 100 MPa) (Gratchev, 2020). In tunnels where rock is in a state of intense elastic deformation, rock popping commonly occurs from the side or the roof. There can also be spalling problem. Spalls are thin slabs of rock that result from extensional fracturing of rock, it is the result of detaching the slabs from the rock mass. If the rock mass strength is lower than the maximum tangential stress, than the rock burst/spalling may occur:

$$\sigma_{cm} < \sigma_{\theta max} \tag{3-18}$$

Where:

- σ_{cm} – Rock mass strength
- $\sigma_{\theta max}$ – Maximum tangential stress

3.3.3. Squeezing

The problem of squeezing is also associated with disintegrated rock mass. It occurs when tunneling through relatively weak rock masses. This results in radial convergence (deformation) of the rock mass around the tunnel due to the plastic zone formed around the tunnel cross section by the weak rock.

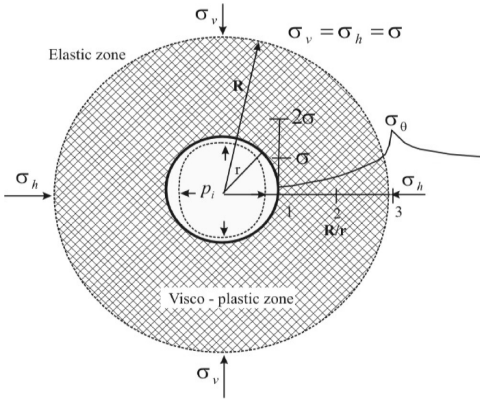


Figure 3. 17 - formation of visco-plastic zone and plastic deformation (squeezing) in a tunnel wall. In the figure, r is the tunnel radius, R is the radius of visco-plastic zone and pi is the support pressure. (Panthi & Broch, 2022)

The tunnel periphery deforms because of plastic deformation prior to and following excavation, the deformation continues even after rock support is applied. There are both time-independent (instantaneous) and time-dependent plastic deformations observed in underground excavations passing through schistose and weak rock mass. Therefore, for a tunnel to remain stable for a

long time, the support design should be considered for both time-dependent and independent deformations.

There are several methods to predict the squeezing phenomena in rock mass:

- Empirical methods
- Semi-analytical methods
- Analytical methods (convergence confinement method)

There are three the most used methods: Empirical method of Singh et al (1992), Goel et al (1995) and semi-analytical method of Hoek and Marinos (2000).

3.3.3.1. Singh et al (1992)

Singh et al (1992) purposed the empirical relation between (Q) value from rock mass classification system and the (H) overburden. As shown in Figure 3. 18, an indication of non-squeezing and squeezing phenomena has been divided by a demarcation line. The equation for the line is given below:

$$H = 350 * Q^{\frac{1}{3}} \quad 3-19$$

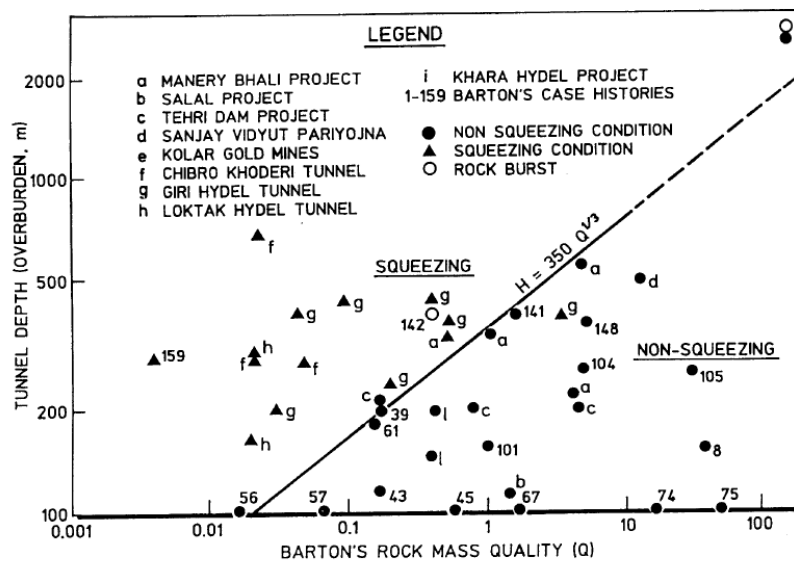


Figure 3. 18 - Singh et al. (1992) approach for predicting squeezing conditions (Barla, 2001)

If overburden depth exceeds the value of (H) given in equation 3-19 than there will be squeezing, otherwise there will be non-squeezing condition.

3.3.3.2. Hoek and Marinos (2000)

Hoek suggested that the ratio between uniaxial compressive strength of the rock mass (σ_{cm}) to in-situ stress (P_o) can predict the rock squeezing. Based on Monte Carlo simulations, the author determined tunnel strain under different tunnel conditions and identified clear patterns of tunnel convergence (Figure 3. 19), which can be predicted using following equation:

$$\varepsilon = 0.2 * \left(\frac{\sigma_{cm}}{P_o} \right)^{-2} \quad 3-20$$

Where:

ε – Strain in percentage

σ_{cm} – Rock mass strength

P_o – In situ stress

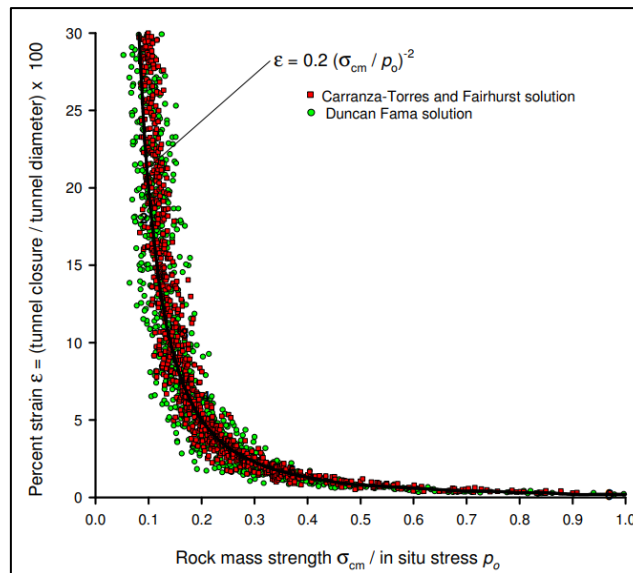


Figure 3. 19 - Tunnel convergence against the ratio of rock mass strength to in-situ stress (Hoek & Marinos, 2000)

After that, Hoek and Marinos extended their equation by including an internal pressure (P_i) in the tunnel to simulate the effects of the support. They purposed the following equations, defining the size of the plastic zone (R) and the total tunnel strain (ε_t):

$$R = r * \left(1.25 - 0.625 * \frac{P_i}{\sigma_v} \right) * \left(\frac{\sigma_{cm}}{\sigma_v} \right)^{\left(\frac{P_i}{\sigma_v} - 0.57 \right)} \quad 3-21$$

$$\varepsilon_t = \frac{\delta_t}{2r} * 100 = \left(0.2 - 0.25 * \frac{P_i}{\sigma_v} \right) * \left(\frac{\sigma_{cm}}{\sigma_v} \right)^{\left(2.4 * \frac{P_i}{\sigma_v} - 2 \right)} \quad 3-22$$

Where:

R – Plastic zone [m]

r – Radius [m]

ε_t – Total inward tunnel strain [%]

δ_t - Total inward tunnel deformation [m]

P_i – Support pressure [MPa]

In order to determine the degree of difficulty that can be encountered at different tunnel strain levels with an approximation, the equation 3-20 is used with Figure 3. 20 and Table 3. 7

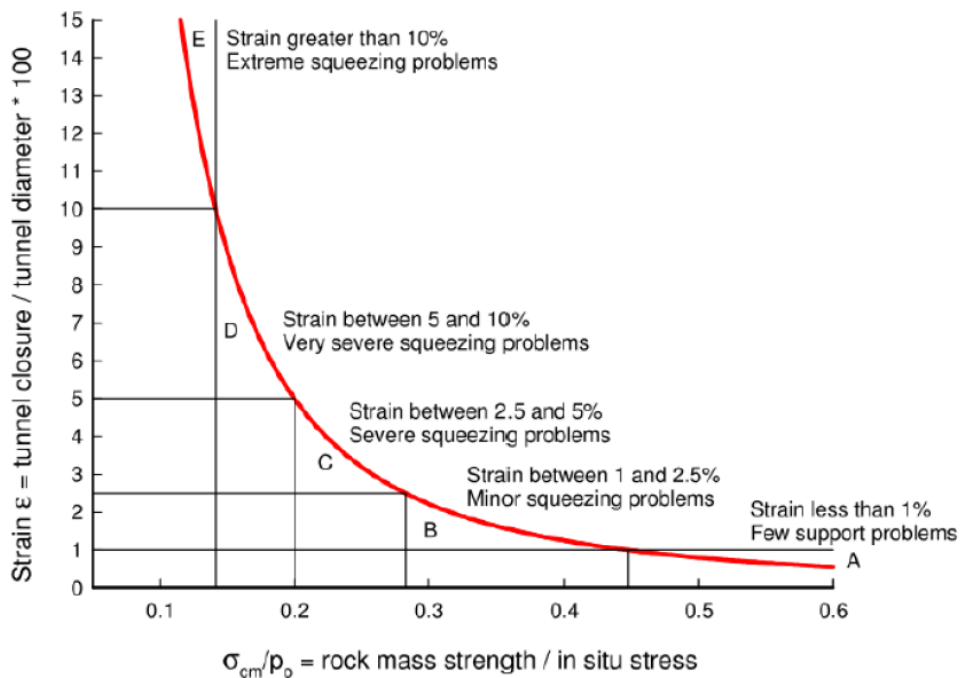


Figure 3. 20 - Relationship between strain and the degree of difficulty associated with tunneling through squeezing rock (Hoek & Marinos, 2000)

Table 3. 7 - Approximate relationship between strain and the degree of difficulty (Hoek & Marinos, 2000)

	Strain ϵ %	Geotechnical issues	Support types
A	Less than 1	Few stability problems and very simple tunnel support design methods can be used. Tunnel support recommendations based upon rock mass classifications provide an adequate basis for design.	Very simple tunnelling conditions, with rockbolts and shotcrete typically used for support.
B	1 to 2.5	Convergence confinement methods are used to predict the formation of a 'plastic' zone in the rock mass surrounding a tunnel and of the interaction between the progressive development of this zone and different types of support.	Minor squeezing problems which are generally dealt with by rockbolts and shotcrete; sometimes with light steel sets or lattice girders are added for additional security.
C	2.5 to 5	Two-dimensional finite element analysis, incorporating support elements and excavation sequence, are normally used for this type of problem. Face stability is generally not a major problem.	Severe squeezing problems requiring rapid installation of support and careful control of construction quality. Heavy steel sets embedded in shotcrete are generally required.
D	5 to 10	The design of the tunnel is dominated by face stability issues and, while two-dimensional finite analyses are generally carried out, some estimates of the effects of forepoling and face reinforcement are required.	Very severe squeezing and face stability problems. Forepoling and face reinforcement with steel sets embedded in shotcrete are usually necessary.
E	More than 10	Severe face instability as well as squeezing of the tunnel make this an extremely difficult three-dimensional problem for which no effective design methods are currently available. Most solutions are based on experience.	Extreme squeezing problems. Forepoling and face reinforcement are usually applied and yielding support may be required in extreme cases.

3.3.3.3. Panthi and Shrestha (2018)

After comprehensive assessment of deformation data taken from three tunnels excavated with drill and blast method, Panthi and Shrestha (2018) have purposed two equations. With equation 3-23 it is possible to estimate instantaneous deformation and with equation 3-24 the final deformation (tunnel strain) can be estimated in the tunnel. Panthi and Shrestha (2018) state that for squeezing analysis, rock mass shear modulus (G) is important parameter in case of thinly foliated/laminated, highly schistose and weak rock mass (Panthi & Broch, 2022).

$$\epsilon_{IC} = 3065 \left(\frac{\sigma_v * \frac{(1+k)}{2}}{2 * G * (1 + P_i)} \right)^{2.13} \quad 3-23$$

$$\epsilon_{FC} = 4509 \left(\frac{\sigma_v * \frac{(1+k)}{2}}{2 * G * (1 + P_i)} \right)^{2.09} \quad 3-24$$

Where:

ε_{IC} – Instantaneous deformation

ε_{FC} - Final deformation

G – Rock mass shear modulus

σ_v – Vertical stress

k – stress ratio

P_i – Support pressure

To calculate rock mass shear modulus (G) the equation proposed by Carranza-Torres and Fairhurst (2000) is used:

$$G = \frac{E_{cm}}{2 * (1 + \mu)} \quad 3-25$$

Where:

G - Rock mass shear modulus

E_{cm} – Rock mass deformation modulus

μ – Poisson's ratio

4. Case description

4.1. Akavreta HPP

Construction area of Akavreta HPP with installed capacity of 20 MW is in Adjara (Georgia) region in the valley of the river Adjaristskali, in the segments between village Namonastrevi and Silibauri, between elevation 465-900 masl. The project area belongs to Qeda municipality. The general layout is shown in Figure 4. 1

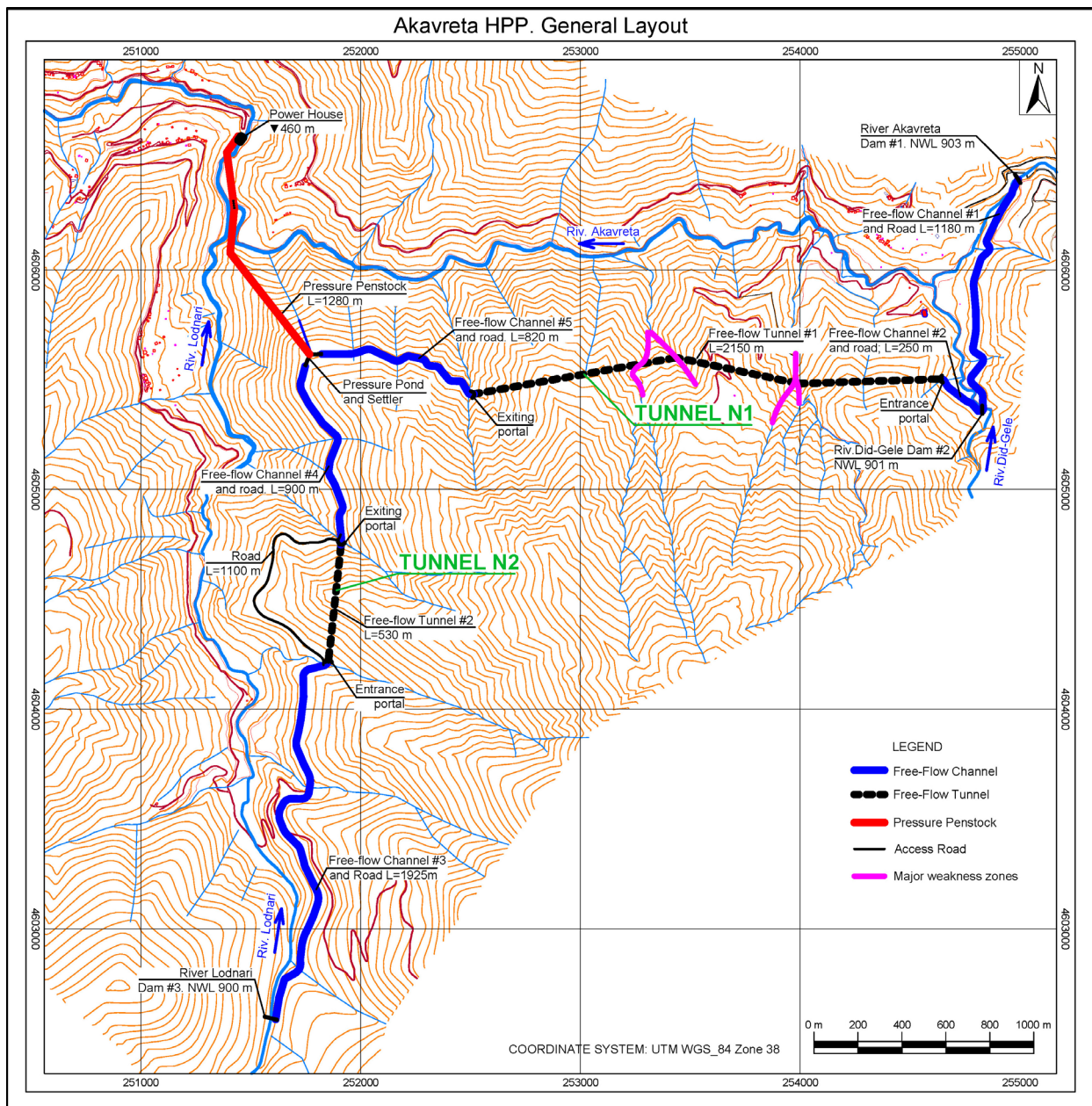


Figure 4. 1 – Akavreta HPP General Layout (modified from GHP’s map data)

4.1.1. River Akavreta catchment area

The river Akavreta flows in Keda region (Figure 4. 1). It is formed for the expense of fusion of two rivers, Tivnarisgele and Did-gele at the village Namonastrevi, at the mark 825 meter. River Akavreta is the most abundant and short among the rivers of the region. Its length is only 19 km, and it joins the river Adjaristskali near a settlement of Keda, at the mark 180 meters from the sea level. River Did-gele takes origin on the northern fold of Shavsheti mountain ridge, at 2400 meter above sea level, while the river Tivnarisgele takes origin on the north fold of the mountain Tsikovela, at 1800 meter above sea level (GHP, 2017).

Area of catchment basin equals to 134 km² with average elevation of 1280 m. River Akavreta is joined by many small and average size tributaries. The greatest among them is the river Lodnari.

4.1.2. Hydraulic structures

The Akavreta HPP hydraulic structures consists of three small dams, five different open flow channels, pressure pond, penstock and powerhouse (Figure 4. 1). Dam #1 is located at Akavreta river, it diverts water through open channel #1 (1180 m in length) to river Did-gele, where it meets the dam #2. Combined discharge enters open channel #2 (250 m in length), following the free-flow headrace tunnel N1 of 2150 m. Finally, the discharge from the headrace tunnel N1 enters 820 m open flow channel #5. From the left side of the map (Figure 4. 1) the dam # 3 is located on river Lodnari, it diverts the discharge to free-flow channel #3 (1925 m in length), after that the discharge enters free flow headrace tunnel N2 (530 m in length) and then goes through free flow channel #4 (900 m in length). The discharge from Lodnari, Akavreta and Did-gele rivers meet at pressure pond, where it is transferred with surface penstock (1280 m in length) to powerhouse. The powerhouse includes two vertical Pelton turbines, each with 10 MW capacity.

4.1.3. Precipitation

Annual and monthly mean precipitation at project territory was taken from nearby measuring stations (MS) located in towns Keda, Shuakhevi and Gundauri. Summary is given in in Table 4. 1 in [mm].

Table 4. 1 - Annual and monthly mean precipitation (modified from (GHP, 2017))

MS Name	I	II	III	IV	V	VI	VII	VIII	IX	X	XI	XII	Annual
Keda	186	166	132	76	74	83	94	98	161	217	202	163	1652
Shuakhevi	133	100	86	59	68	69	57	54	79	125	132	114	1076
Gundauri	174	131	112	78	89	90	75	70	103	165	172	148	1407

Snow can be characterized by its thickness, days of formation of snow cover, snow cover standing and melting time. For the project region the parameters for description are taken from Keda and Merisi (Gundauri) meteorological stations (MS), which are given in Table 4. 2 and Table 4. 3

Table 4. 2 – Average decade snow cover height [cm] (modified from (GHP, 2017))

MS Name	December	January			February			March		Summary		
	21-31	1-10	11-20	21-31	1-10	11-20	21-28	1-10	11-20	Ave.	max	min
Keda	9	14	17	25	29	25	21	13	11	55	29	9
Shuakhevi	6	9	10	27	32	26	21	17	11	52	32	6
Gundauri	10	15	16	34	43	40	32	22	19	68	43	10

Table 4. 3 - Number of days with snow cover [cm] (modified from (GHP, 2017))

MS Name	December	January			February			March	
	21-31	1-10	11-20	21-31	1-10	11-20	20-28	1-10	11-21
Keda	4	3	4	6	6	5	4	4	3
Gundauri	5	4	5	7	7	6	5	4	3

4.1.4. Hydrology

The hydrograph and duration curve were calculated based on discharge data provided by Georgian Hydro Power LLC, using 50 years of daily discharge observation data taken from Gundauri gauging station, with catchment area of $F=88.2 \text{ m}^2$. The hydrographs for different dams with 10%,50% and 90% provisions were plotted. The scaling method was used to scale discharge from known to unknown catchment area.

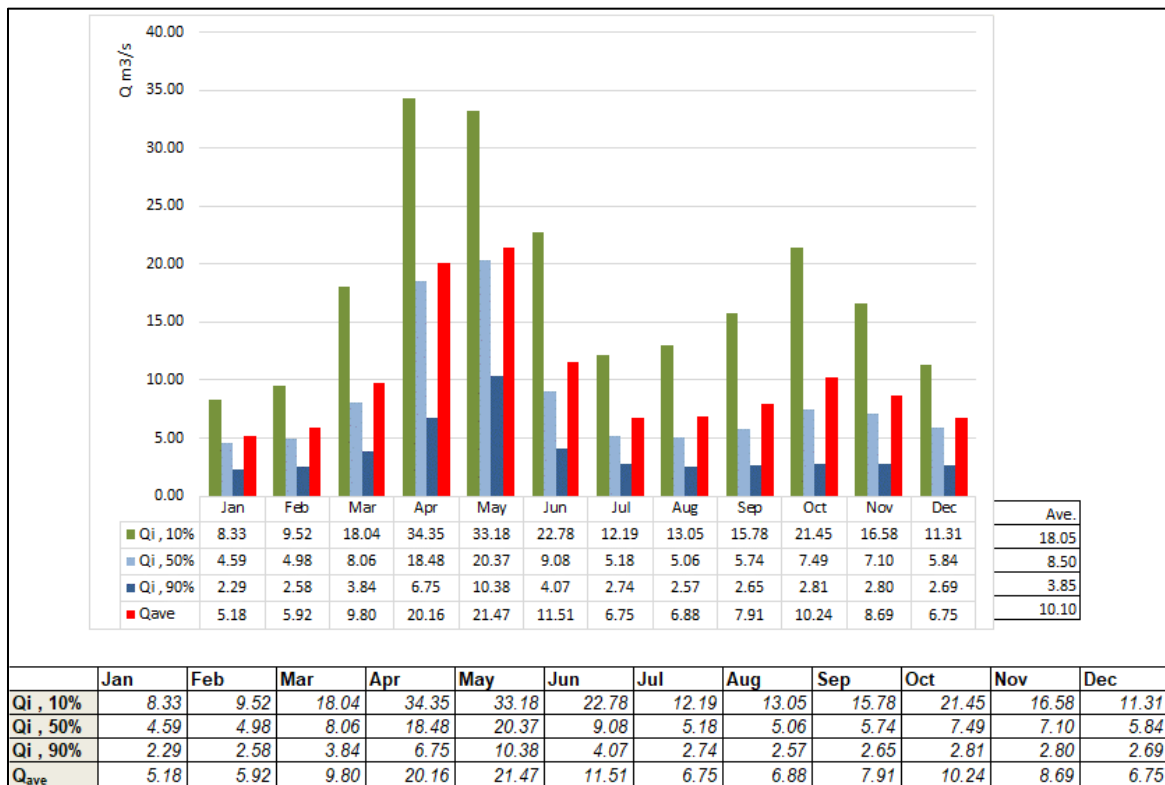


Figure 4. 2 – Hydrograph with discharge data at Gundauri gauging station ($F=88.2 \text{ m}^2$) with different provisions (based on 50 year daily discharge data from (GHP, 2017))

Three different calculations were performed. First (Figure 4. 2) for the gauging station Gundauri, second (Figure 4. 3) with combination of Akavreta dam #1 (F=11.4 m²) and dam #2 (F=22.1 m²) and the third (Figure 4. 5) calculation was made just for dam N3 (F=24 m²), which is located on Lodnari river. The dam locations and numbering can be found in Figure 4. 1

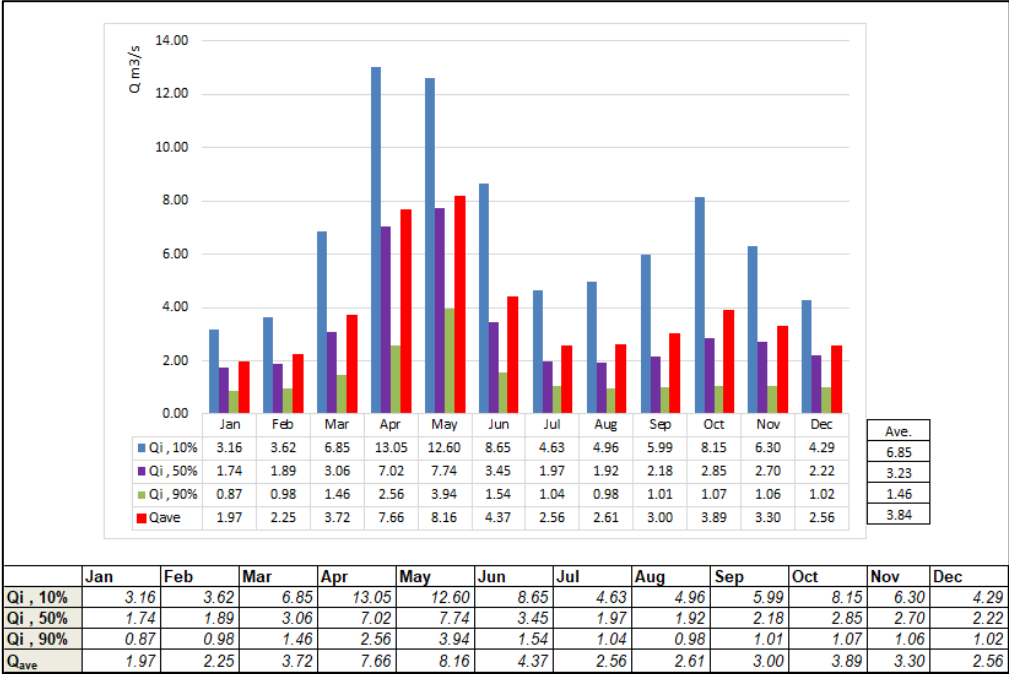


Figure 4. 3 – Hydrograph with discharge data at Akavreta dam #1 and #2 combination with different provisions (based on 50 year daily discharge data from (GHP, 2017))

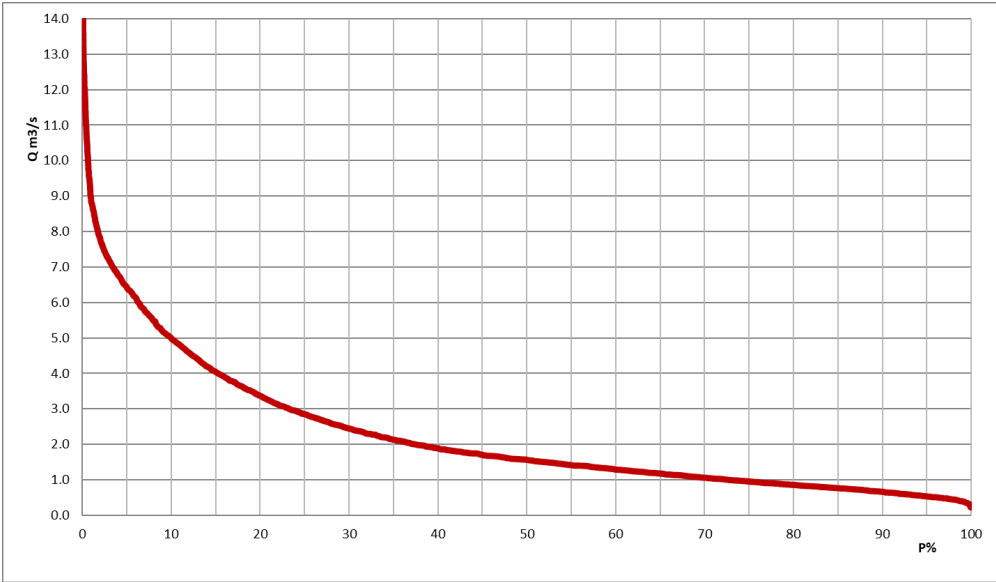


Figure 4. 4 - Duration curve of discharge at Akavreta dam #1 and dam #2 combination (based on 50 year daily discharge data from (GHP, 2017))

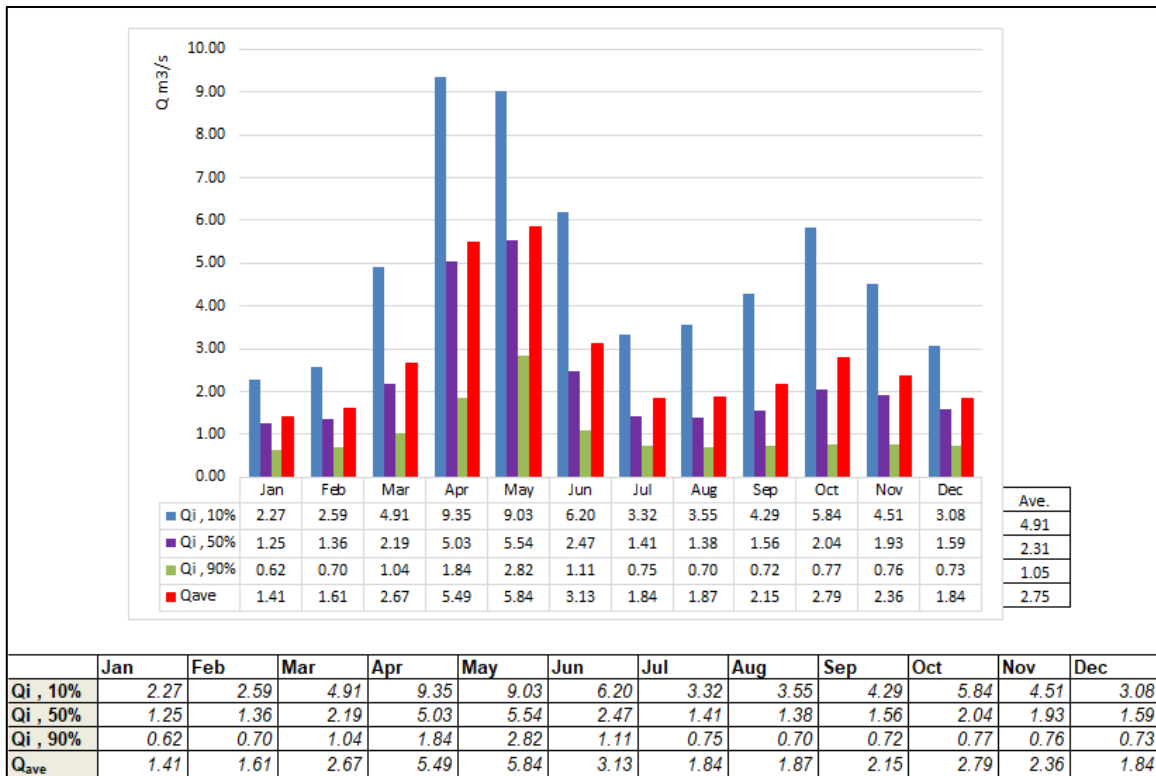


Figure 4. 5 – Hydrograph with discharge data at Lodnari river dam #3 with different provisions (based on 50 year daily discharge data from (GHP, 2017)

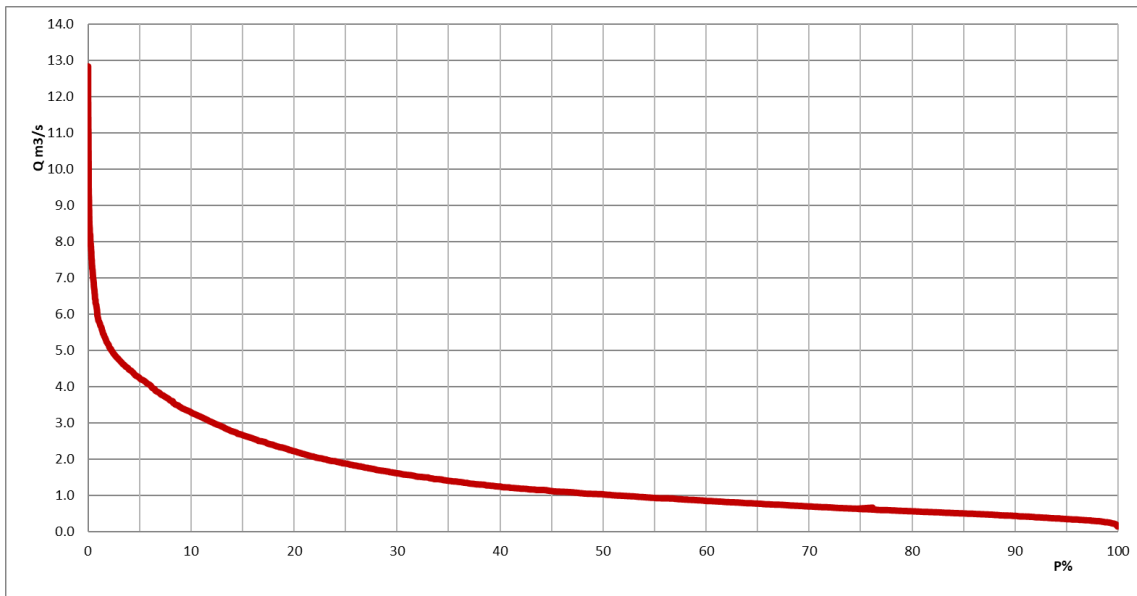


Figure 4. 6 - Duration curve of discharge for at Lodnari dam #3 (based on 50 year daily discharge data from (GHP, 2017)

4.1.5. Climate

Classification of Georgian climate according to districts and sub-districts is based on Koppen climate classification system, which is the most well-formulated and spread system among the classification systems based on mean values of climate elements. According to this classification there are 3 districts and 23 zones on the territory of Georgia. Catchment basin of the river Akavreta is in the 3rd, 4th and 5th zones of sea subtropical humid district (Figure 4. 7).

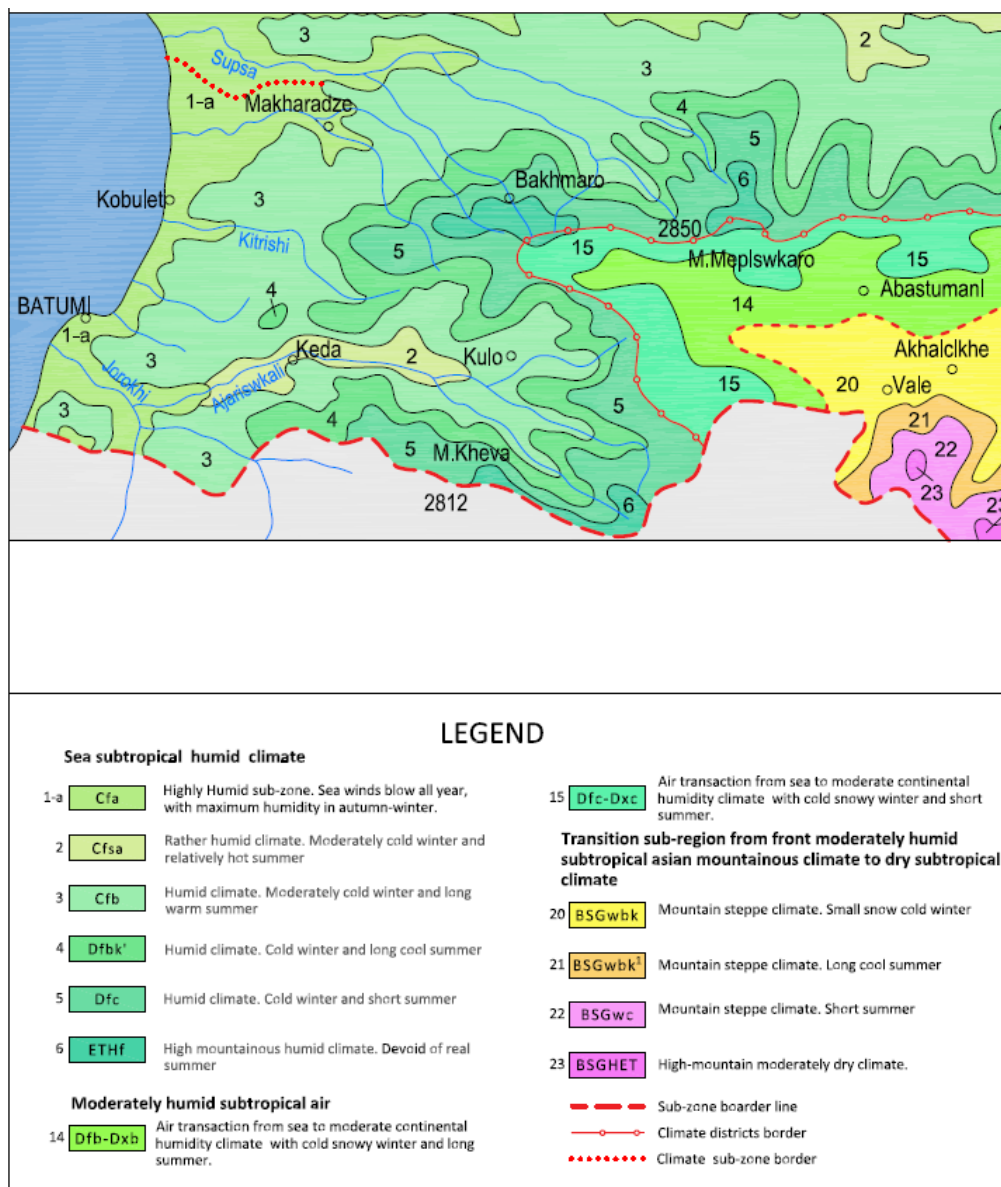


Figure 4. 7 - Adjara region climate data (GHP, 2017)

4.2. General geology of Georgia

Georgia belongs to the Caucasus segment of the Mediterranean collisional orogenic belt (Alpine-Himalayan) (Gamkrelidze et al., 2018). Geographically, it ranges from the northern slopes of the Greater Caucasus to the southern slopes of the Lesser Caucasus, situated in between the Afro-Arabian (Gondwana) and the Eurasian plates. More specifically it consists of the Greater Caucasus Range with Mount Kazbegi as the highest peak to the north and the Transcaucasia to the south (Figure 4. 9) (Adamia et al., 1992).

Caucasus mountains are marked by relief mobility and are affected by a variety of processes, including unidirectional seismic oscillations of the crust and magmatic processes. The Caucasian region is one of the world's most dangerous seismic zones and is known for its frequent earthquakes. In Georgia, its mountainous regions are in a magnitude 8–9 zone, while its coastal regions are in a magnitude 7 zone.

Georgia is divided into several main tectonic zones, each having a different level of stability and liability. Georgian tectonic zones (Figure 4. 10):

- The Great Caucasus and Achara-Trialeti fold-thrust mountain belts
- The Rioni and Kura forelands
- The Georgian and Artvin-Bolnisi Blocks
- The Javakheti volcanic highlands

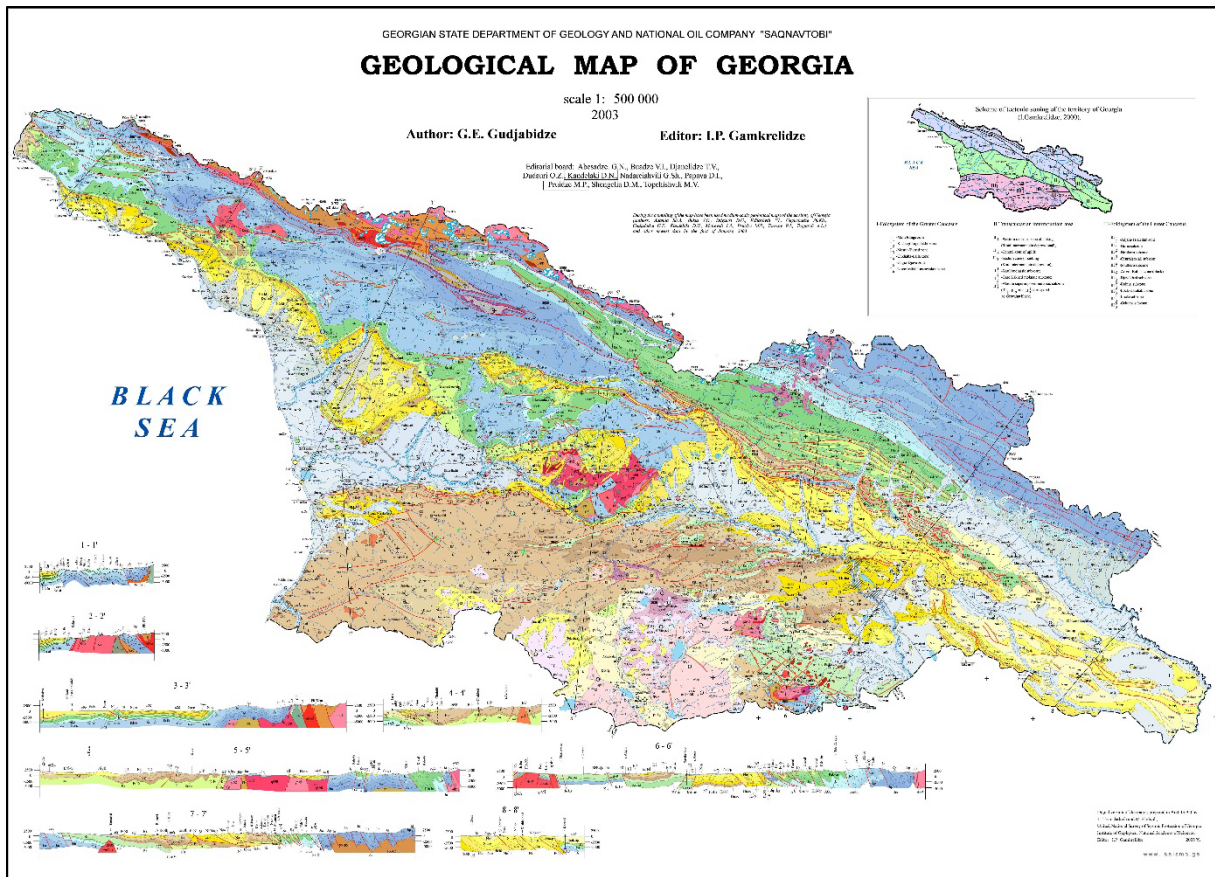


Figure 4. 8 - Geological map of Georgia (Gudjabidze & Gamkrelidze, 2003)

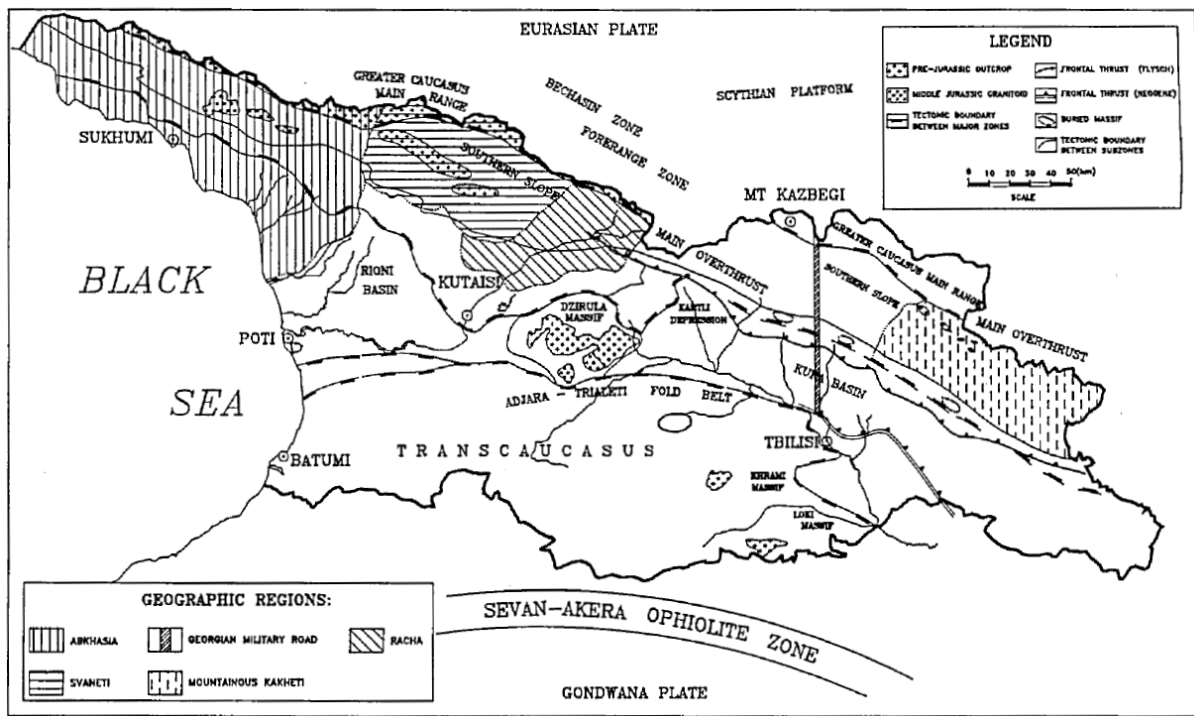


Figure 4. 9 - Geographic and geological map of Georgia (Adamia et al., 1992)

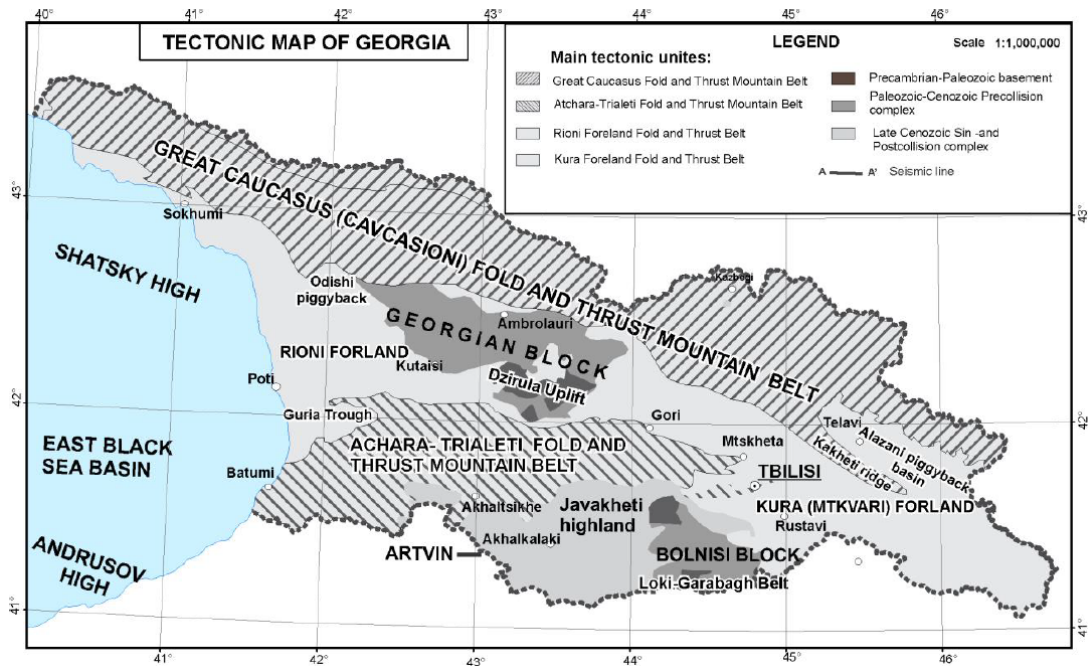


Figure 4. 10 - Tectonic map of Georgia (Adamia et al., 2011)

4.2.1. Regional geology

Akavreta HPP project is in Adjara region. This region is dominated by reversed faults and thrusts. The detailed geological outcrop from Figure 4. 8 of Adjara region is shown in Figure 4. 11. As stated by (Gudjabidze & Gamkrelidze, 2003) the area mainly consists of the following types of rocks:

- Plutons - upper eocene syenite and syenit-diorites
- Upper part of the Middle Eocene. Adjara-Trialetian zone: massive, thick-bedded heteroclastic volcanic breccias, tuffs and lava sheets of subalkalic, alkalic and calc-alkalic basaltoids, rarely andesite-basalts, andesites, dellenites and trachytes, tuff conglomerates, olistostromes, tephro and sandstone-siltstone turbidites. In upper part rarely tuffites, gritstones, tufogenic sandstones, marls (Chidila and Dviri suites)
- Volcanic rocks (submarine and subaeral) – Subalkalic

In tectonic zone point of view, the Adjara region is in fold system of the Lesser Caucasus, at III₁ subdivision section, which is called Adjara-Trialeti Zone (Figure 4. 12).

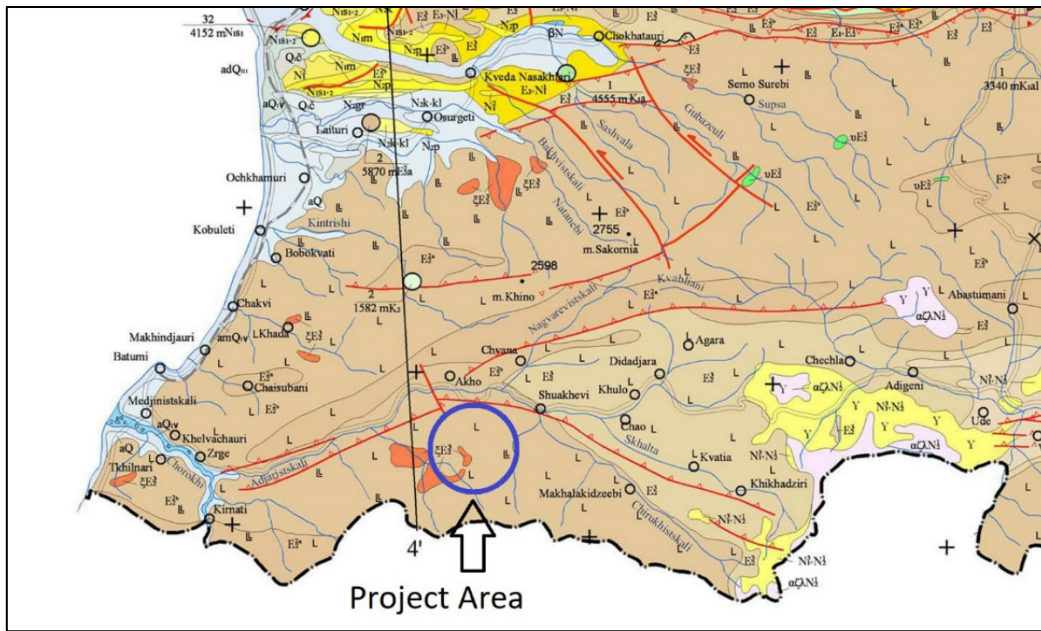


Figure 4. 11 - Adjara regional geology (modified from (Gudjabidze & Gamkrelidze, 2003))

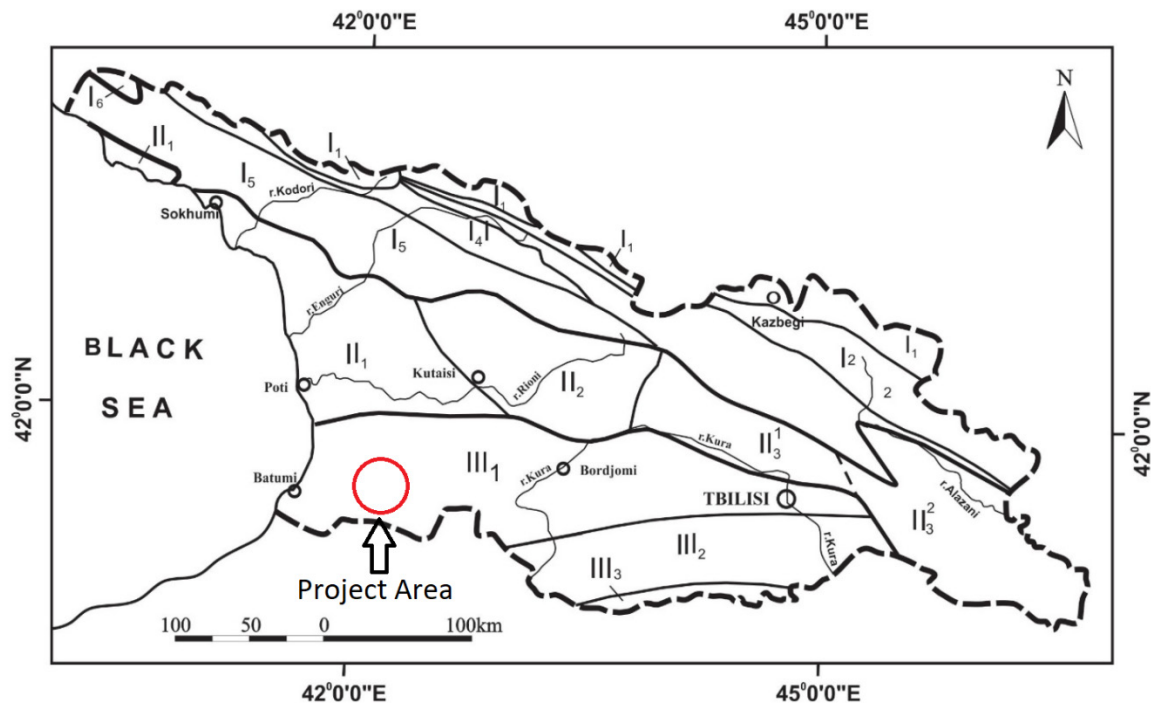


Figure 4. 12 - Simplified tectonic subdivision of the territory of Georgia (Gamkrelidze et al., 2018)

4.2.2. Project geology

In following chapter, project geology description is based on Georgian Hydro Power LLC (GHP) geological report (2016). The project site and the surrounding region, in terms of geomorphology, are represented by medium and high mountainous erosion/denudation relief. It is situated within the left slope of the river Acharistskali valley. The Acharistskali valley is situated between the Meskheta mountain range on the north and the Shavsheti mountain range on the south. The height of the Meskheta mountain range crest reaches 2600-2700m, and the height of the Shavsheti mountain range crest is within 2300-2450 m.

According to academician P. Gamkrelidze's Scheme of Geotectonic Zoning, the project area and its adjacent zone represent part of the Ajara-Trialeti fold system (Figure 4. 10) and are structured by Paleogenic, namely Eocene (P_2) volcanic formations, among which mid-Eocene intrusive (γP_2^2) are also found (Figure 4. 13).

Within the construction site and its neighborhood, among Eocene sediments several suites are distinguished, including Perangi, Naghvarevi, Chidili, Shuakhevi, Makhuntseti and Vaio suites (GHP, 2016). Brief description of the Shuakhevi and Makhuntseti suites, which are part of the 2150 m tunnel system are given below.

Makhuntseti suite is represented on the southern and northern parts of the Adjaristskali syncline, on the area adjacent to village Makhuntseti, and is structured by volcanic/sedimentary and terrigenous deposits (GHP, 2016). In terms of lithology, Makhuntseti suite is divided into three parts:

- First sub-suite of micro fragmental, micro bedded tuffs and tuff breccias ($P_2^3mh_1$).
- Second sub-suite of thin-bedded tuffs, tuff breccias and lavas ($P_2^3mh_2$).
- Third sub-suite of micro-bedded pelitic tuffs, tuff breccias ($P_2^3mh_3$).

Shuakhevi suite sediments within the project area are represented on the right slope of the Akavreta river valley, as well as on the lower part of the valley (GHP, 2016). According to geological report, presented by Georgian Hydro Power LLC the suite is mainly structured by lava lateral extensions and volcanoclastic trachyandesites and trachybasalts. The suite is divided into three parts:

- First sub-suite of coarsely-stratified lava breccias, lavas and tuff breccias ($P_2^3sh_1$);
- Second sub-suite of coarsely-stratified tuff breccias and conglomerates ($P_2^3sh_2$);
- Third sub-suite of coarsely-stratified lava breccias, lavas and tuff breccias ($P_2^3sh_3$);

The first sub-suite is best defined on the right bank of the river Acharistskali. It gradually transfers into the second sub-suite, where the conglomerate of uniform structure is well seen (GHP, 2016).

According to P. Gamkrelidze's, the region is within Aspindza-Manglisi and Abastumani-Boshuri sub-zones. Within the region, Acharistskali syncline and Chakvistavi anticline should be mentioned. Acharistskali syncline is one of the biggest structural units in the southern part of the region and is spread along the river Acharistskali valley. On this area, a tectonic fault, second largest in the region, is observed along villages Makhinjauri and Sakhalvasho (GHP, 2016). Within the construction site itself, no significant tectonic faults are mentioned in geological literature, though relatively small-scale tectonic faults are not excluded here (GHP, 2016).

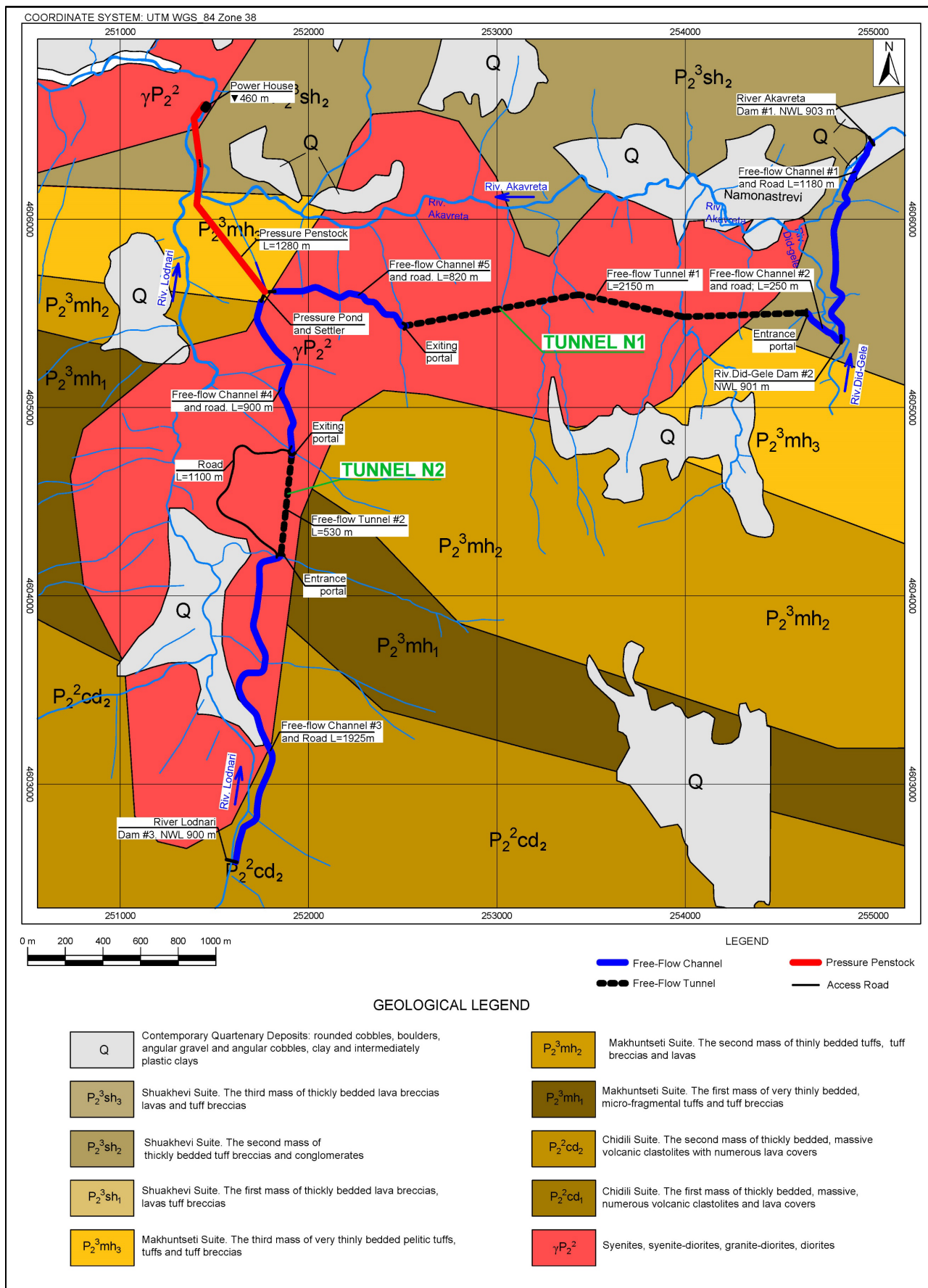


Figure 4. 13 - Geological map (modified from (GHP, 2016))

4.2.2.1. Engineering geological investigations

In 2016 the in-situ and lab investigations were performed in Georgia concerning Akavreta HPP. Study program at this stage did not include boreholes and trial-pits. Therefore, for preliminary general assessment of physical-mechanical features of soils and rocks, laboratory analyses were done on the samples taken from the local outcrops. The geological map based on investigations is shown in Figure 4. 13. The flow chart of the main conducted geological investigations is shown in Figure 4. 14.

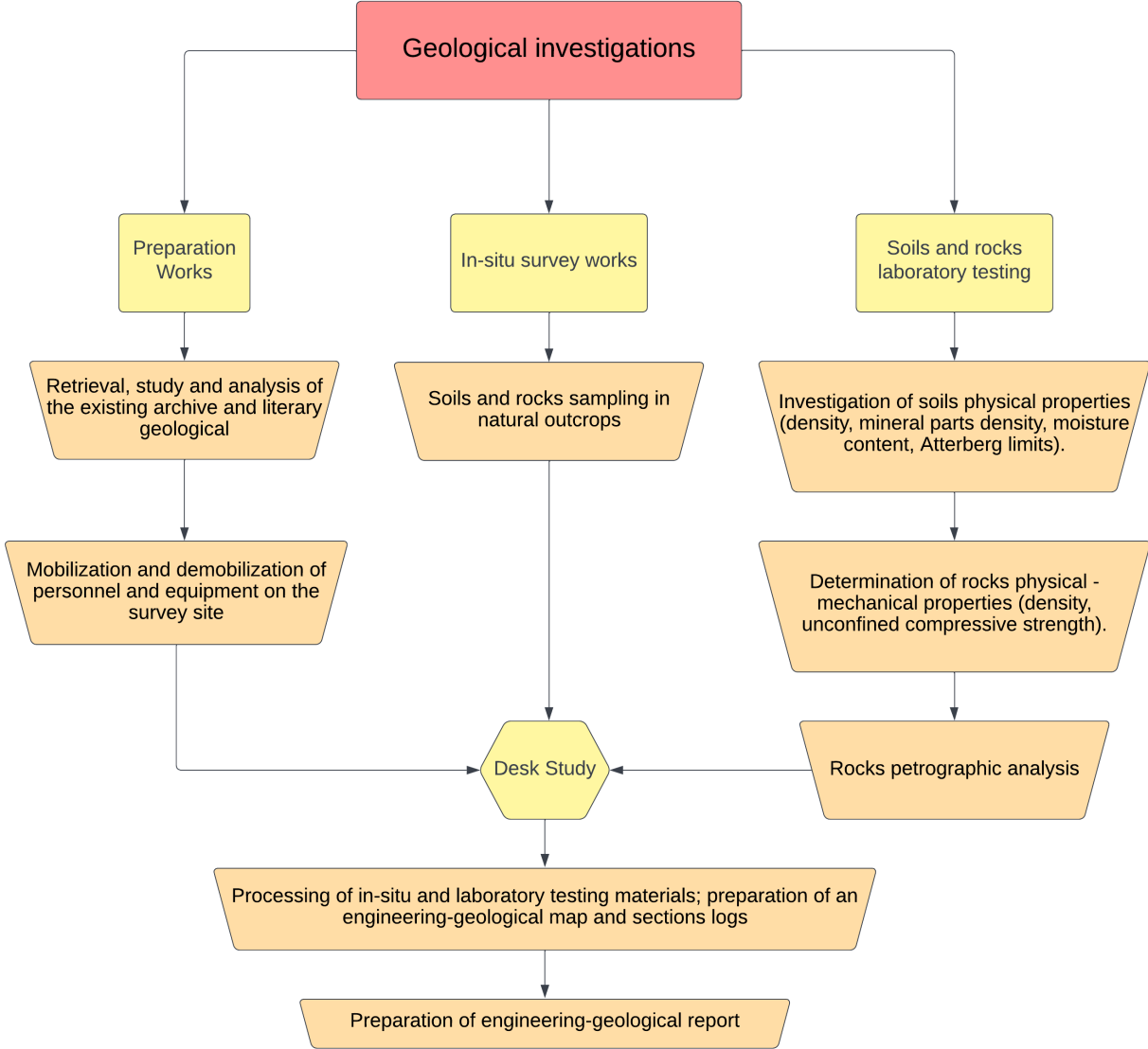


Figure 4. 14 - Conducted geological investigations (based on (GHP, 2016))

4.2.2.2. Laboratory testing

(γP_2^2) Sub-suite of Mid-Eocene syenites, syenite-diorites, granodiorites and diorites has been found on the surface in many places within the project area, further in the chapters this rock type will be referred to as syenite-diorites. Therefore, most of the project structures will be in contact with these rocks. Rock density and strength properties have been studied using the samples taken from the outcrops. In total, 16 samples of different lithologies of the sub-suite have been tested. Laboratory testing data and averaged values of the obtained results are presented in Table 4. 4 below.

Table 4. 4 - Laboratory results (modified from (GHP, 2016))

Outcrop N	Natural density [t/m ³]	compressive strength in natural moisture state [MPa]	Rock type
1	2.59	127	syenite
2	2.56	105	syenite
3	2.56	115	syenite
4	2.62	133	syenite
5	2.64	133	syenite
6	2.46	114	syenite
7	2.49	43	syenite
8	2.41	63	syenite
9	2.64	73	syenite
18	2.59	105	granodiorite
19	2.62	128	tectonic breccia
20	2.55	50	granodiorite
21	2.52	163	tectonic breccia
22	2.54	97	granodiorite
24	2.53	146	granodiorite
26	2.56	156	crystalline breccia/ granodiorite
Min	2.41	43	
Max	2.64	163	
St Dev	0.06	36	
Average		109	

As seen from the Table 4. 4, the average uniaxial compressive strength (UCS) of intact rock is 109 MPa. Samples with high strength, were presumably less weathered and free of hidden fractures. Relatively less strength was revealed in more weathered samples, as well as the samples with hidden fractures inside them. According to ISRM (1978) (Appendix D) the rock with strength of 109 MPa is classified as grade R5 with description “Very strong”

($P_2^3sh_2$) Coarsely stratified tuff breccias and conglomerates, further in the chapters this rock type will be referred to as tuff-breccias. This stratum has been observed at some sections of the Tunnel N1. According to geological report, uniaxial compressive strength of ($P_2^3sh_2$) Coarsely stratified tuff breccias and conglomerates is 30 MPa. The rock strength classification of tuff breccias and conglomerates is R3 (medium strong).

Table 4. 5 - Summary of rock strength lab results and its classification (According to (GHP, 2016))

Rock type	Density [kg/m ³]	Specific weight [MN/m ³]	UCS of intact rock [MPa]	Rock strength classification according to ISRM (1978)
($P_2^3sh_2$) tuff-breccias and conglomerates	2500	0.025	30	R3 (medium strong)
(γP_2^2) syenite-diorites and granodiorites	2600	0.026	109	R5 (Very strong)

4.2.2.3. Rock jointing

Rock jointing has been studied on 2 different outcrops for rock type of syenite-diorites. As general characteristic of volcanic formations, rock joint systems are not clearly expressed everywhere, though in both outcrops selected for jointing study, such systems are well determined. In each of the outcrops, they were registered with almost similar joint orientation (Appendix E). The joint rosette was constructed (Figure 4. 15) according to dip angle-direction given in appendix E.

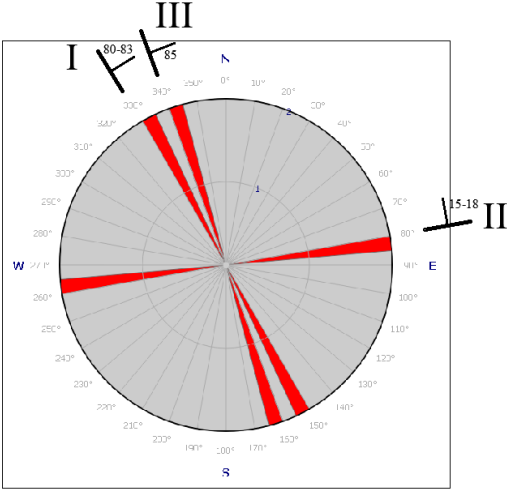


Figure 4. 15 - Joint rosette (based on (GHP, 2016))

4.3. Rock mass quality along the headrace tunnels

4.3.1. Modulus of deformation

To calculate modulus of deformation of rock mass, first modulus ratio (MR) was approximated using guidelines for the selection of modulus ratio (MR) values (Appendix F), because there is no available laboratory data for modulus of deformation of intact rock. Young's modulus of intact rock was calculated using 3-4 and The Poisson's ratio was approximated using Gercek table (Appendix F). Results are given in Table 4. 7

After knowing all the necessary input parameters, several different equations taken from Table 3. 6, including Hoek & Diederichs (2006), Barton (2002), Panthi (2006) and Hoek & Brown (1997) were used. For numerical model the results of Hoek and Diederichs (2006) will be used. Results are given in below tables and figures.

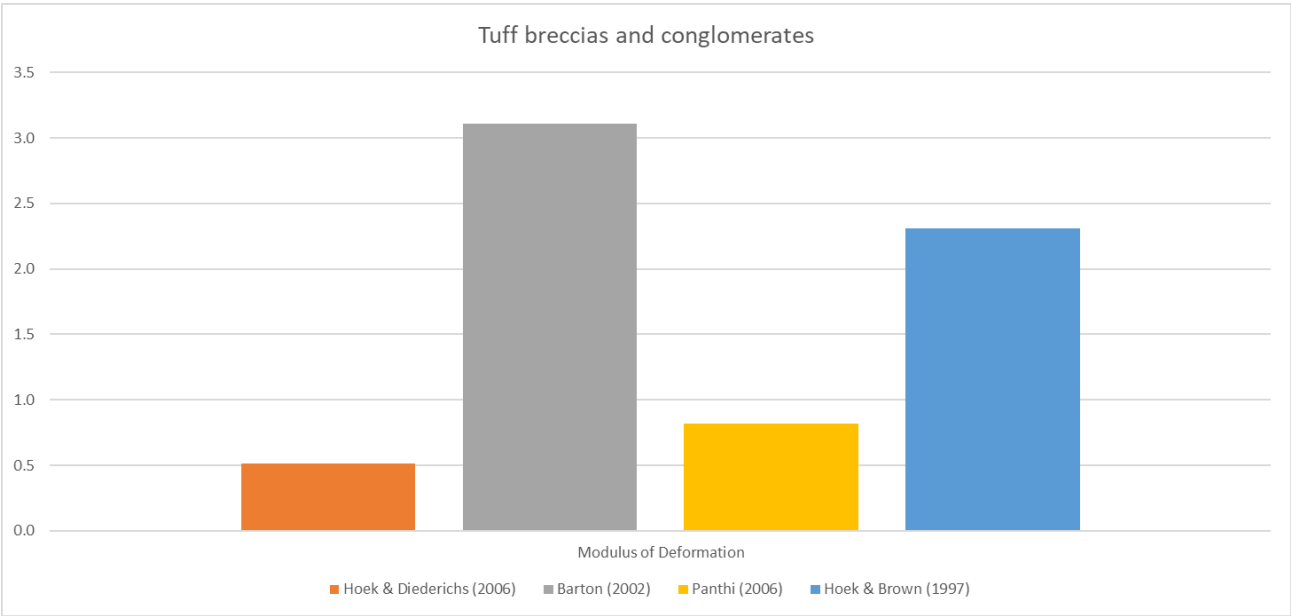


Figure 4. 16 - Modulus of Deformation for tuff breccias and conglomerates

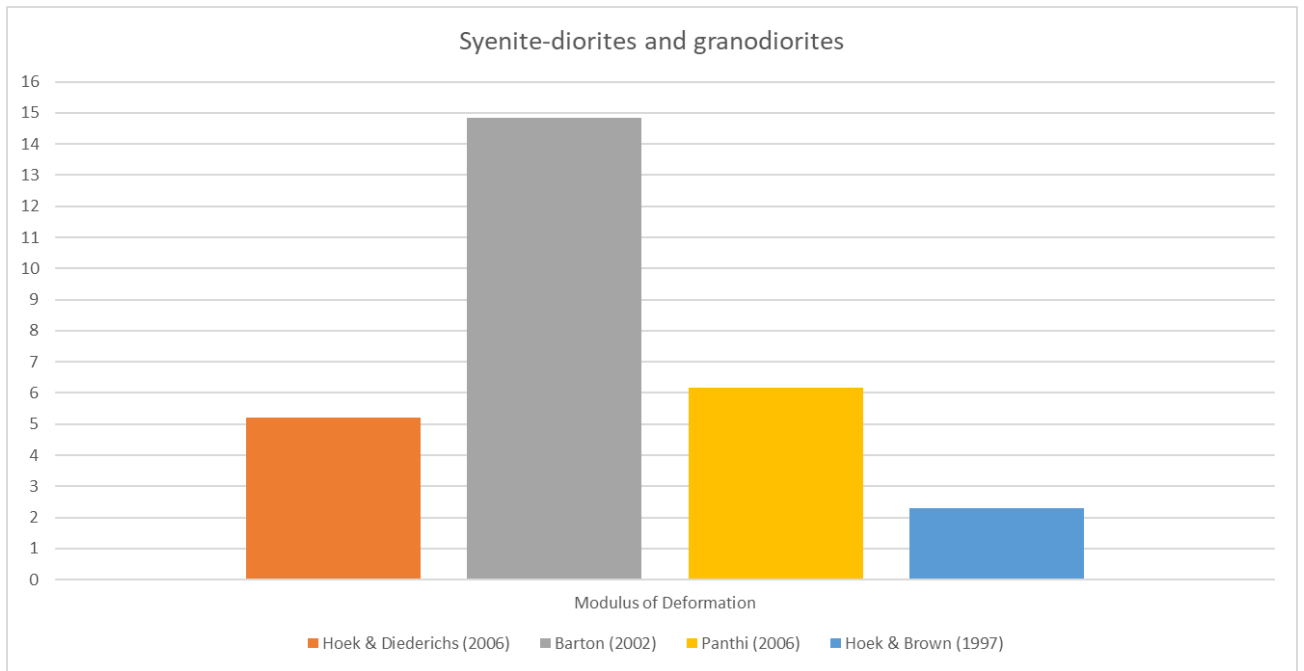


Figure 4. 17 - Modulus of deformation for syenite-diorites and granodiorites

Table 4. 6 - Modulus of deformation (E_m) calculated using four different equations in [GPa]

Rock Type	Panthi (2006)	Barton (2002)	H & D (2006)	H & B (1997)	Min	Max	Mean	Std
Tuff-breccias	1	3	1	2	1	3	2	1.23
Syenite-diorites	6	15	5	10	5	15	9	4.42

Table 4. 7 – Summary of Young’s modulus and Poisson’s ratio approximation

Rock Type	Poisson’s ratio	Modulus ratio (MR)	Young’s modulus [GPa]
Tuff-breccias	0.18	300	9
Syenite-diorites	0.22	325	35

4.3.2. Rock mass strength

To determine rock mass strength four different equations from Table 3. 5 were used for comparison purpose. For tuff-breccias Panthi (2006) equation is used, because this rock type, as described in geological report is moderately fissured. For syenite-diorites rock type Panthi (2018) equation is used, as this type is very strong and with less fissures. The results in Table 4. 8 show that Panthi’s and Barton’s values are very similar. Panthi’s values will be used for

further empirical and semi-analytical calculation methods. The graphical results and comparisons are given in below figures.

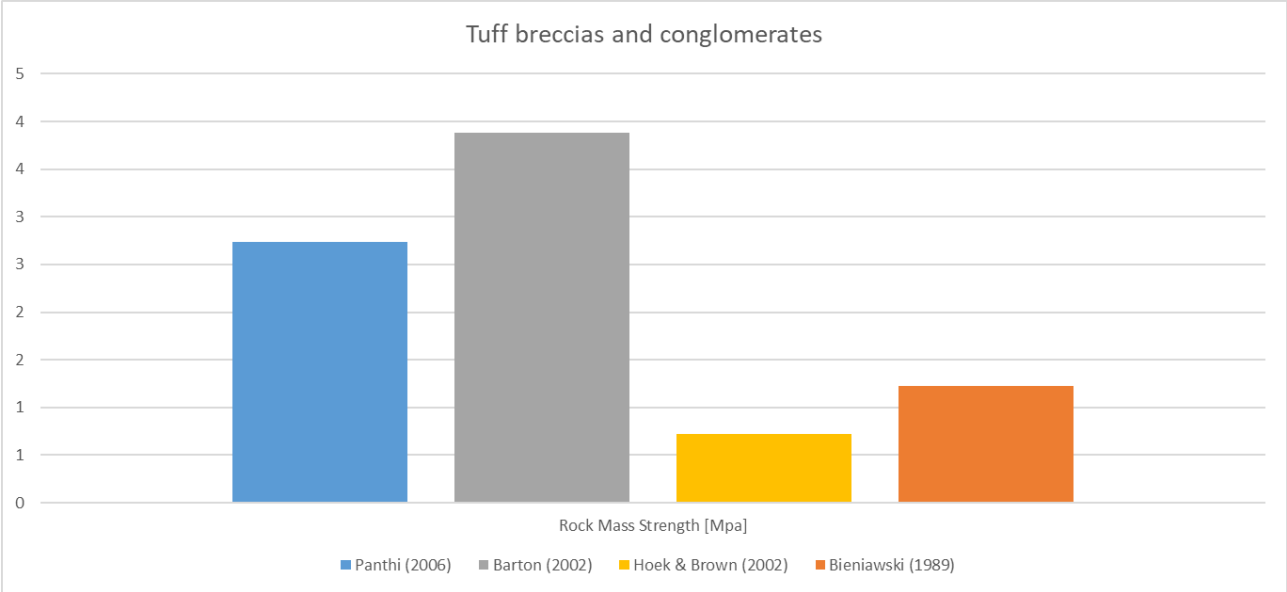


Figure 4. 18 - Rock mass strength for tuff breccias and conglomerates

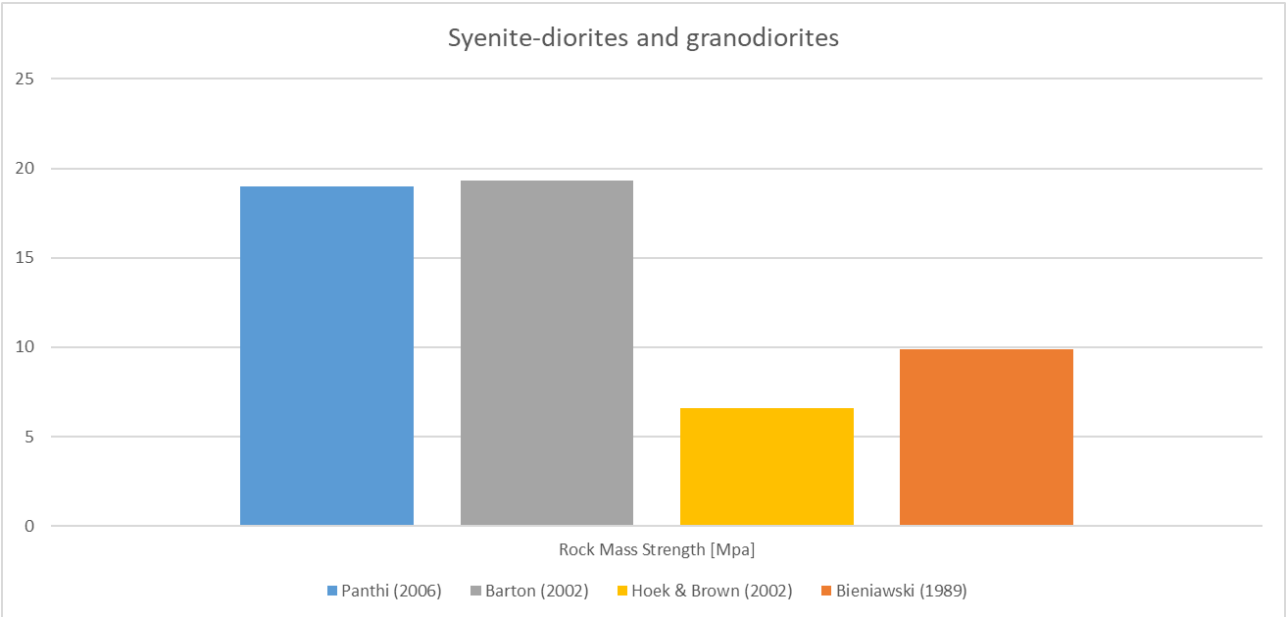


Figure 4. 19 - Rock mass strength for syenite-diorites and granodiorites

Table 4. 8 - Comparison of rock mass strength results for different equations in [MPa]

Rock Type	Panthi (2006)	Barton (2002)	H & B (2002)	Bieniawski (1989)	Min	Max	Mean	Std
Tuff-breccias	3	4	1	1	1	4	2	1.44
Syenite-diorites	19	19	7	10	7	19	14	6.44

4.3.3. Rock mass classification

GSI value for each rock type was derived based on in-situ observations and geological report from Georgian geological team (from Georgian Hydro Power LLC company). The RMR value was calculated using equation 3-3.

Q values are estimated using Table 4. 9 provided by Panthi (2006). The results are given in Table 4. 10. As the Q values were estimated, it will be more appropriate to write the range of possible Q values. For further calculations, the Q value from column “Q-Values for calculations” will be used.

Table 4. 9 - Rock mass classes used for comparison of the four tunnel projects (modified from (Panthi, 2006))

Description		Range of Q-values		Range of RMR-values	
Rock Class	Quality Description	Minimum	Maximum	Minimum	Maximum
Class 1	Very good to excellent	100	1000	85	100
Class 2	Good	10	100	65	85
Class 3	Fair to good	4	10	56	65
Class 4	Poor	1	4	44	56
Class 5	Very poor	0.1	1	35	44
Class 6	Extremely poor	0.01	0.1	20	35
Class 7	Exceptionally poor	0.001	0.01	5	20

Table 4. 10 – Rock mass classification systems

Rock Type	RMR	GSI	Q - Value (Range)	Q - Value used in Calculations
Tuff-breccias	40	35	0.1 - 1	0.1
Syenite-diorites	55	50	1 - 4	3

5. Critical assessment of existing design

5.1. Brief description of current design

Current design consists of two free flow headrace tunnels, five open flow channels, pressure pond and penstock. Headrace tunnel N1 total length is 2150 m and tunnel N2 is 530 m. Full detailed description of the whole hydropower system is given in chapter 4.1.2.

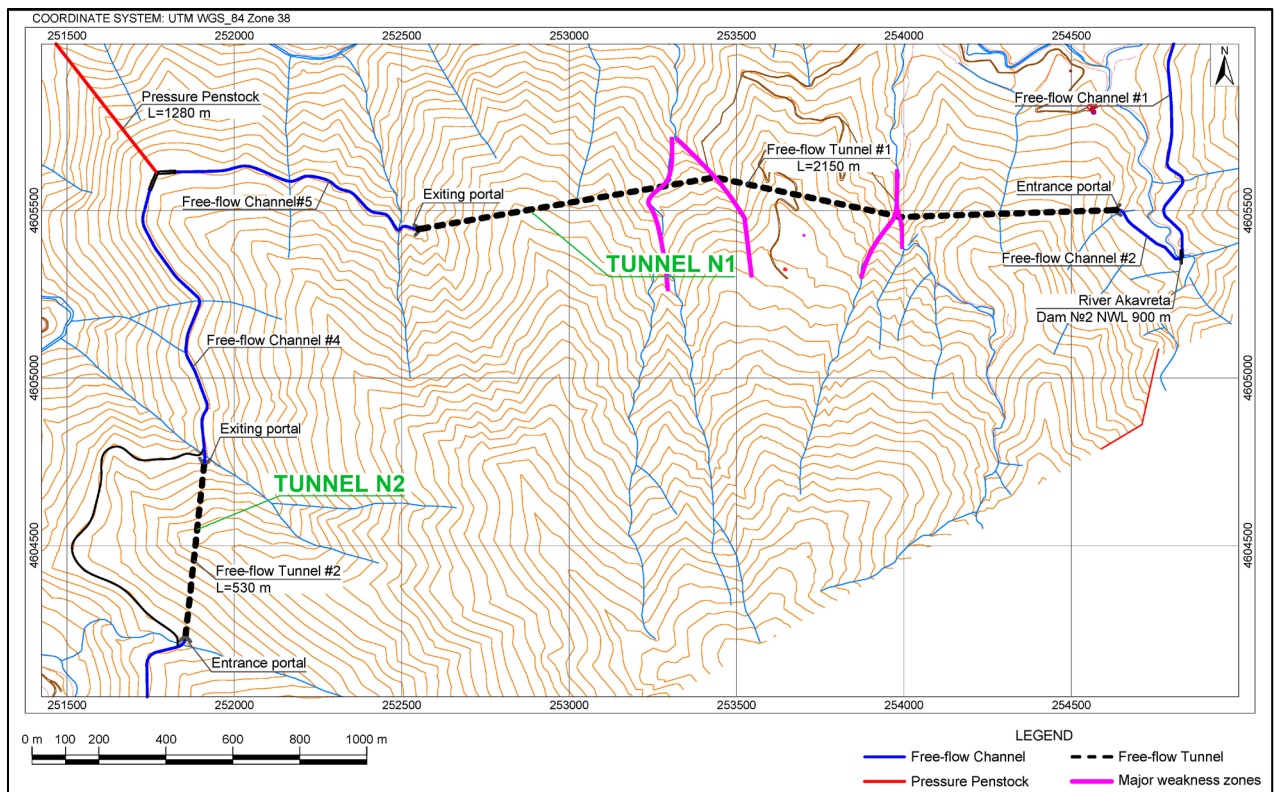


Figure 5. 1 – Headrace tunnels N1 and N2 layout (modified from GHP’s map data)

The Figure 5. 1 shows general layout of both headrace tunnels, five open flow channels, pressure pond and penstock. Tunnel N1 has two bends in two different locations. Inlet and outlet of the headrace tunnel N1 is connected to free flow channels. The first channel at inlet is 250 m and second channel at outlet is 820 m long. Similar idea is applied to headrace tunnel N2. The inlet to tunnel N2 is connected to 1925 m long free flow channel and outlet is connected to 900 m free flow channel. The water coming from both tunnels meet at pressure pond, where it is delivered to powerhouse with 1280 m long penstock.

5.2. Evaluation of current design

Figure 5. 2 shows closer look at geological layout of the headrace tunnels. The headrace tunnel N1 meets two rock types, first is (γP_2^2) syenite-diorites and granodiorites, and second is ($P_2^3 sh_2$) tuff-breccias and conglomerates. The headrace tunnel N2 meets only with (γP_2^2) syenite-diorites type of rock. After studying topographical map of the area, the major weakness zones which headrace tunnel N1 meets were drawn on the map in purple lines (Figure 5. 3) and in green on geological map (Figure 5. 2). To analyze alignment of the headrace tunnels, the detailed longitudinal profiles Figure 5. 4 and Figure 5. 5 were created in AutoCAD Civil 3D software based on 3D contour lines provided by GHP. On longitudinal profile for headrace tunnel N1 two major weakness zones and their overburden is shown.

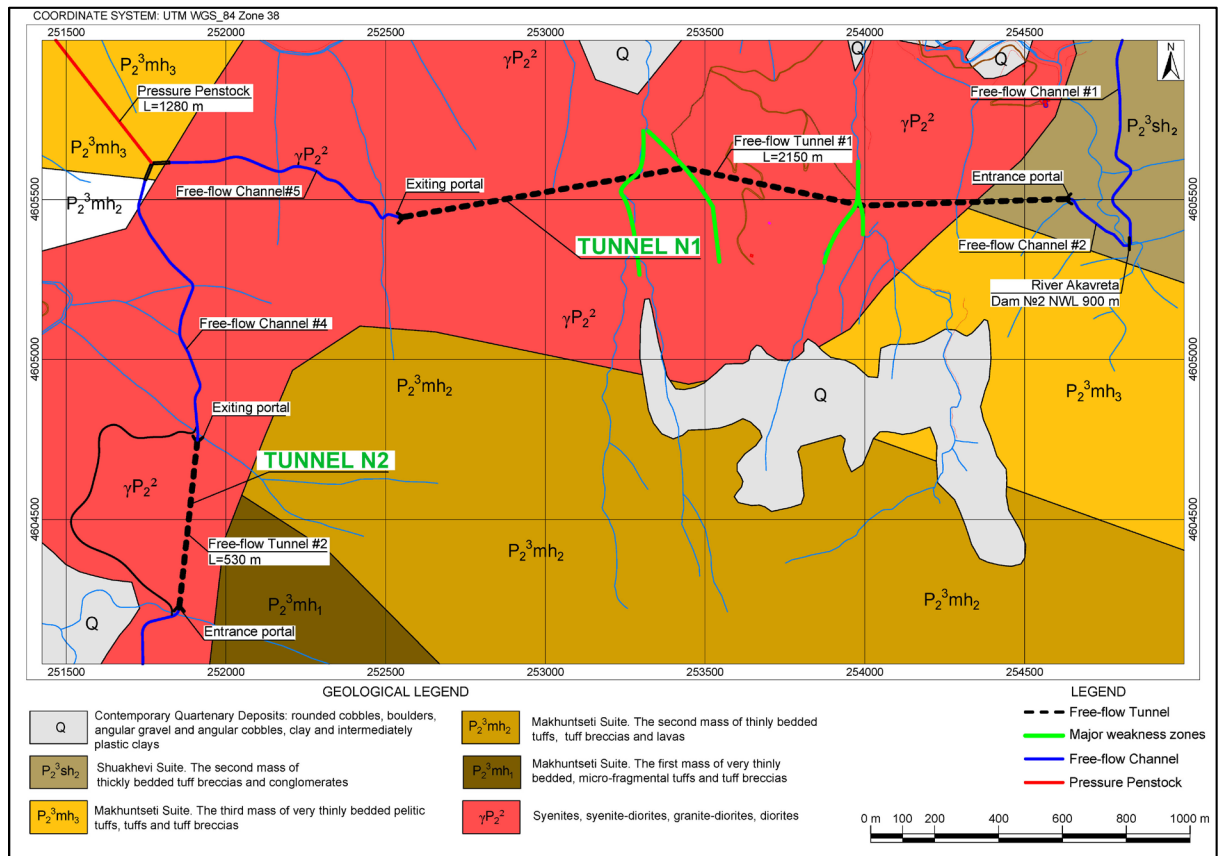


Figure 5. 2 - Geological map of Akavreta HPP headrace tunnel layout (modified from (GHP, 2016))

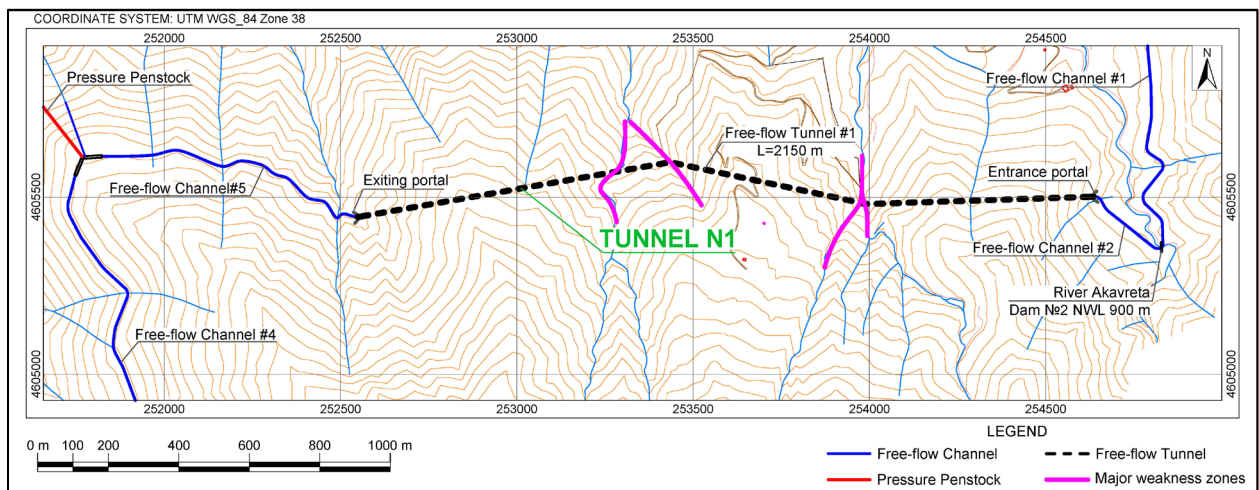


Figure 5. 3 – Major weakness zones, which headrace tunnel N1 alignment meets (modified from GHP’s map data)

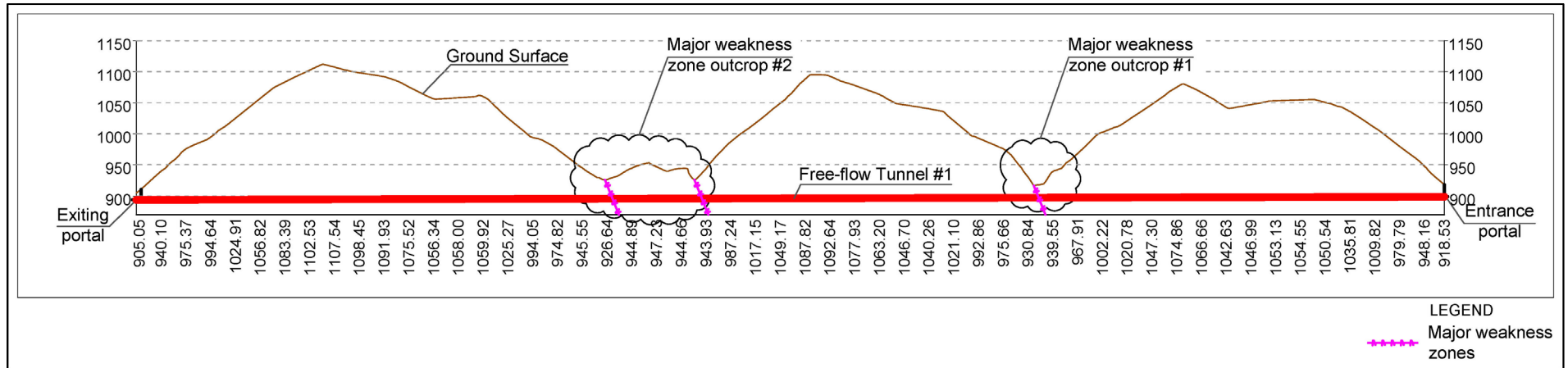


Figure 5. 4 – Headrace tunnel N1 longitudinal cross section of Akavreta HPP with major weakness zones

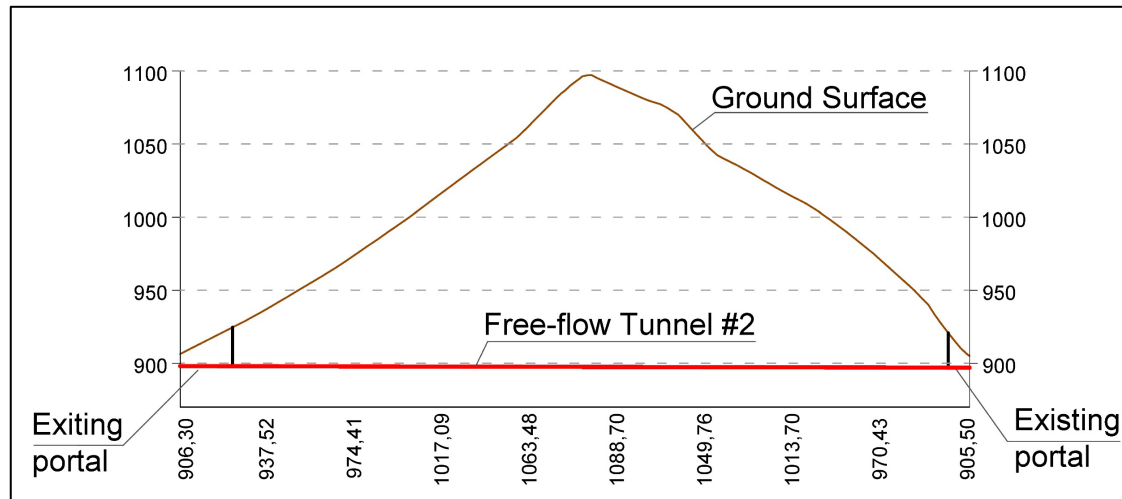


Figure 5. 5 – Headrace tunnel N2 longitudinal cross section of Akavreta HPP

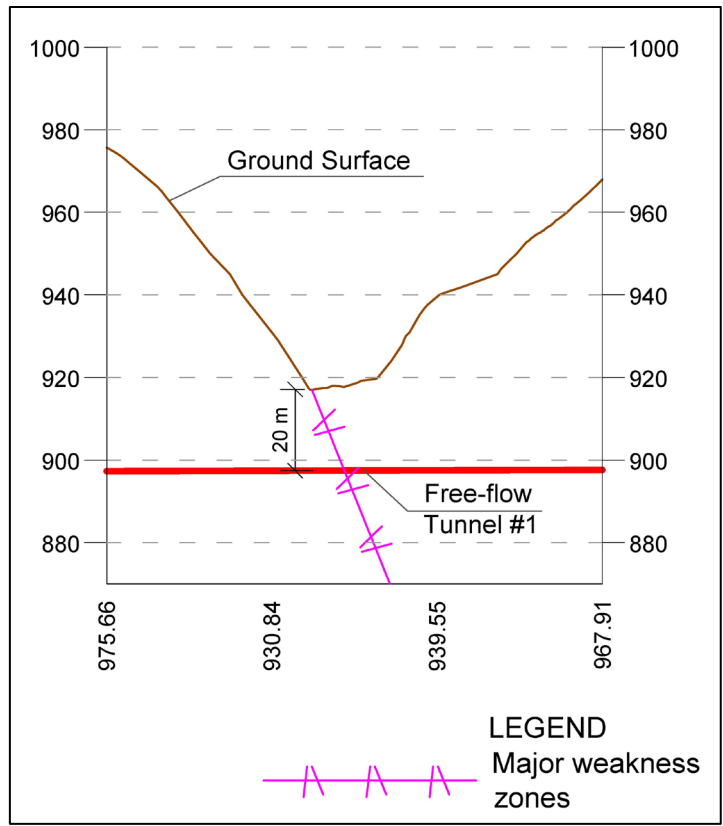


Figure 5. 6 - Outcrop of the major weakness zone #1 for headrace tunnel N1 of Akavreta HPP

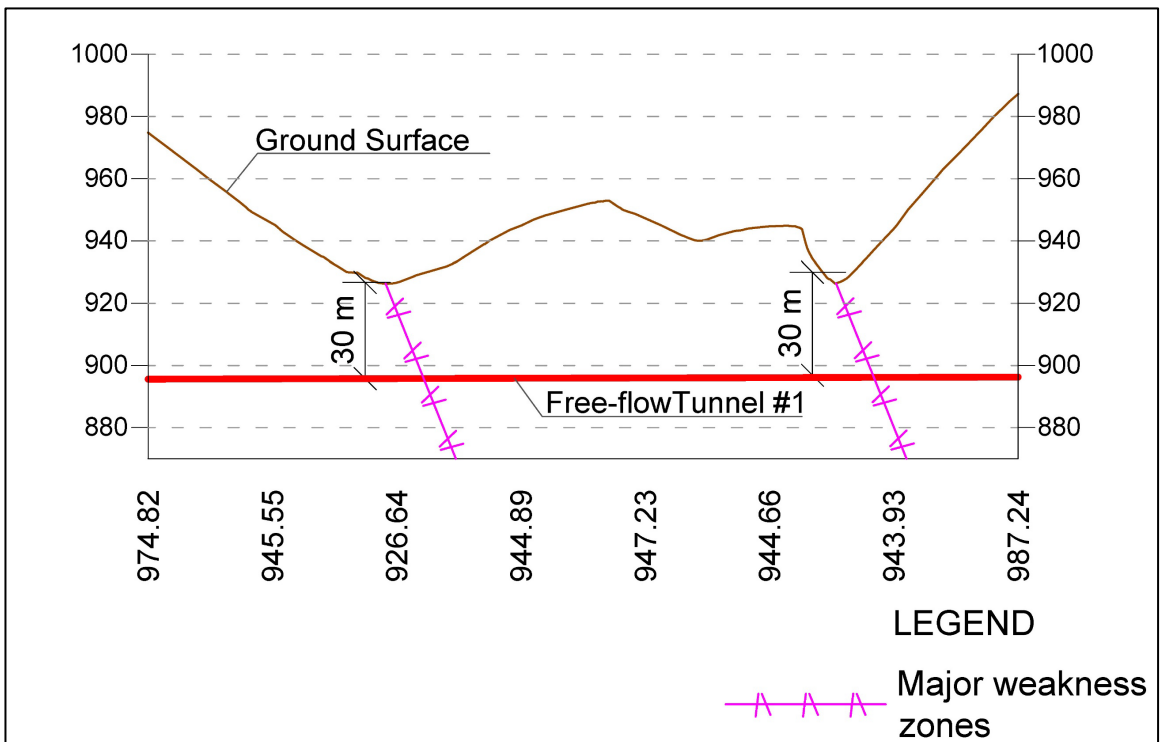


Figure 5. 7 – Outcrop of the major weakness zone #2 for headrace tunnel N1 of Akavreta HPP

In case of headrace tunnel N1 the smallest overburden is 20 m, which is located at outcrop #1, which is also major weakness zone (Figure 5. 6). At outcrop #2, there is second major weakness zone, where the minimum overburden is 30 m (Figure 5. 7).

The small overburden for headrace tunnel N1 case at major weakness zones will impose tunnel instabilities. It was concluded based on extremely small overburden that current alignment for headrace tunnel N1 was not reliable and safe, that is why no further analysis were conducted for current design. With cooperation of Georgian Hydro Power LLC (GHP) the second alternative was developed for headrace tunnel N1. Headrace tunnel N2 has sufficient overburden (200 m) and the rock mass consists of syenite-diorite rock type (Figure 6. 4), which is very strong rock type (Table 4. 5). Further in the chapters, headrace tunnel N1 alternative version will be discussed in detail with full analysis.

6. Alternative possibility

6.1. Evaluation on the possible alternative

As for alternative possibility, the alignment of the headrace tunnel N1 is changed (Figure 6. 1), while headrace N2 remained the same. Headrace tunnel N1 now is one straight line without any bending and will be connected directly to the open flow channel #4 coming from the headrace tunnel N2. The minimum overburden at outcrop #1 increased from 20 m to 55 m (Figure 6. 6) and minimal overburden at outcrop # 2 increased from 30 m to 95 m (Figure 6. 7). The headrace tunnel N1 length is increased from 2150 m to 2750 m. The 820 m of the channel, which was connecting outlet of the headrace tunnel N1 to the pressure pond is removed. Also, there will be no more necessity of building the 820 m extra road which would be following the open flow channel. As concluded from given topography, the construction of the road would be difficult and costly, taking into consideration the extra work for Environmental Impact Assessment of the construction area.

Considering prices in Georgia and upper mentioned changes, although, the tunnel length increased by 600 m, the total cost of the construction will not increase much. Further analysis and calculations will be conducted only for headrace tunnel N1, because headrace tunnel N2 shares similar geological characteristics and doesn't require alternative design.

Similar to original design, the alternative headrace tunnel N1 passes through two types of rocks, tuff-breccias and syenite-diorites, as shown on geological map Figure 6. 2 and geological longitudinal cross section Figure 6. 3

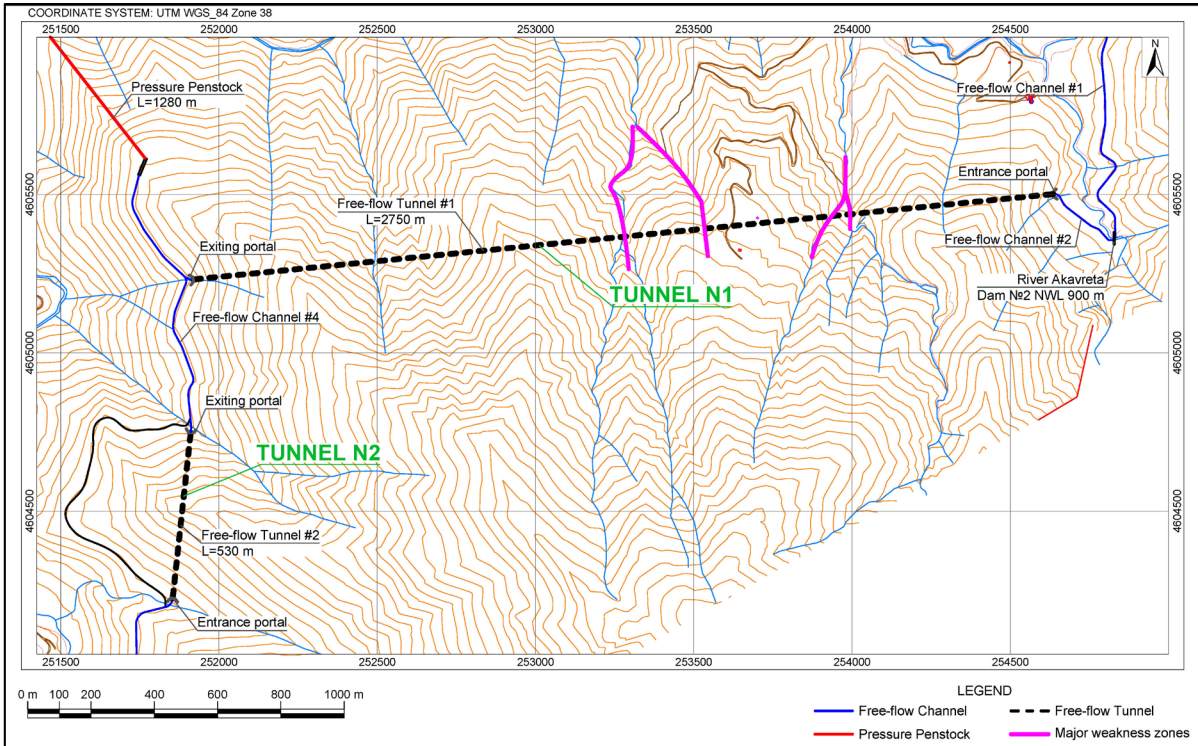


Figure 6. 1 - Alternative alignment of the headrace tunnel N1 with major weakness zones (modified from GHP's map data)

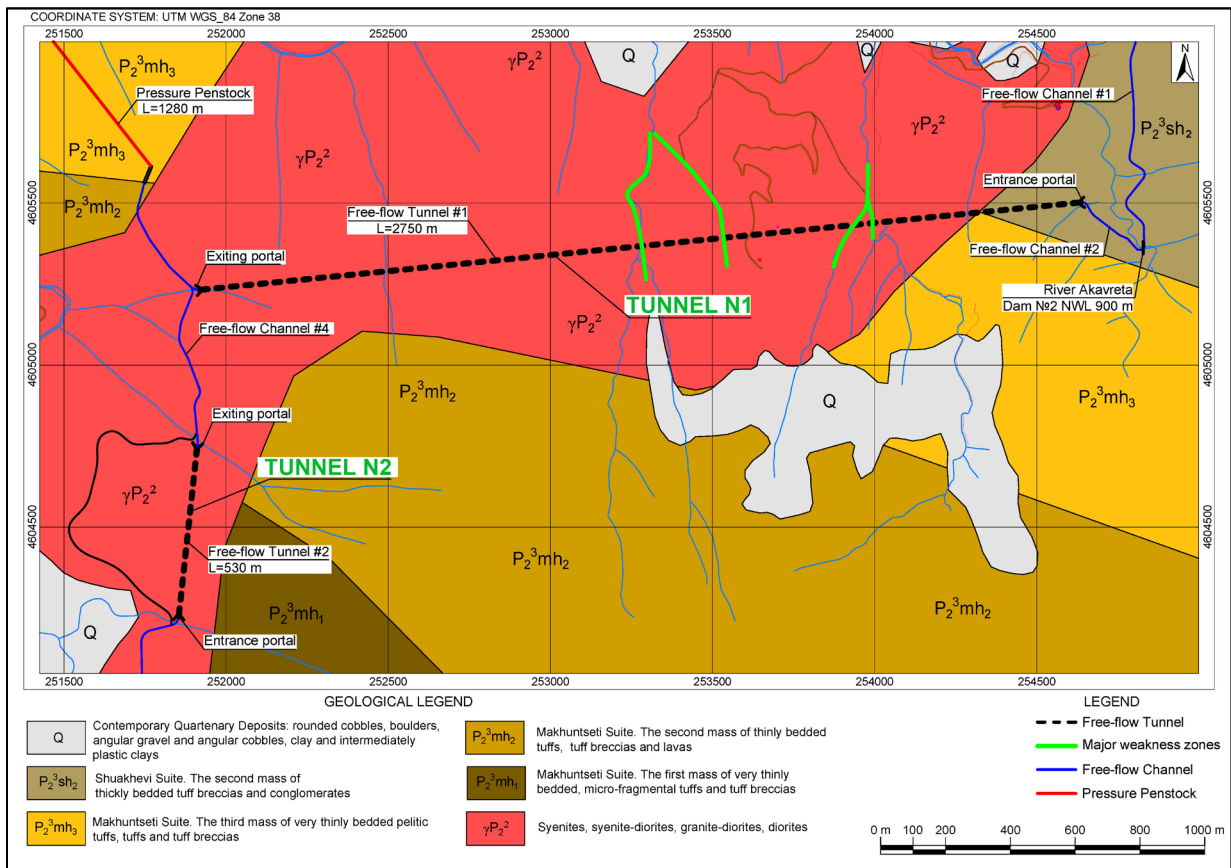


Figure 6. 2 - Geological map of alternative alignment of headrace tunnel N1 (modified from (GHP, 2016))

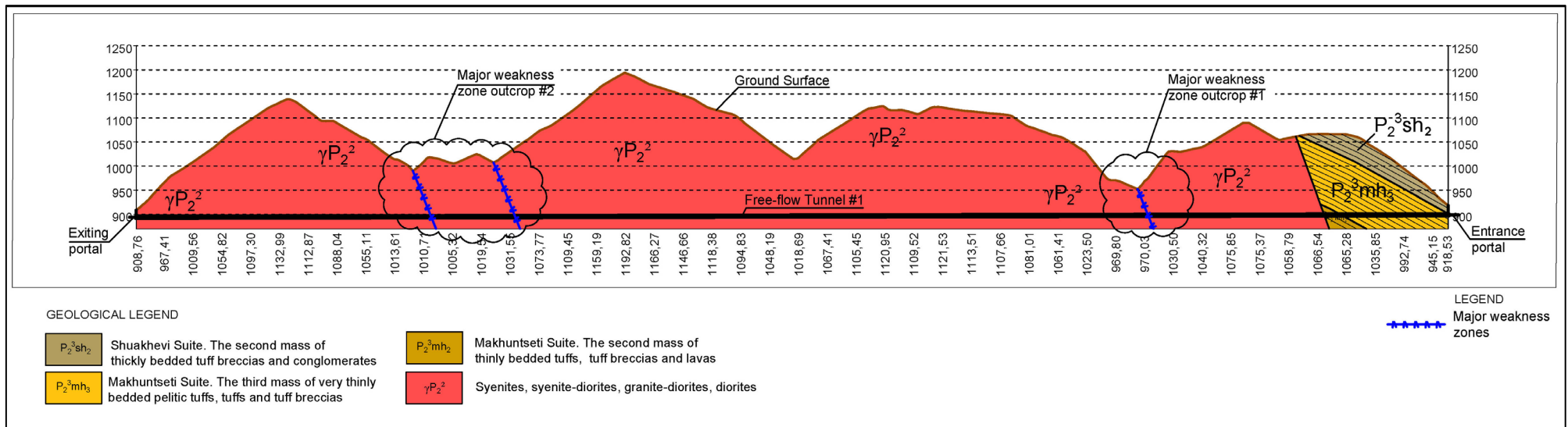


Figure 6. 3 - Geological cross section of the tunnel N1 of Akavreta HPP with major weakness zones (based on (GHP, 2016))

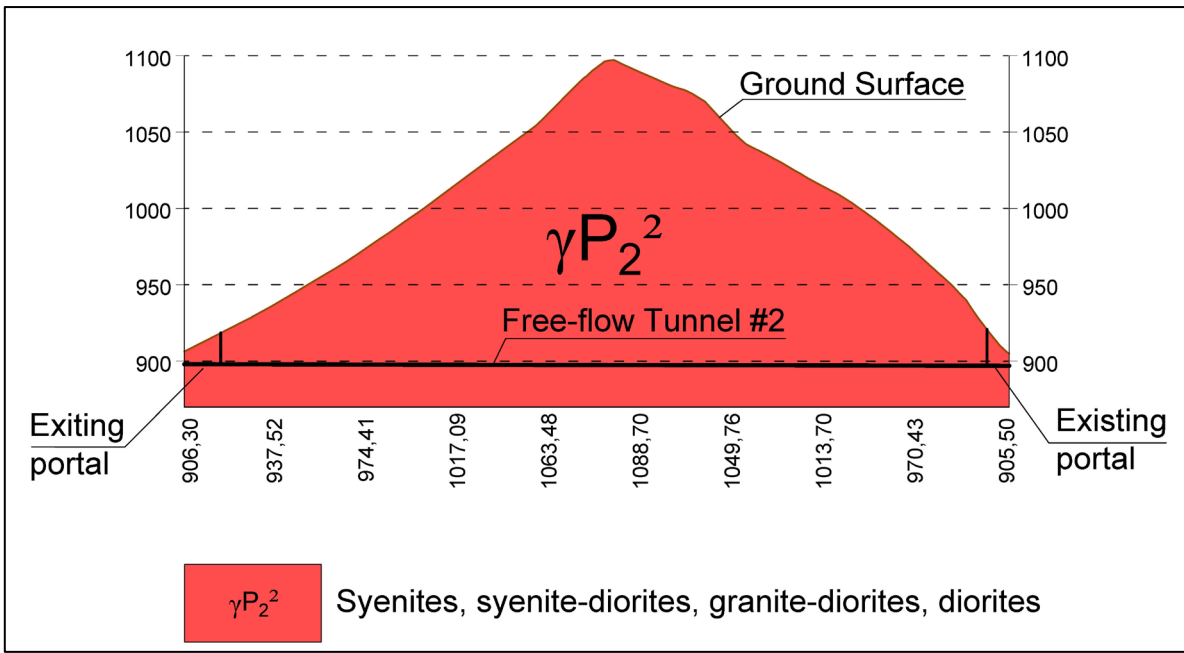


Figure 6. 4 – Geological longitudinal cross section of the headrace tunnel N2 of Akavreta HPP (based on (GHP, 2016))

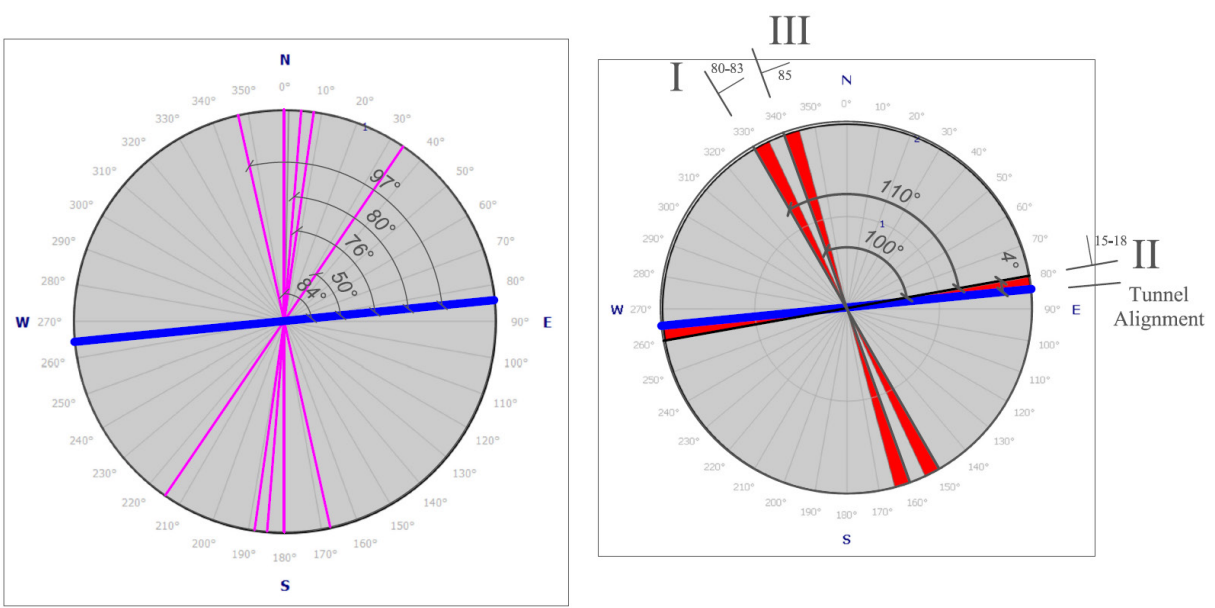


Figure 6. 5 - Weakness zones (Left), joints with orientation (Right) (based on (GHP, 2016))

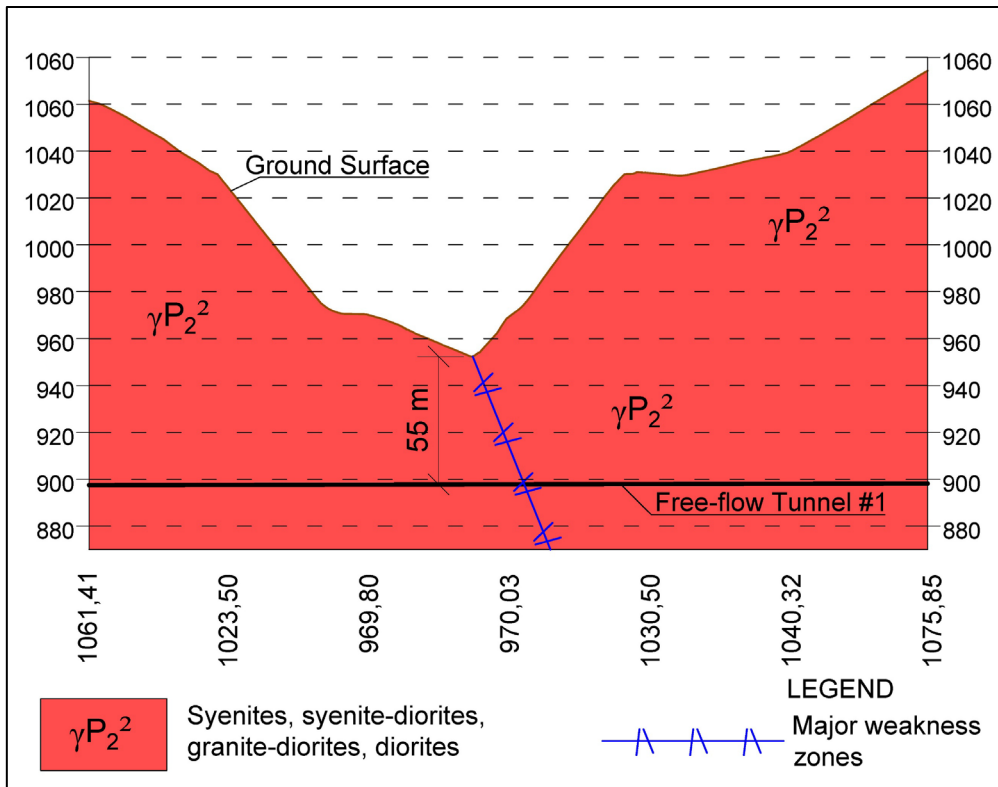


Figure 6. 6 - Outcrop of the major weakness zone #1 of Akavreta HPP tunnel N1

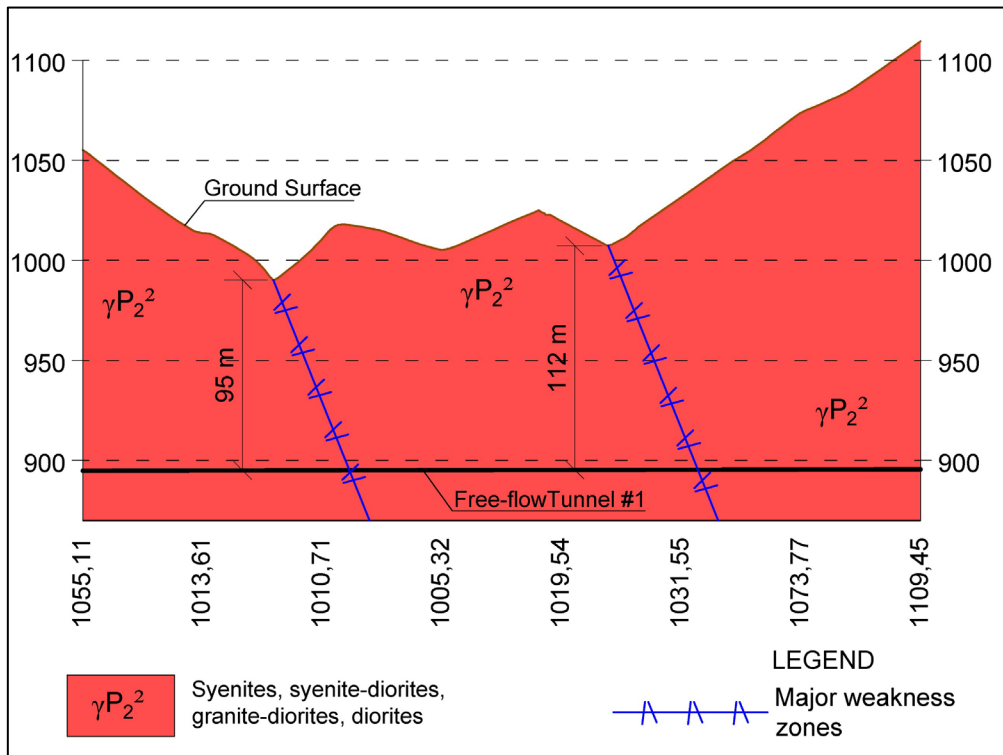


Figure 6. 7 - Outcrop of the major weakness zone #2 of Akavreta HPP tunnel N1

In hydropower tunneling systems topography should be taken into consideration. Desk work with the map is very important part of the planning phase. The major weakness zone is shown in Figure 6. 1. The major and minor weakness zones were plotted on joint rosette diagram in Figure 6. 5 (left). The tunnel alignment crosses each of them nearly perpendicular, which is the best-case scenario. As shown on joint rosette Figure 6. 5 (right) the main dominating joints are Joint set I and III, they cross the headrace tunnel N1 alignment at 100 and 110 degrees, which is favorable condition. The joint set II is almost parallel to the headrace tunnel N1 alignment, but it may not occur frequently in the rock mass.

For analysis purpose the headrace tunnel N1 and N2 was chosen to be inverted D shape with dimensions shown on Figure 6. 8.

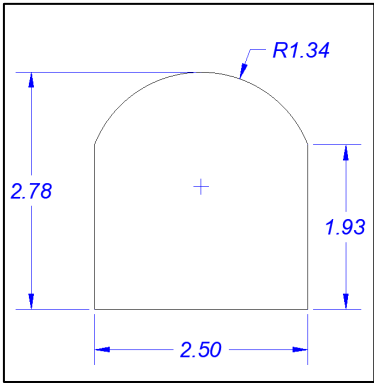


Figure 6. 8 – Headrace tunnel shape and size of Akavreta HPP tunnel N1 and N2 (according to GHP)

6.2. Stability assessment and rock support design

6.2.1. Squeezing and rock burst/spalling analysis

For squeezing analysis empirical and semi-analytical methods, discussed in Chapter 3 were used, which are: Singh et al (1992), Q-system, Hoek and Marinos (2000), Panthi and Shrestha (2018). For each rock type the analysis were made at three different cross sections, for smallest, medium and highest overburden. For vertical and horizontal stresses, the equations 3-5 and 3-6 were used. After discussion with Prof. Panthi (2022/05/16) and geological team in Georgian Hydro Power LLC, the horizontal tectonic stress for tuff-breccias was decided to be taken as 1.5 MPa and for syenite-diorites 3 MPa. The squeezing analysis were not conducted for the syenite-diorites, because there will not be squeezing given the strength of the rock, instead the rock burst/spalling analysis were carried out using equation 3-18. As for rock mass strength, Panthi’s values were used from Table 4. 8

Table 6. 1 – Input parameters for squeezing and rock burst analysis

Rock type	Distance from inlet [m]	Overburden [m]	σ_1 [MPa]	σ_3 [MPa]	σ_{tec} [MPa]	$\sigma_{\phi max}$ [MPa]	σ_{cm} [MPa]
Tuff-breccias	53	67	1.7	1.9	1.5	3.16	3.00
	133	127	3.2	2.2	1.5	7.33	3.00
	253	169	4.2	2.4	1.5	10.25	3.00
Syenite-diorites	653	55	1.4	3.4	3.0	0.89	19.00
	1352	120	3.1	3.9	3.0	5.49	19.00
	1712	300	7.8	5.2	3.0	18.22	19.00

Table 6. 2 – Results of squeezing and rock burst analysis

Rock type	Overburden [m]	Singh et al. (1992)		Q-System		Hoek and Marinos (2000)		Panthi and Shrestha (2018)			Rock burst possibility
		Limiting value of H [m]	Squeezing condition	$\sigma_{\phi max} / \sigma_{cm}$	Squeezing condition	Strain without support [%]	Squeezing condition	k	ϵ_{ci} without support [%]	ϵ_{FC} without support [%]	
Tuff-breccias	67	162	NO	1.05	Mild squeezing	0.1	Very small squeezing	1.12	0.01	0.01	
	127	162	NO	2.44	Mild squeezing	0.2	Very small squeezing	0.69	0.02	0.04	
	169	162	YES	3.42	Mild squeezing	0.4	Very small squeezing	0.58	0.04	0.08	
Syenite-diorites	55										NO
	120										NO
	300										NO

As seen from above Table 6. 2, there will be small squeezing for tuff-breccias rock type, while for syenite-diorites there will be no squeezing and no rock burst/spalling. Further numerical analysis will be carried out.

6.2.2. Support design

For support estimation the Q-System will be used. The appropriate support measures depend on the relationship between Q and the excavation's equivalent dimension. Anchor (l_a) and bolt (l_b) length depends on tunnel width (B) and height (H) respectively in meters. In calculations tunnel width is used for roof analysis and height for wall support calculations. Baron (1974) has purposed equations for anchor and bolt length calculations:

$$l_{b(roof)} = 2 + \frac{0.15 * B}{ESR} \tag{6-1}$$

$$l_{b(wall)} = 2 + \frac{0.15 * H}{ESR} \tag{6-2}$$

$$l_{a(roof)} = \frac{0.40 * B}{ESR} \tag{6-3}$$

$$l_{a(wall)} = \frac{0.40 * H}{ESR} \tag{6-4}$$

For the Akavreta tunnel ESR value was taken from Table 3. 3 as for hydropower tunnel project ESR = 1.6. The tunnel dimensions were taken from Figure 6. 8. Bolt lengths are calculated with upper mentioned equations and results given in Table 6. 3.

Table 6. 3 - Rock bolts calculation

Tunnel dimensions		Bolt dimensions	
Width (B) [m]	Wall height (H) [m]	Roof bolt length [m]	Wall bolt length [m]
2.5	1.93	2.23	2.18

The calculations of equivalent dimension (De) with equation 3-2 is given in Table 6. 4. Full tunnel height was taken for calculations, the dimensions are shown at Figure 6. 8.

Table 6. 4 - (De) value calculation

Tunnel height [m]	ESR	Equivalent dimension (De)
2.8	1.6	1.8

The (De) and Q values (Table 4. 10) were used to estimate the support based on Q system graph (Figure 3. 7) and the results are given in Table 6. 5.

Table 6. 5 - Support system according to Q system

Rock type	Class N	Support description	Bolt spacing [m]	Shotcrete thickness [cm]
Tuff-breccias	4	Fibre reinforced shotcrete and bolting	1.3	6-9
Syenite-diorites	1	No support		

7. Numerical assessment

For further numerical analysis two cross sections will be taken with highest overburden for each rock type. For numerical assessment the Rocscience RS2 software was used for deformation and support calculations and for failure criteria calculations RSDdata software was used. For cross sections AutoCAD Civil 3D and AutoCAD was used.

7.1. Input parameters

In upcoming chapters, In RS2 software both elastic and plastic analysis will be carried out for tuff-breccias and syenite-diorites. Two different cross sections were taken for analysis purpose (Figure 7. 2). They were made in Civil 3D using 3D contour lines, one with highest overburden for tuff-breccias and second for highest overburden of syenite-diorites cases (Figure 7. 1).

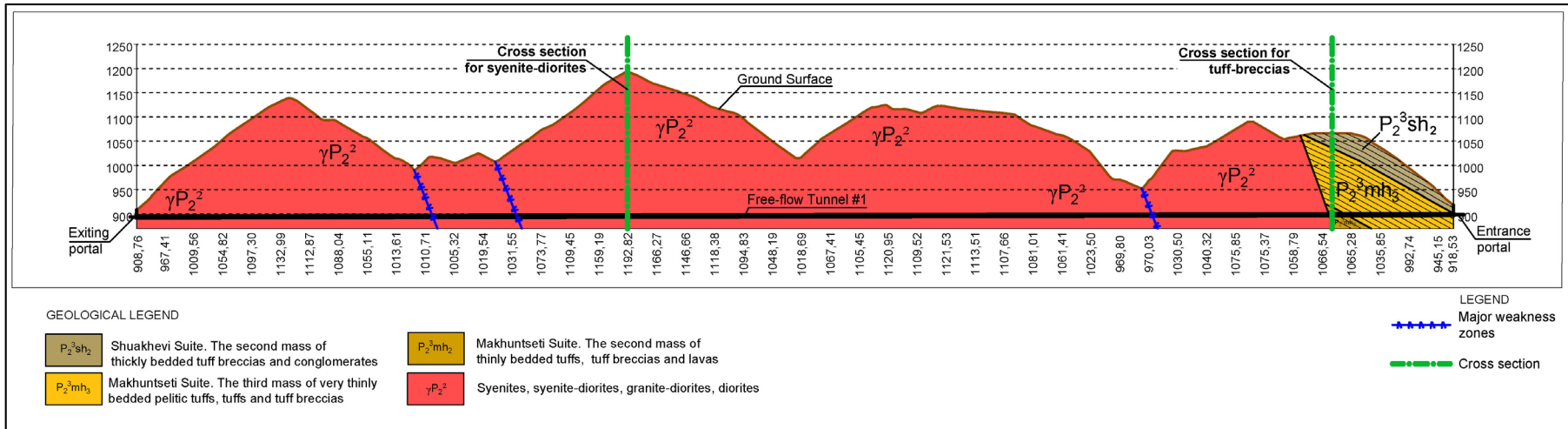


Figure 7. 1 - Cross section locations on the geological longitudinal cross section profile of Akavreta HPP headrace tunnel N1(based on (GHP, 2016))

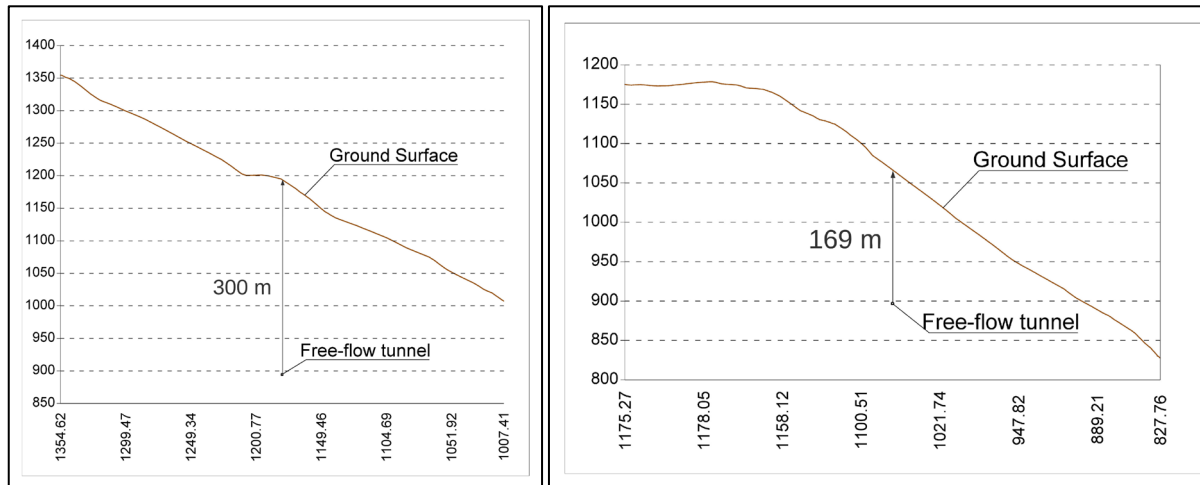


Figure 7. 2 - Cross sections for each rock type in Akavreta HPP headrace tunnel N1, left for syenite-diorites and right for tuff-breccias

The input parameters for both rock types used in plastic and elastic analysis are summed up in Table 7. 1.

Table 7. 1 - Input parameters for both rock types for elastic and plastic analysis

Rock type	Overburden [m]	σ_{ci} [MPa]	Specific weight [MN/m ³]	Poisson's ratio	E_{ci} [GPa]	MR	m_i	Tectonic stress [MPa]	GSI	σ_1 [MPa]	σ_3 [MPa]
Tuff-breccias	169	30	0.025	0.18	9	300	13	1.5	35	4.2	2.4
Syenite-diorites	300	109	0.026	0.22	35	325	25	3	50	7.8	5.2

For both elastic and plastic analysis Generalized Hoek-Brown failure criteria was used. The input parameters were taken from Table 7. 1 and calculations were made in RSData software, the results are given below (Table 7. 2) with disturbance factor 0.5.

Table 7. 2 - Generalized Hoek-Brown failure criteria calculations for tuff-breccias (left) and for syenite-diorites (right) (Extracted from RSData software)

Tuff		Syenite	
Hoek Brown Classification		Hoek Brown Classification	
UCS of intact rock (MPa)	30	UCS of intact rock (MPa)	109
GSI	35	GSI	50
m_i	13	m_i	25
disturbance factor	0.5	disturbance factor	0.5
Intact Modulus (MPa)	9000	Intact Modulus (MPa)	35425
Hoek Brown Criterion		Hoek Brown Criterion	
m_b	0.588	m_b	2.312
s	0.000172	s	0.00127
a	0.516	a	0.506

7.2. Principle stress direction

It is important to know the direction of principle stresses and how the topography influence its angle. For this purpose, RS2 software was used with cross section of each rock type taken from Figure 7. 2. The elastic mode was used for calculations with field stress type “gravity” and actual ground surface parameter on. In the first stage there is a full cover above ground surface line (Figure 7. 3) and in the second stage the ground above surface line was excavated (Figure 7. 4). The sides of the model are restrained in X direction and has fixed restrain at the corners. According to Panthi (05/05/2022) above mentioned technique gives reliable results.

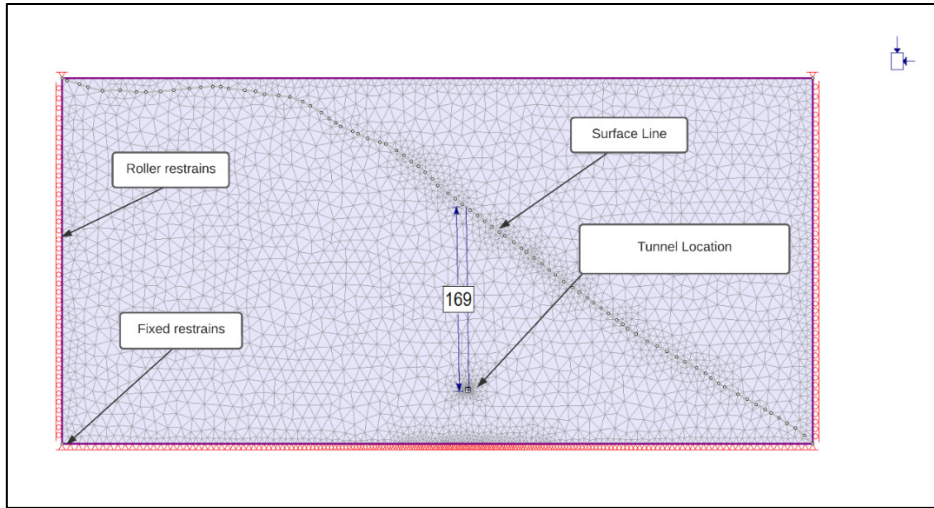


Figure 7. 3 - Excavation stages for tuff-breccias, with full cover above surface

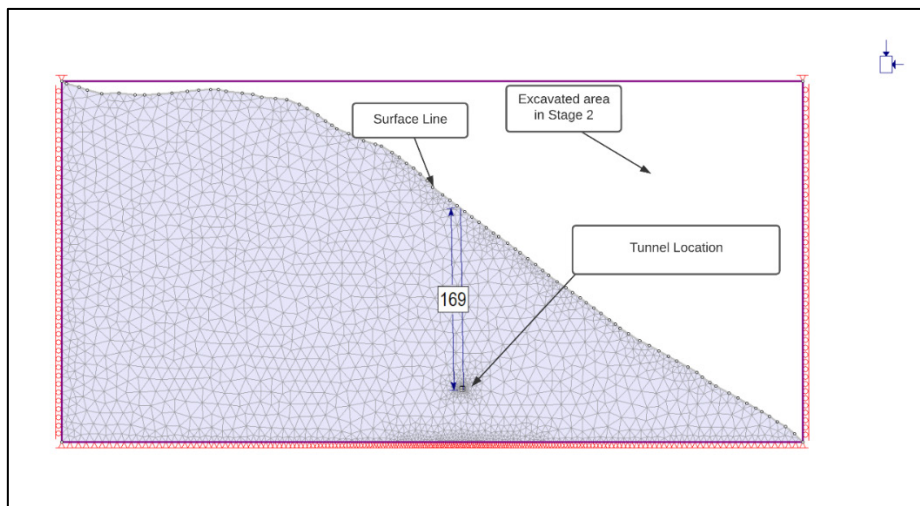


Figure 7. 4 - Excavation stages for tuff-breccias, with excavated part above surface

As seen from results for tuff-breccias on Figure 7. 5 the direction of major principal stress is 132°NE . The reason is steep topography, which affected the direction of principle stresses.

The same procedures were carried out for syenite-diorite cross section for principal stress direction analysis. As expected, major principal stress direction is near vertical (Figure 7. 6), because the tunnel is deep enough (300 m) which has minimal topographical effect on the direction of principle stresses.

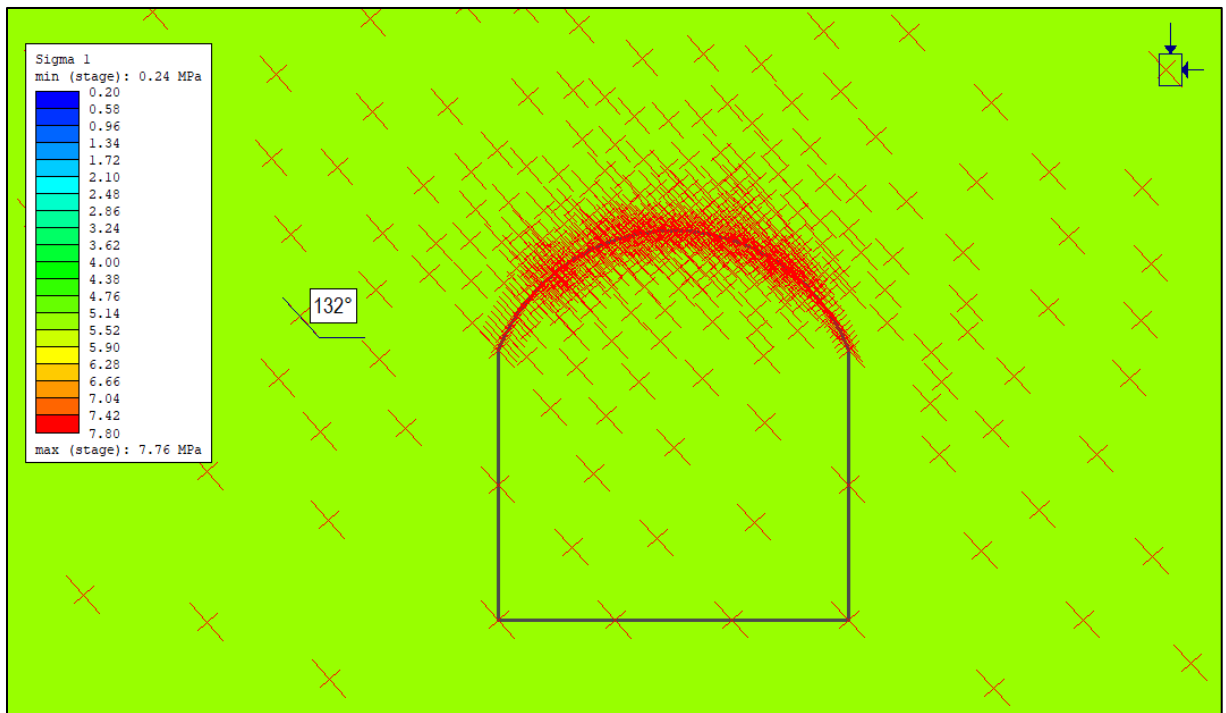
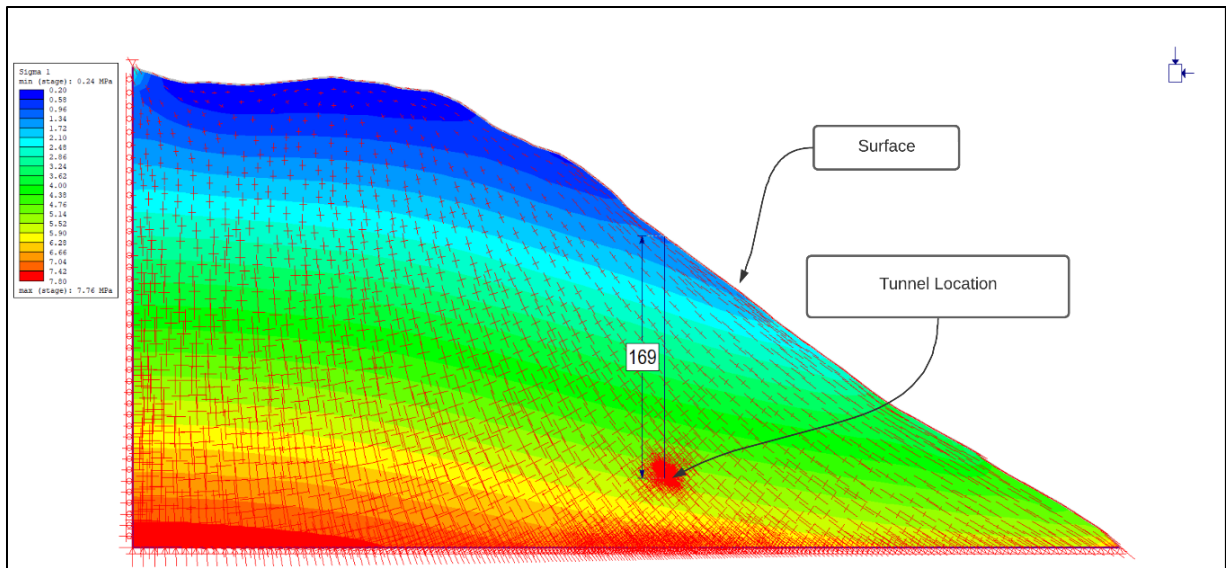


Figure 7. 5 - Direction of principle stresses for tuff-breccias

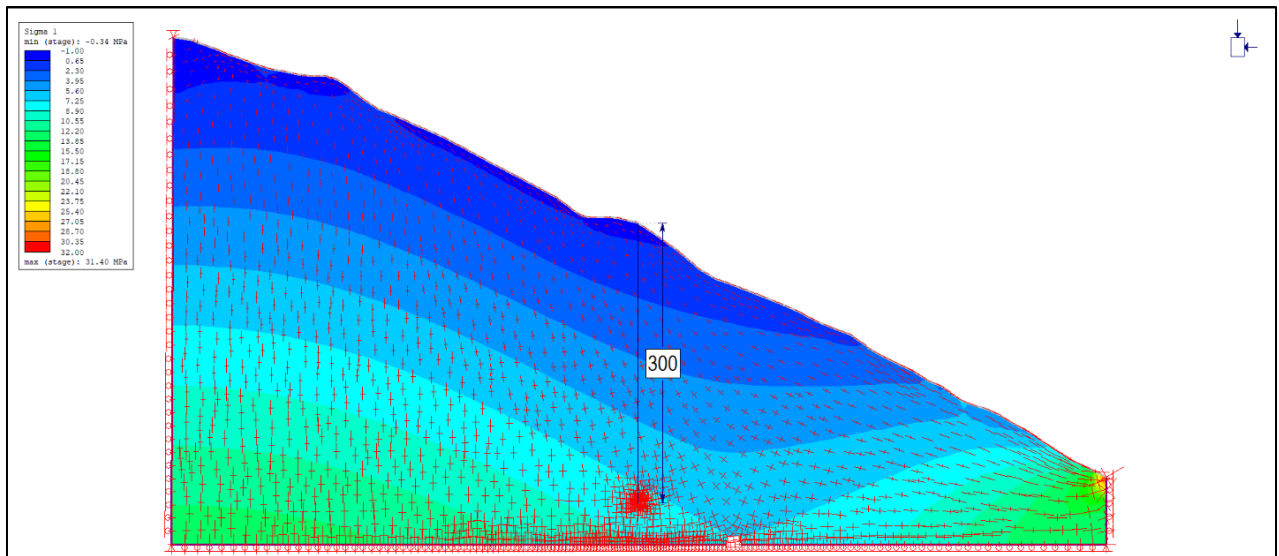


Figure 7. 6 - Direction of principle stresses for syenite-diorites

7.3. Elastic analysis

First elastic analysis was carried out to determine strength factor and stress distribution around tunnel excavation. The strength factor is the ratio of available rock mass strength to induced stress at a given point. Input parameters were taken from Table 7. 1 and Table 7. 2. The simulation was done in confined box model (Figure 7. 9) with major principal stress oriented vertically for syenite-diorites case and 132°NE for tuff-breccias case (Figure 7. 7). First the analyses were carried out for tuff-breccias and then for syenite-diorites. As shown on Figure 7. 8 and Figure 7. 10 the strength factor around tunnel is less than 1 for both rock types, it means that the tunnel will have instabilities and will fail (yield). The Figure 7. 8 and Figure 7. 10 shows the stress concentrations, for both rock types, which occurs at the corners and crown of the tunnel. Further step will be to conduct plastic analysis to determine the deformation of the headrace tunnel N1 due to stresses and to compute the required support system.

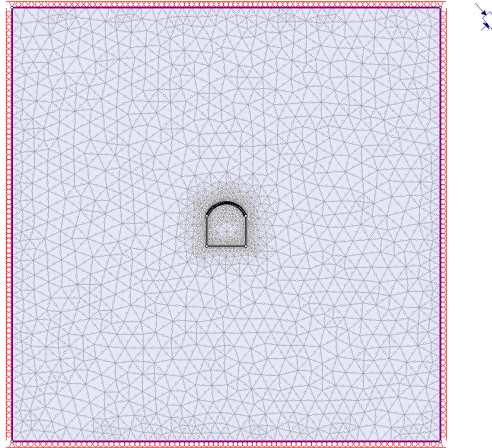


Figure 7.7 - Confined box for simulation for tuff-breccias in RS2 software

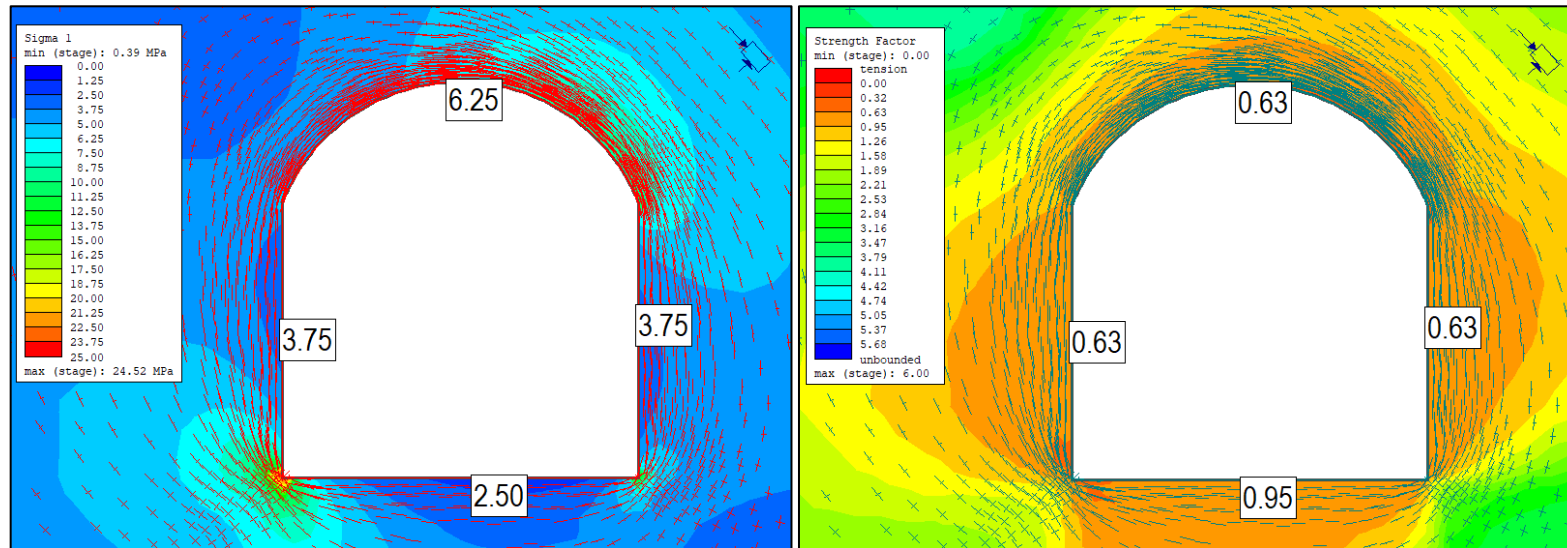


Figure 7.8 - Stress concentration (left) and strength factor (right) for tuff-breccias

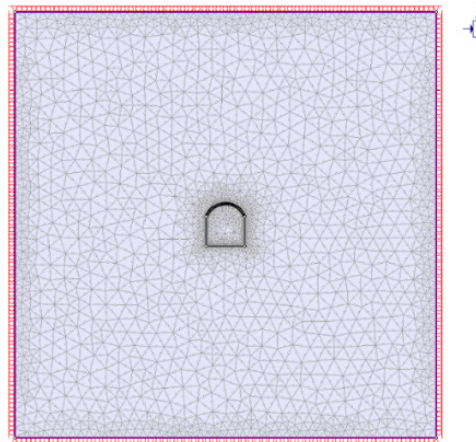


Figure 7. 9 - Confined box for simulation for syenite-diorites

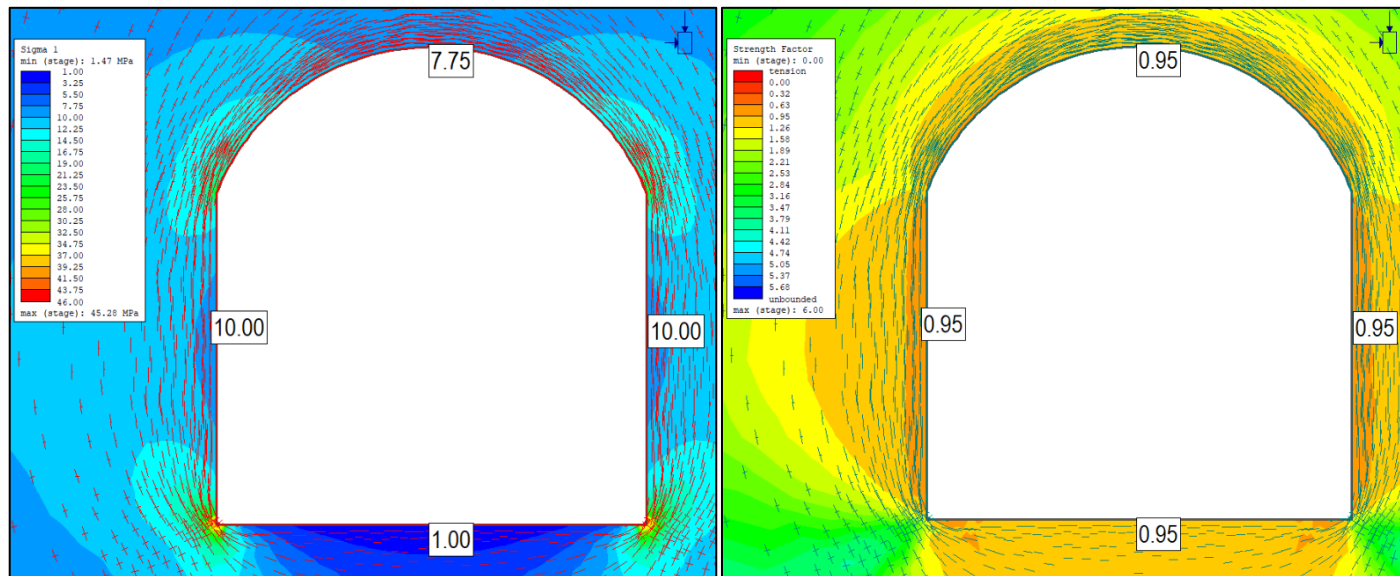


Figure 7. 10 - Stress concertation (left) and strength factor (right) for syenite-diorites

7.4. Plastic analysis

After elastic analysis, there is need for plastic analysis to see actual deformation of the tunnel due to stresses with and without support system installed. For plastic analysis same Generalized Hoek-Brown criteria is used and same input parameters as for elastic model, with addition of residual parameters, which were calculated for residual GSI. To calculate residual GSI value the equation 7-1 (Cai et al., 2007) was used.

$$GSI_r = GSI^{-0.0134*GSI} \quad 7-1$$

Results of original and residual GSI values are given in the table below:

Table 7. 3 – Original and residual GSI values

Rock type	GSI	Residual GSI
Tuff-braccias	35	22
Syenite-diorites	50	26

The residual parameters for Generalized Hoek-Brown criteria were calculated for the case when disturbance factor and dilation parameter is equals to 0.

Table 7. 4 - residual parameters for Generalized Hoek-Brown criteria

Rock type	GSI	Residual GSI	Residual parameters		
			mb	s	a
Tuff-braccias	35	22	0.8	0.0001	0.54
Syenite-diorites	50	26	1.8	0.0003	0.53

As shown in Figure 7. 15, for both rock types two similar materials were created with same parameters, except one was with disturbance factor 0.5 and second with 0. This is because after tunnel blasting near the tunnel there will be disturbance and after certain distance from the excavation the disturbance factor will be 0 again.

As seen from Figure 7. 12 for tuff-breccias maximum displacement is 5.3 cm at the right wall and as seen on Figure 7. 14 for syenite-diorites, maximum displacement is very small, which is only 6 mm (0.24% of the tunnel width).

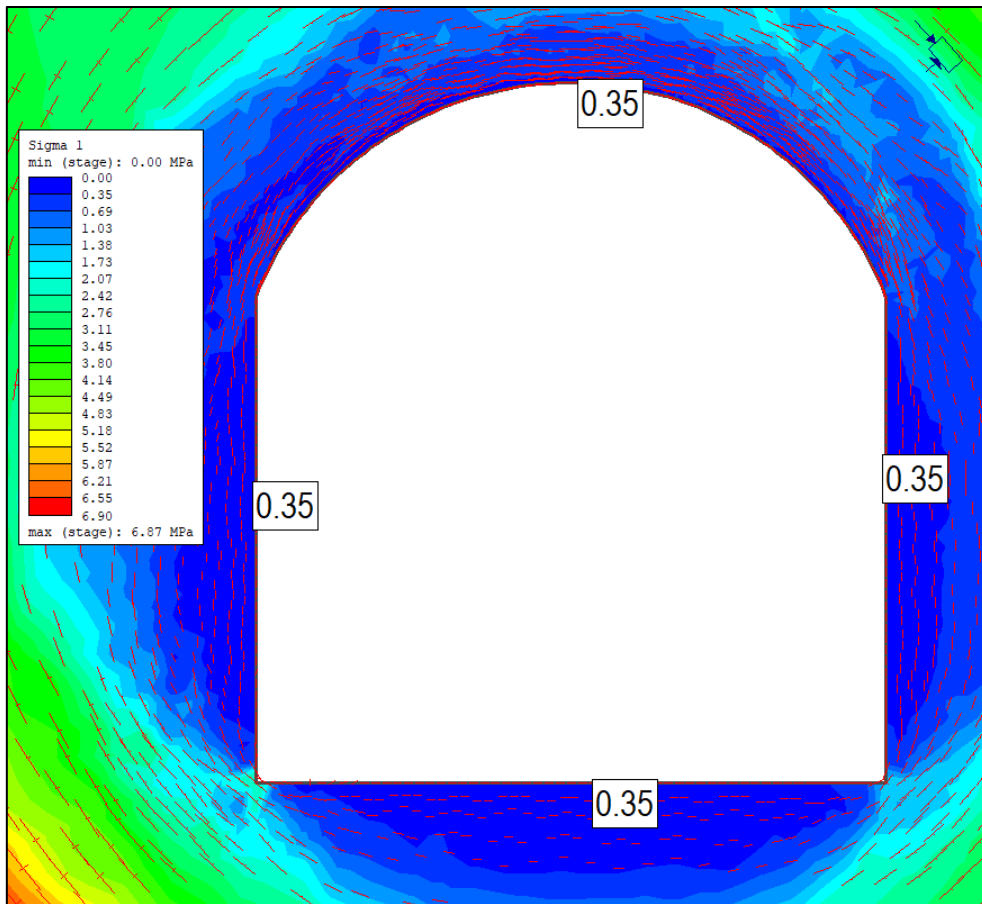


Figure 7. 11 - Major principal stress distribution around excavation for tuff-breccias

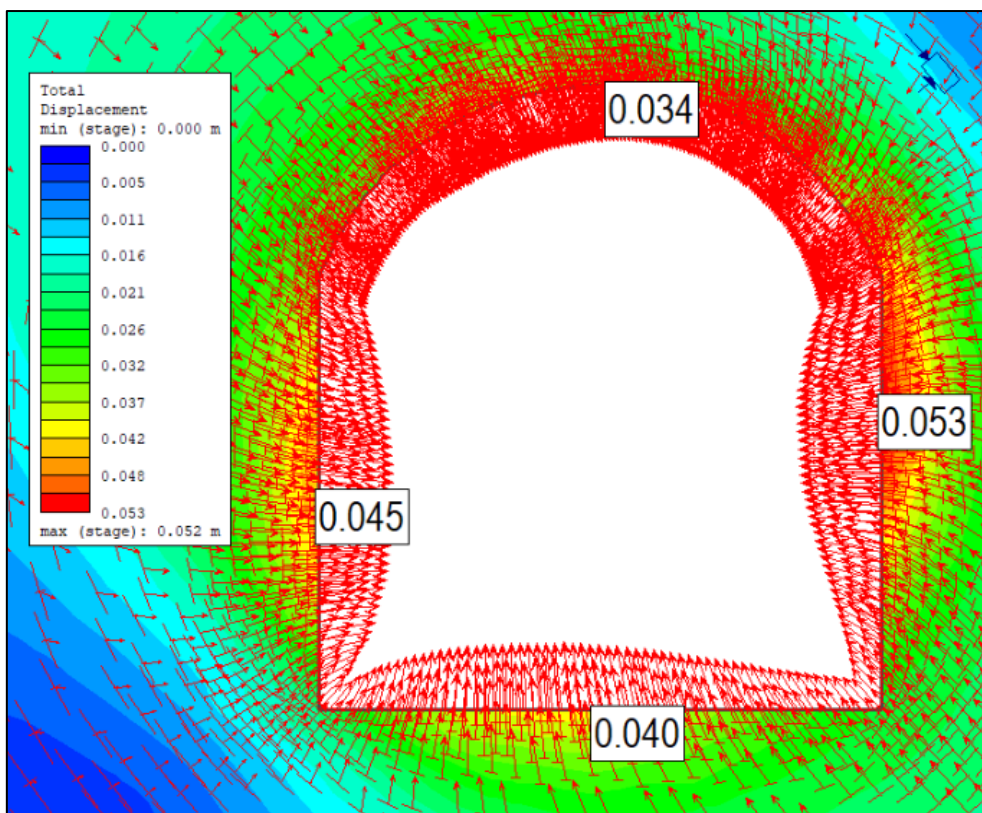


Figure 7. 12 – Total displacement for tuff-breccias

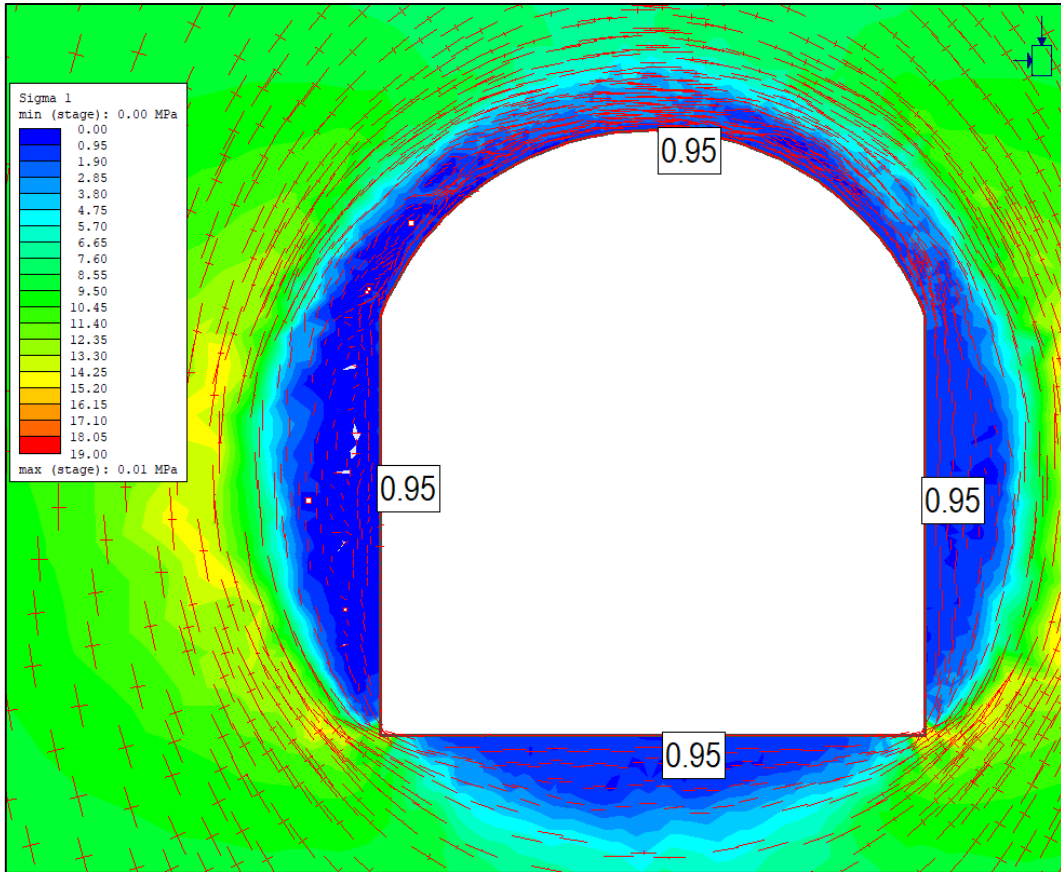


Figure 7. 13 - major principal stress distribution around excavation for syenite-diorites

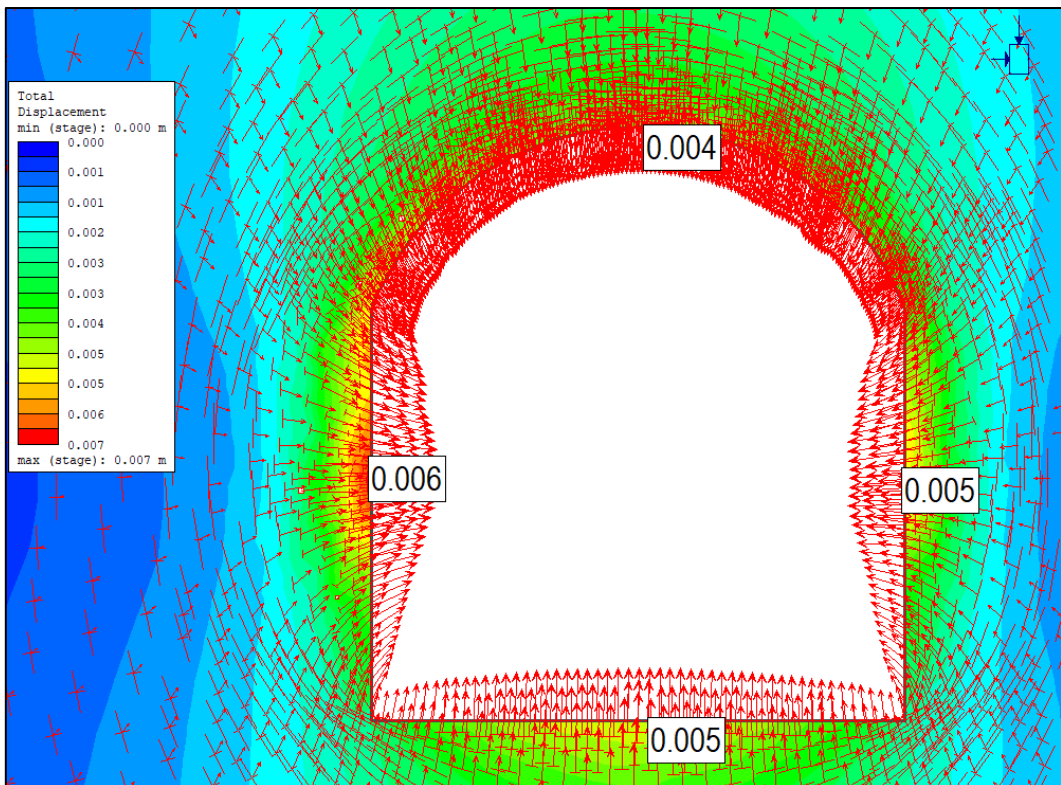


Figure 7. 14 –Total displacement for syenite-diorites

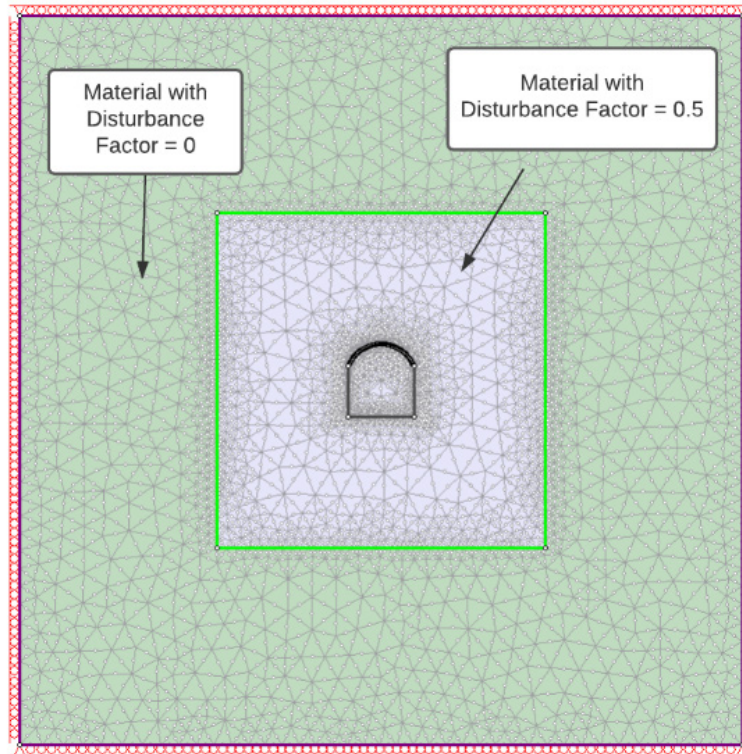


Figure 7. 15 - Confined box for plastic analysis

Further analyses were carried out to find yielding area and depth, which will be useful for making choice in support system.

As shown on Figure 7. 16 and Figure 7. 17 the yielding area for tuff-breccias is much larger than syenite-diorites. It was expected to behave like this, because of low strength and rock type specifications. For both rock types the dominating failure is due to the tension.

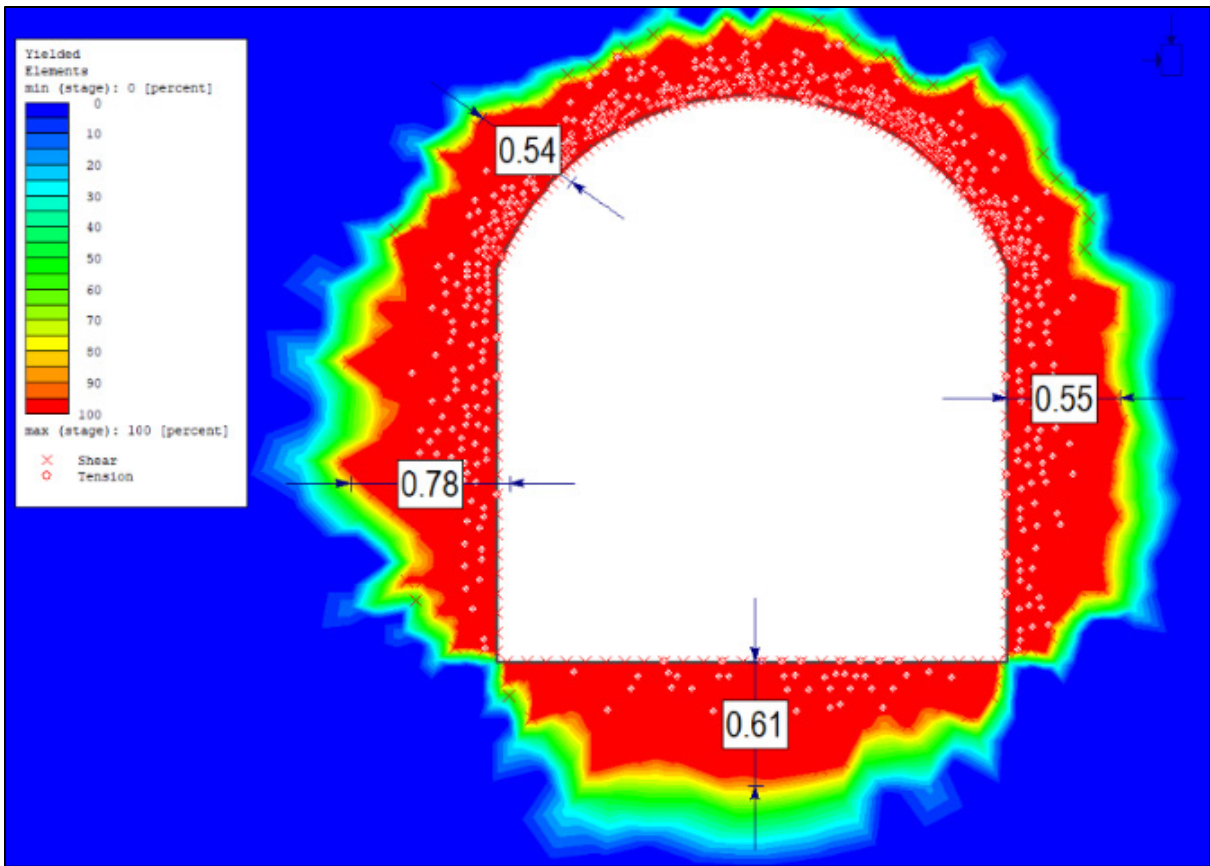


Figure 7. 16 - Yielding area with depth for syenite-diorites

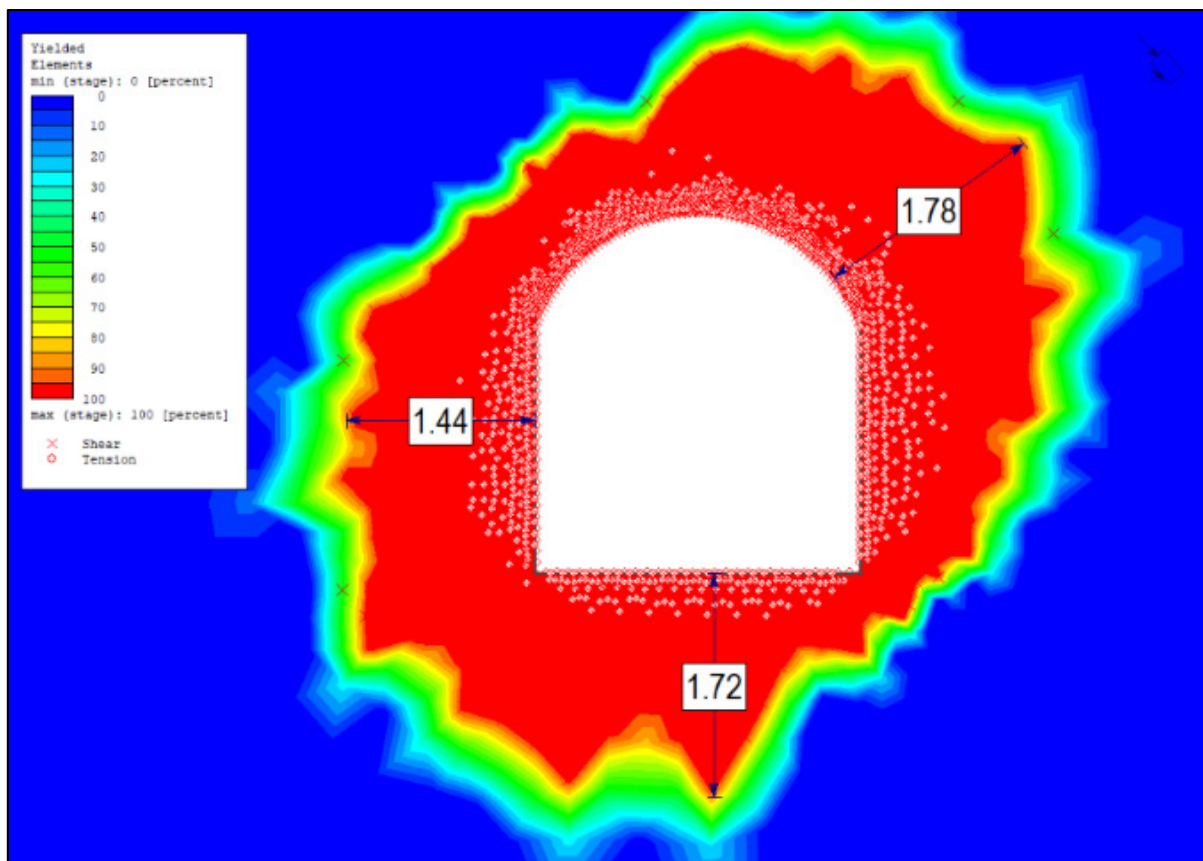


Figure 7. 17 – Yielding area with depth for tuff-breccias

7.5. Support system

As shown in Table 6. 5 the Q system was used to determine probable support used for this project. Bolt length with 2 m was used for calculations, the value is different from calculated in Table 6. 5, because tunnel width is 2.5 m and it will be difficult installing 2.3 m bolts. For both rock types the shotcrete will be applied at walls and crown for more reliable support system.

In case for tuff-breccias, in Figure 7. 18 shows the supports installed and Figure 7. 19 shows the 2.1 cm deformation at the right and left walls after support installation, which is 0.84% of total width, which is acceptable. The maximum deformation from wall was reduced from 5.3 cm to 2.1 cm. Also, the yielding area was significantly reduced with increase of strength factor.

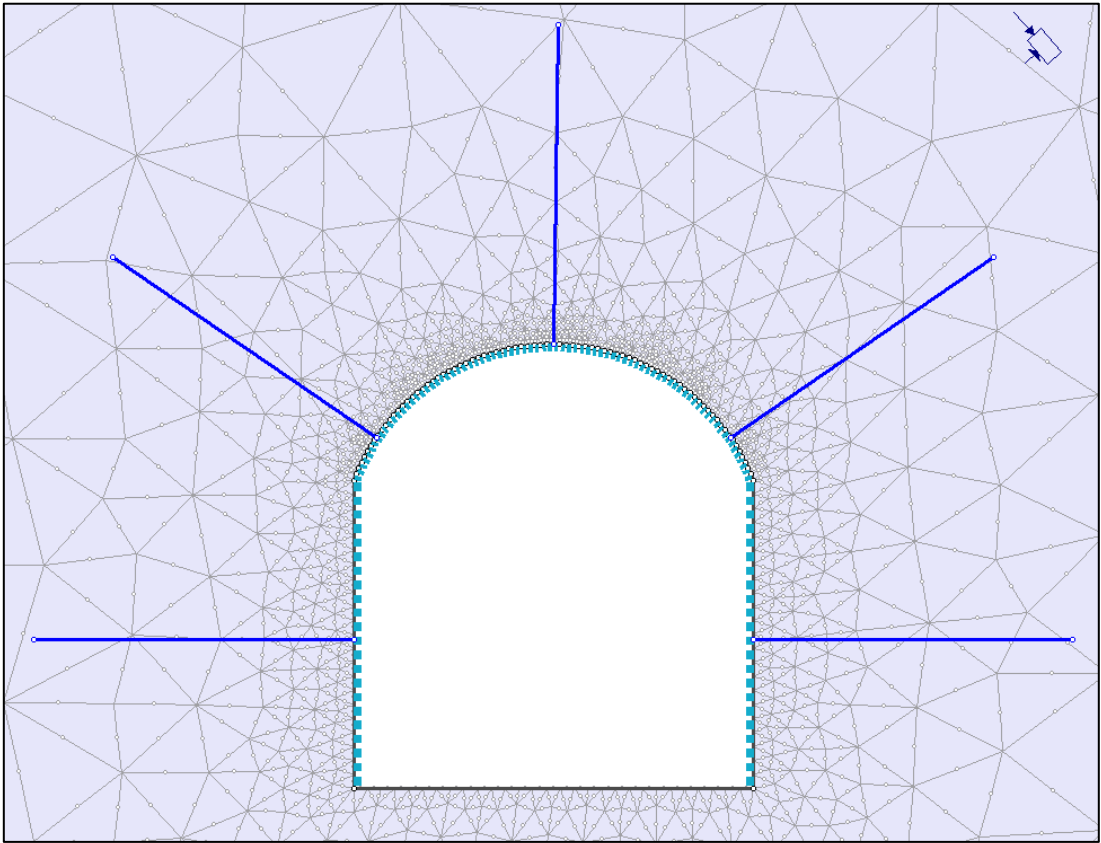


Figure 7. 18 – Installed support for tuff-breccias case in RS2 software

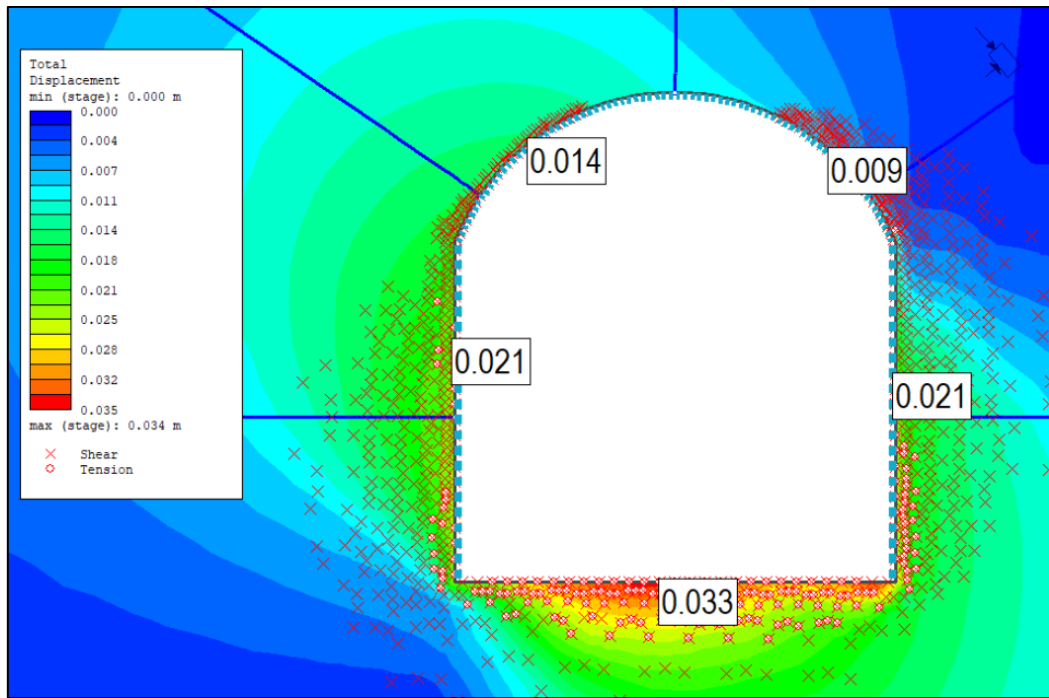


Figure 7. 19 - Total displacement for tuff-breccias after support installation

The summary of support system used in plastic analysis in RS2 software is shown in Table 7. 5 and Table 7. 6

Table 7. 5 – Bolt, shotcrete and reinforcement for tuff-breccias case

Number of bolts	Bolt spacing [m]	Bolt length [m]	Shotcrete type	Shotcrete thickness [m]	Reinforcement type	Reinforcement diameter [mm]
5	1.3	2	Reinforced concrete	0.1	Wire mesh	10

Table 7. 6 - Bolt specifications for tuff-breccias case

Rock type	Bolt type	Bolt diameter [mm]	Bolt modulus E [MPa]	Bolt tensile Capacity [MN]
Tuff-breccias	Dextra ASTEC thrust bolt solid bar 25	25	45000	0.69

Unfortunately, not always Q values are good representatives of the real-world condition of the rock mass, because the judgment of Q value depends mainly on experience and expertise of the geologist evaluating the rock mass condition. For syenite-diorites there will be support installed despite being in “unsupported” class. As a result, it provides better stability, significantly decreases the yielding area and increase the strength. In this case only 3 bolts will be installed with spacing of 1.9 m. The summary of support system used is shown in Table 7. 7. The total displacement is 5 mm, which is 0.2% of tunnel width and is acceptable.

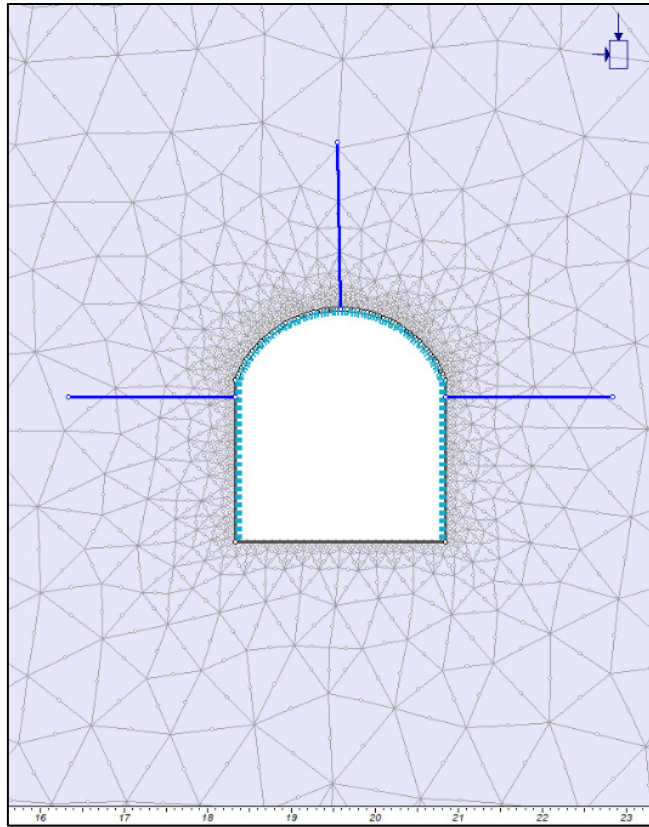


Figure 7. 20 – Support installed for syenite-diorites case in RS2 software

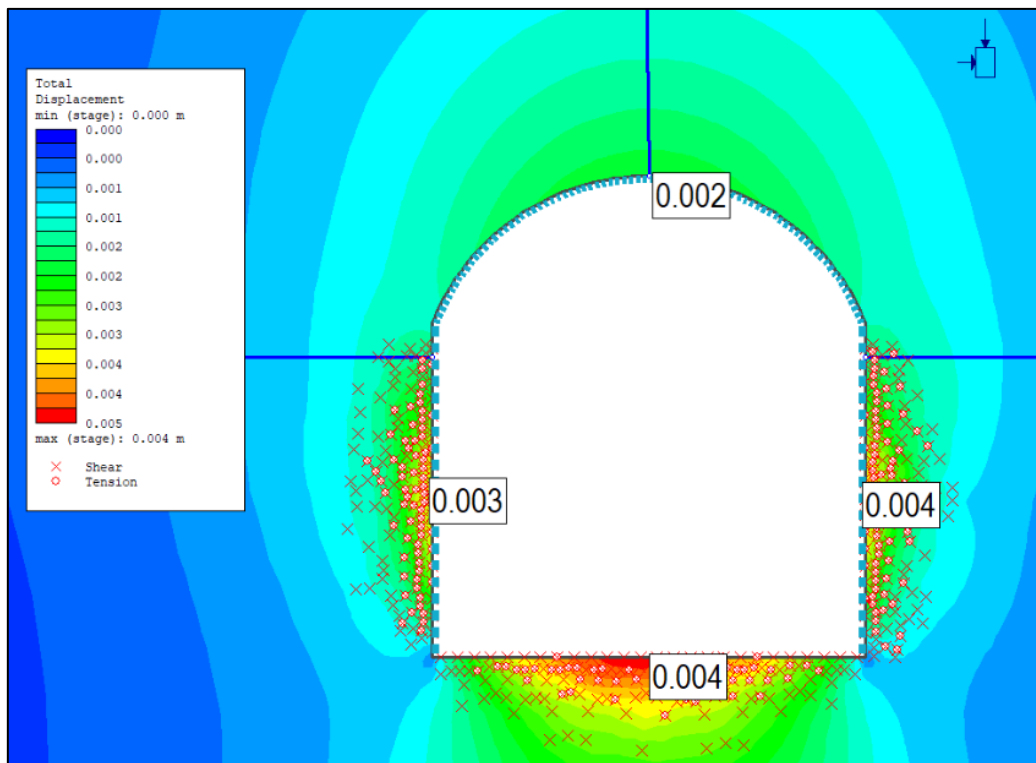


Figure 7. 21 - Total displacement for syenite-diorites after support installation

Table 7. 7 - Bolt, shotcrete and reinforcement for syenite-diorites case

Number of bolts	Bolt spacing [m]	Bolt length [m]	Shotcrete type	Shotcrete thickness [m]	Reinforcement type	Reinforcement diameter [mm]
3	1.9	2	Reinforced concrete	0.1	Wire mesh	10

Table 7. 8 - Bolt specifications for syenite-diorite case

Rock type	Bolt type	Bolt diameter [mm]	Bolt modulus E [MPa]	Bolt tensile Capacity [MN]
Syenite-diorites	Dextra ASTEC thrust bolt solid bar 25	20	50000	0.2

8. Conclusion and recommendations

8.1. Conclusion

There were two headrace tunnels given for study on Akavreta HPP in Georgia. Current project is under feasibility study and is planned to be constructed in the future. First, the current design of the two free flow headrace tunnels were evaluated. After doing excessive desk study, working with topography, geological map, making cross sections and analyzing tunnel alignment several conclusions were made:

- The headrace tunnel N1 alignment has very small overburden at two major weakness zones, which can easily be the risk factor for high instability problems in the tunnel and in case of construction, will need heavy support to stay safe and reliable.
- The difficulty of tunnel N1 construction arises with introducing the angles in the tunnel alignment, which requires very precises survey work to stay on the track.
- Tunnel N2 is safe to be constructed with original design

After deciding that current design of headrace tunnel N1 will introduce instabilities because of small overburden in major weakness zones, alternative version was introduced in cooperation with Georgian Hydro Power LLC. Alternative version not only solves small overburden problems (minimal overburden increased from 20 m to 55 m), but also eliminates 820 m of road and open channel construction necessity. The headrace tunnel N1 size increases by from 2150 m to 2750 m, but after discussion with Georgian Hydro Power LLC, it was concluded that the benefits overweight the overall project price increase because of tunnel lengthening.

Elimination of road and open channel construction is considered very beneficial for project area, because according to topography and Georgian Hydro Power LLC the difficulty of construction and cost would be high. Further detailed analysis was carried out only for tunnel N1 as Tunnel N2 shares similar geological characteristics, doesn't require alternative design and has smaller highest overburden. As shown on geological cross section Figure 6. 3, starting from inlet, at first 250 m headrace tunnel N1 meets tuff-breccia type of rock and further along alignment syenite-diorites are only rock type coming into contact with the headrace tunnel N1. Empirical and semi-empirical assessments were carried out for three different cross section for each rock type, with highest, medium and smallest overburden cases (Table 6. 2). Results showed that in case of tuff-breccias there will be small squeezing and in case of syenite-diorites there will not be any rock burst/spalling. After that, numerical analysis was performed on two cross sections, one for highest overburden for tuff-breccias case and second highest overburden for syenite-diorites case. As was expected, numerical analysis showed (Figure 7. 12) that there will be squeezing for tuff-breccias with total deformation of 5.3 cm. Support system was chosen (Table 7. 5) based on Q values (Table 4. 10) and Q system graph (Figure 3. 7) with small modifications. After support system installation, deformation at the walls reduced from 5.3 cm to 2.1 cm. In case of syenite-diorites, according to Q system, there was no need for support, but for safety purpose it was decided to install minimum amount of support (Table 7. 7), because according to Table 6. 1 maximum tangential stress was nearly equal to rock mass strength at highest (300 m) overburden. It is worth pointing out that numerical modeling is much more versatile than empirical or semi-analytical. It gives more possibilities to find best support for the given case by choosing different types of supports e.g. bolts, shotcrete, rebars and so on, with different parameters.

8.2. Recommendations

Following recommendations can be applied for this project:

- In case of severe squeezing, headrace tunnel measurements of deformation must be performed and correlations to rock mass parameters and stress conditions may be made using the RS2 software. By calibrating the input parameters, it will give opportunity to have better predictions and possibility to give more optimum suggestions about support system.

- It is important to have proper in situ stress measurements, because it is essential input parameter not only for numerical modeling, but also for verification of different estimated values from different analysis methods.
- More excessive field investigations and lab tests should be carried out. For accurate analysis of rock mass properties, field observations and laboratory tests are crucial, since input parameters are the most important for numerical modeling and different analysis methods.
- Using actual monitored deformation data during construction phase with mapped geological conditions and lab tests, can assist in verifying the plastic deformation analysis of squeezing rock mass done with numerical, empirical and semi-analytical methods.
- It is recommended for analysis to be performed using numerical models, since these types of models are very versatile and can incorporate more complexities such as groundwater effects, weakness zones and so on.

References

- Adamia, S., Akhvlediani, K., Kilasonia, V., M. Nairn, A., Papava, D., & Patton, D. (1992). Geology of the republic of Georgia: a review. *International Geology Review*, 34(5), 447-476.
- Adamia, S., Alania, V., Chagelishvili, R., Chabukiani, A., Enukidze, O., Jaoshvili, G., Razmadze, A., & Sadradze, N. (2011). Tectonic setting of Georgia (Caucasus). 3rd International Symposium on the Geology of the Black Sea Region,
- Aksoy, C. (2008). Review of rock mass rating classification: historical developments, applications, and restrictions. *Journal of mining science*, 44(1), 51-63.
- Barla, G. (2001). Tunnelling under squeezing rock conditions. *Eurosummer-school in tunnel mechanics, Innsbruck*, 169-268.
- Barton, N. (2002). Some new Q-value correlations to assist in site characterisation and tunnel design. *International journal of rock mechanics and mining sciences*, 39(2), 185-216.
- Barton, N. (2015). Forty Years with the Q-system—Lessons and Developments. *Keynote lecture, Underground Design and Construction Projects. Hong Kong Inst. of Materials, Minerals & Mining, IoM3*, 1-25.
- Brown, E. T. (1993). The nature and fundamentals of rock engineering. *Comprehensive rock engineering*, 50, 1-23.
- Cai, M., Kaiser, P., Tasaka, Y., & Minami, M. (2007). Determination of residual strength parameters of jointed rock masses using the GSI system. *International journal of rock mechanics and mining sciences*, 44(2), 247-265.
- Celada, B., & Bieniawski, Z. (2020). *Ground Characterization and Structural Analyses for Tunnel Design*. CRC Press.
- Chapman, D., Metje, N., & Stärk, A. (2018). *Introduction to tunnel construction*. Crc Press.
- Factsheet: Renewable Energy in Georgia 2021. (2021). In *UNECE Renewable Energy Uptake: Building Support for Renewable Energy Investments in Georgia* (pp. 6). Ren21 Renewables now https://www.ren21.net/wp-content/uploads/2019/05/Factsheet_Georgia-HardTalk-2021.pdf
- Gamkrelidze, I., Koiava, K., Mosar, J., Kvaliashvili, L., & Mauvilly, J. (2018). Main features of geological structure and a new tectonic map of Georgia. EGU General Assembly Conference Abstracts,
- Georgia. (2008). In (2018 ed.): *Encyclopædia Britannica*. <https://www.britannica.com/place/Georgia#/media/1/230186/61878>
- Georgia Energy Policy Review 2020*. (2020). International Energy Agency. https://www.euneighbours.eu/sites/default/files/publications/2020-07/Georgia_2020_Energy_Policy_Review.pdf
- Georgian Hydro Power LLC (GHP). (2016). *Akavreta HPP on river Akavreta geological investigation technical report*.
- Georgian Hydro Powr LLC (GHP). (2017). *Akavreta HPP on river Akavreta hydrological investigation technical report*.
- Gratchev, I. (2020). *Rock Mechanics Through Project-based Learning*. CRC Press.
- Gudjabidze, G., & Gamkrelidze, I. (2003). *Geological map of Georgia*. Georgian State Department of Geology.
- Hoek, E. (2007). Practical rock engineering. *Internet reference: www.roscience.com*.
- Hoek, E., & Bray, J. D. (1981). *Rock slope engineering*. CRC Press.
- Hoek, E., & Brown, E. T. (1997). Practical estimates of rock mass strength. *International journal of rock mechanics and mining sciences*, 34(8), 1165-1186.
- Hoek, E., & Marinos, P. (2000). Predicting tunnel squeezing problems in weak heterogeneous rock masses. *Tunnels and tunnelling international*, 32(11), 45-51.

- Hudson, J., & Harrison, J. (1997). *Engineering Rock Mechanics: an Introduction to the Principles*. In: Pergamon, Oxford.
- Hudson, J. A., & Harrison, J. P. (2000). *Engineering rock mechanics: an introduction to the principles*. Elsevier.
- Kolymbas, D. (2008). *Tunnelling and tunnel mechanics: A rational approach to tunnelling*. Springer Science & Business Media.
- Marinos, P., & Hoek, E. (2000). GSI: a geologically friendly tool for rock mass strength estimation. ISRM international symposium,
- Panthi, K., & Nilsen, B. (2005). Comparison between predicted and actual rock mass conditions: a review based on tunnel projects in Nepal Himalaya.
- Panthi, K. K. (2006). Analysis of engineering geological uncertainties related to tunnelling in Himalayan rock mass conditions.
- Panthi, K. K. (2012). Evaluation of rock bursting phenomena in a tunnel in the Himalayas. *Bulletin of Engineering Geology and the Environment*, 71(4), 761-769.
- Panthi, K. K. (2015). Himalayan rock mass and possibility of limiting concrete lined pressure tunnel length in hydropower projects in the Himalaya. *Geosystem Engineering*, 18(1), 45-50.
- Panthi, K. K. (2020). *Design approach for underground openings*. Lecture Notes , Norwegian University of Science and Technology (NTNU), Department of Geoscience and Petroleum.
- Panthi, K. K., & Basnet, C. B. (2016). Review on the major failure cases of unlined pressure shafts/tunnels of Norwegian hydropower projects. *Hydro Nepal: Journal of Water, Energy and Environment*, 18, 6-15.
- Panthi, K. K., & Broch, E. (2022). 6.07 - Underground Hydropower Plants. In T. M. Letcher (Ed.), *Comprehensive Renewable Energy (Second Edition)* (pp. 126-146). Elsevier. <https://doi.org/https://doi.org/10.1016/B978-0-12-819727-1.00077-7>
- Selmer-Olsen, R., & Broch, E. (1978). General design procedure for underground openings in Norway. In *Storage in Excavated Rock Caverns: Rockstore 77* (pp. 219-226). Elsevier.
- Ten-Year Network Development Plan of Georgia 2021-2031*. (2021). https://www.gse.com.ge/sw/static/file/TYNDP_GE-2021-2031_ENG_NEW.pdf
- Vásárhelyi, B. (2009). A possible method for estimating the Poisson's rate values of the rock masses. *Acta Geodaetica et Geophysica Hungarica*, 44(3), 313-322.
- Zhang, L. (2017). *Engineering properties of rocks*. Butterworth-Heinemann.
- Zuo, J., & Shen, J. (2020). *The Hoek-Brown Failure Criterion--From Theory to Application*. Springer.

APPENDICES





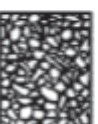
APPENDIX A

RMR classification of rock mass (Bieniawski, 1989 in (Panthi, 2006))

A. Classification parameters and their ratings									
Parameters			Range of values or ratings						
1	Strength of Intact Rock	Point load strength index (MPa)	> 10	4 - 10	2 - 4	1 - 2	Low range uniaxial strength is preferred		
		Uniaxial compressive strength (MPa)	> 250	100-250	50-100	25-50	5- 25	1 - 5	< 1
	Rating	15	12	7	4	2	1	0	
2	Drill core quality, RQD (%)		90-100	75-90	50-75	25-50	< 25		
	Rating		20	17	13	8	5		
3	Spacing of discontinuities (m)		> 2	0.6-2	0.2-0.6	0.06-0.2	< 0.06		
	Rating		20	15	10	8	5		
4	Condition of discontinuities	Length, persistence (m)	< 1	1-3	3-10	10-20	> 20		
		Rating	6	4	2	1	0		
		Separation (mm)	none	< 0.1	0.1-1	1-5	> 5		
		Rating	6	5	4	1	0		
		Roughness	very rough	rough	slightly rough	smooth	slickensided		
		Rating	6	5	3	1	0		
		Infilling (gouge) (mm)	none	hard filling		soft filling			
		Rating	6	< 5	> 5	< 5	> 5		
Weathering	un-weathered	slightly weathered	moderately weathered	highly weathered	decomposed				
Rating	6	5	3	1	0				
5	Ground water	Inflow per 10 meter tunnel length (l/min)	none	< 10	10-25	25-125	> 125		
		ρ_w / σ_1	0	0.0.1	0.1-0.2	0.2-0.5	> 0.5		
		General conditions	dry	damp	wet	dripping	flowing		
		Rating	15	10	7	4	0		
here, ρ_w is joint water pressure and σ_1 is major principle stress									
B. Rating adjustment for discontinuity orientation									
Tunnel alignment			very favorable	favorable	fair	unfavorable	very unfavorable		
Rating adjustment			0	-2	-5	-10	-12		
C. Rock mass classes determined from total ratings									
Rating	100-80	80-61	60-41	40-21	< 20				
Class No.	I	II	III	IV	V				
Description	Very good	Good	Fair	Poor	Very poor				
D. Meaning of rock mass classes									
Class No.	I	II	III	IV	V				
Average stand-up time	Can be estimated from Figure 4-4								
Cohesion of the rock mass (kPa)	> 400	3-400	2-300	1-200	< 00				
Friction angle of the rock mass (degrees)	< 45	35-45	25-35	15-25	< 15				






APPENDIX B

Characterization of rock masses based on interlocking and joint alteration. (Based on Hoek, E., Brown, E.T., 1997. Practical estimates of rock mass strength. Int. J. Rock Mech. Min. Sci. 34, 1165–1186.) (Zhang, 2017)

<p>Geological Strength Index (GSI)</p> <p>From the description of structure and surface conditions of the rock mass, pick an appropriate box in this chart. Estimate the average value of GSI from the contours. Do not attempt to be too precise. Quoting a range of GSI from 36 to 42 is more realistic than stating that GSI = 38.</p>		<p>Surface conditions</p>				
<p>Structure</p>		Very good Very rough and fresh unweathered surfaces	Good Rough, maybe slightly weathered or iron stained surfaces	Fair Smooth and/or moderately weathered and altered surfaces	Poor Slickensided or highly weathered surfaces or compact coatings with fillings of angular fragments	Very poor Slickensided and highly weathered surfaces with soft clay coatings or fillings
		Decreasing surface quality ⇒				
	Intact/Massive – intact rock specimens or massive in-situ rock masses with very few widely spaced discontinuities	90			N/A	N/A
	Blocky – very well interlocked undisturbed rock mass consisting of cubical blocks formed by three orthogonal discontinuity sets	80				
	Very Blocky – interlocked, partially disturbed rock mass with multifaceted angular blocks formed by four or more discontinuity sets	70				
	Blocky/Disturbed – folded and/or faulted with angular blocks formed by many intersecting discontinuity sets	60	50			
	Disintegrated – poorly interlocked, heavily broken rock mass with a mixture of angular and rounded rock pieces		40	30	20	
	⇐					10

APPENDIX C

Guidelines for estimating disturbance factor D (Hoek, 2007)

Rock mass appearance	Description of rock mass	Suggested value of D
	<p>Excellent quality controlled blasting or excavation by Tunnel Boring Machine results in minimal disturbance to the confined rock mass surrounding a tunnel</p>	<p>$D = 0$</p>
	<p>Mechanical or hand excavation in poor quality rock masses (no blasting) results in minimal disturbance to the surrounding rock mass. Where squeezing problems result in significant floor heave, disturbance can be severe unless a temporary invert, as shown in the photograph, is placed</p>	<p>$D = 0$ $D = 0.5$ No invert</p>
	<p>Very poor quality blasting in a hard rock tunnel results in severe local damage, extending 2 or 3 m, in the surrounding rock mass</p>	<p>$D = 0.8$</p>
	<p>Small scale blasting in civil engineering slopes results in modest rock mass damage, particularly if controlled blasting is used as shown on the left hand side of the photograph However, stress relief results in some disturbance</p>	<p>$D = 0.7$ Good blasting $D = 1.0$ Poor blasting</p>
	<p>Very large open pit mine slopes suffer significant disturbance due to heavy production blasting and also due to stress relief from overburden removal In some softer rocks excavation can be carried out by ripping and dozing and the degree of damage to the slopes is less</p>	<p>$D = 1.0$ Production blasting $D = 0.7$ Mechanical excavation</p>

APPENDIX D

Rock strength classification according to ISRM (1978) (Hoek, 2007)

Grade*	Term	Uniaxial Comp. Strength (MPa)	Point Load Index (MPa)	Field estimate of strength	Examples
R6	Extremely Strong	> 250	>10	Specimen can only be chipped with a geological hammer	Fresh basalt, chert, diabase, gneiss, granite, quartzite
R5	Very strong	100 - 250	4 - 10	Specimen requires many blows of a geological hammer to fracture it	Amphibolite, sandstone, basalt, gabbro, gneiss, granodiorite, limestone, marble, rhyolite, tuff
R4	Strong	50 - 100	2 - 4	Specimen requires more than one blow of a geological hammer to fracture it	Limestone, marble, phyllite, sandstone, schist, shale
R3	Medium strong	25 - 50	1 - 2	Cannot be scraped or peeled with a pocket knife, specimen can be fractured with a single blow from a geological hammer	Claystone, coal, concrete, schist, shale, siltstone
R2	Weak	5 - 25	**	Can be peeled with a pocket knife with difficulty, shallow indentation made by firm blow with point of a geological hammer	Chalk, rocksalt, potash
R1	Very weak	1 - 5	**	Crumbles under firm blows with point of a geological hammer, can be peeled by a pocket knife	Highly weathered or altered rock
R0	Extremely weak	0.25 - 1	**	Indented by thumbnail	Stiff fault gouge

* Grade according to Brown (1981).

** Point load tests on rocks with a uniaxial compressive strength below 25 MPa are likely to yield highly ambiguous results.

APPENDIX E

Rock jointing for syenite-diorites rock type (GHP, 2016)

Outcrop #	Joint Set No.	Dip. Azimuth degrees	Dip. degrees	Joint Spacing, [cm]	Joint Length, [m]	Aperture [mm]
1	I	60	80-83	70	3.6	2.03
				25	5	
				50	1.7	
				30	3.3	
				20	4.8	
				35	1.6	
				38.33	3.33	
	II	350	85	15	5	
				25	2.1	
				18	2.1	
				35	3.3	
				30	4.4	
				22	4.8	
	24.17	3.62				
	III	250	15-18	25	1.2	
				25	1	
				15	2.2	
				37	1.5	
				25	1.4	
				20	1.5	
				24.50	1.47	

Outcrop #	Joint Set No.	Dip. Azimuth degrees	Dip. degrees	Joint Spacing, cm	Joint Length, [m]	Aperture [mm]
2	I	60	80	60	3.8	0.41
				65	10	
				50	4.2	
				44	1.8	
				31	3.15	
				28	2.1	
				47.0	4.18	
	II	350	85	27	1.5	
				35	3	
				40	4	
				17	2.5	
				28	3	
				65	3.5	
	35.33	2.92				
	III	250	15-18	17	0.35	
				14	0.7	
				25	2.2	
				15	1.7	
				27	3	
				33	2.7	
				21.83	1.78	

APPENDIX F

Guidelines for the selection of modulus ratio (MR) values - based on Deere (1968) and Palmstrom and Singh (2001) (Hoek, 2007)

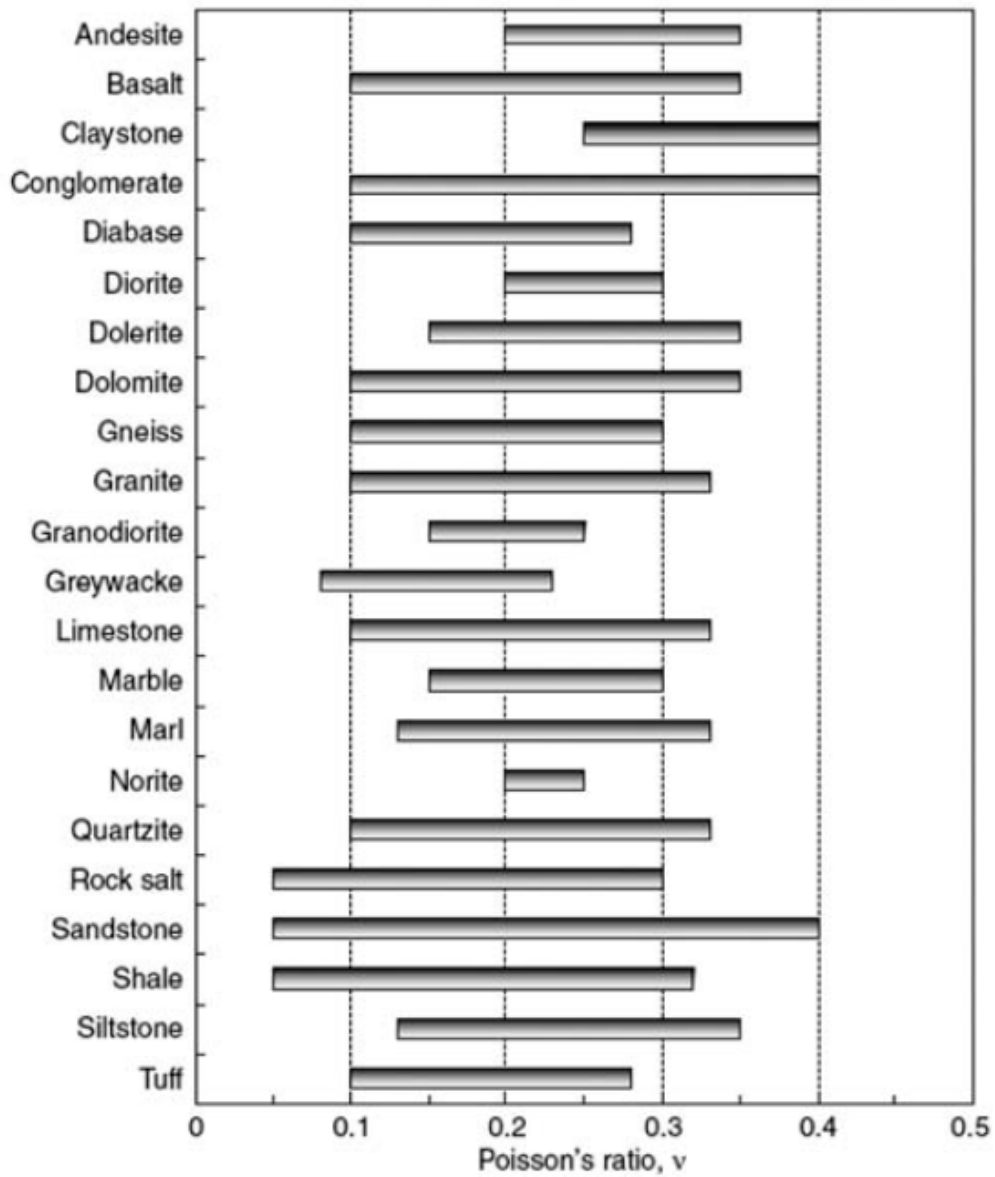
	Class	Group	Texture			
			Coarse	Medium	Fine	Very fine
SEDIMENTARY	Clastic		Conglomerates 300-400	Sandstones 200-350	Siltstones 350-400	Claystones 200-300
			Breccias 230-350		Greywackes 350	Shales 150-250 * Marls 150-200
	Non-Clastic	Carbonates	Crystalline Limestone 400-600	Sparitic Limestones 600-800	Micritic Limestones 800-1000	Dolomites 350-500
		Evaporites		Gypsum (350)**	Anhydrite (350)**	
Organic					Chalk 1000+	
METAMORPHIC	Non Foliated		Marble 700-1000	Hornfels 400-700 Metasandstone 200-300	Quartzites 300-450	
	Slightly foliated		Migmatite 350-400	Amphibolites 400-500	Gneiss 300-750*	
	Foliated*			Schists 250-1100*	Phyllites /Mica Schist 300-800*	Slates 400-600*
IGNEOUS	Plutonic	Light	Granite+ 300-550 Granodiorite+ 400-450	Diorite+ 300-350		
		Dark	Gabbro 400-500 Norite 350-400	Dolerite 300-400		
	Hypabyssal		Porphyries (400)**		Diabase 300-350	Peridotite 250-300
	Volcanic	Lava		Rhyolite 300-500 Andesite 300-500	Dacite 350-450 Basalt 250-450	
		Pyroclastic	Agglomerate 400-600	Volcanic breccia (500)**	Tuff 200-400	

* Highly anisotropic rocks: the value of MR will be significantly different if normal strain and/or loading occurs parallel (high MR) or perpendicular (low MR) to a weakness plane. Uniaxial test loading direction should be equivalent to field application.

+ Felsic Granitoids: Coarse Grained or Altered (high MR), fined grained (low MR).

** No data available, estimated on the basis of geological logic.

Poisson's ratio range for different rock type (collected by Gercek 2007 in (Vásárhelyi, 2009))



Values of the constant m_i for intact rock (Marinos & Hoek, 2000)

Rock type	Class	Group	Texture			
			Coarse	Medium	Fine	Very fine
SEDIMENTARY	Clastic		Conglomerates *	Sandstones 17 ± 4	Siltstones 7 ± 2	Claystones 4 ± 2
			Breccias *		Greywackes (18 ± 3)	Shales (6 ± 2) Marls (7 ± 2)
	Non-Clastic	Carbonates	Crystalline Limestone (12 ± 3)	Sparitic Limestones (10 ± 2)	Micritic Limestones (9 ± 2)	Dolomites (9 ± 3)
		Evaporites		Gypsum 8 ± 2	Anhydrite 12 ± 2	
Organic					Chalk 7 ± 2	
METAMORPHIC	Non Foliated		Marble 9 ± 3	Hornfels (19 ± 4) Metasandstone (19 ± 3)	Quartzites 20 ± 3	
	Slightly foliated		Migmatite (29 ± 3)	Amphibolites 26 ± 6	Gneiss 28 ± 5	
	Foliated**			Schists 12 ± 3	Phyllites (7 ± 3)	Slates 7 ± 4
IGNEOUS	Plutonic	Light	Granite 32 ± 3	Diorite 25 ± 5		
		Dark	Gabbro 27 ± 3 Norite 20 ± 5	Dolerite (16 ± 5)		
	Hypabyssal			Porphyries (20 ± 5)	Diabase (15 ± 5)	Peridotite (25 ± 5)
	Volcanic	Lava		Rhyolite (25 ± 5) Andesite 25 ± 5	Dacite (25 ± 3) Basalt (25 ± 5)	
		Pyroclastic	Agglomerate (19 ± 3)	Breccia (19 ± 5)	Tuff (13 ± 5)	

